High Resolution Infrared Spectroscopy Of Some Molecules In The Gas Phase

by

Konstadinos Tavladorakis

A thesis submitted to the University of London in partial fulfilment of the regulations of the Ph.D. degree.

Department of Chemistry

University College London

1990

This work is dedicated to my parents
for their financial support
and to Katerina
for her support and encouragement
throughout the years.

Aknowledgments

I would like to thank Dr. J.E.Parkin for supervising this work and for his assistance in the recording of FTIR spectra, supplying of computer programs and helpful advice on all of the analysis.

I am also indebted to Simon Edwards for making available to me samples of $C_2H.CDO$ and $C_2D.CDO$.

Abstract

A nineteen-parameter harmonic in-plane force field for the s-trifluorobenzene-h_3 molecule was constructed. Internal force constants, symmetry force constants, normal coordinates and Cartesian displacements were calculated. The observed data included fundamental frequencies, first order Coriolis constants and centrifugal distortion constants for both s-trifluorobenzene-h_3 and -d_3. Some of the data were obtained from our study of the mid-infrared spectrum of s-trifluorobenzene-h_3.

A seven-parameter harmonic out-of-plane force field for the same molecule was also re-investigated, utilising two accurately obtained fundamental frequencies.

The mid-infrared spectrum of s-trifluorobenzene-h_3 was examined at a resolution of ca. Ø.Ø6 cm^{-1}. An analysis of the two partially resolved fundamental a_2'' vibrations was completed using the method of simulation with synthetic spectra.

The five e′ fundamental bands of the same molecule in the mid-infrared region were investigated for the estimation of first order Coriolis constants. A modified computer program was used to simulate the effects of l-resonance which were present in some of the fundamentals.

The infrared spectra of some of the overtones and combination bands were also investigated and in some cases effective first order Coriolis constants were estimated either using computer simulation techniques or zeta sum rules or both.

The mid-infrared spectra of two deuterium substituted propynal molecules , namely $C_2H.CDO$ and $C_2D.CDO$ were recorded at a resolution of ca. Ø.Ø8 cm^{-1}. A detailed analysis of the partially resolved $\nu_1(a')$, $\nu_5(a')$,

$\nu_6,\nu_{10}(a',a'')$ bands of $C_2H.CDO$ molecule was completed. An analysis of ν_7 and ν_{11} bands of the same molecule was also performed. Again, the method which was used was the simulation of the observed bands with synthetic spectra taking into account the effects of second order Coriolis interactions between the energy levels of the two bands.

Finally, the $\nu_6(a'),\nu_{10}(a'')$ pair of bands of $C_2D.CDO$ species were also analysed, again using the 'Band Contour Method'.

Contents

Chapter 1

Introduction

1.1 Introduction

High resolution spectroscopy of polyatomic molecules is an area of expanding research activity over the last decades. This has led to a number of advances in the experimental techniques together with important developments in the theory of rovibrational spectra. Despite the considerable efforts by a large number of research workers in this field, problems remain relating to the complexity of large molecules and the large amount of computation involved.

During the 1960s and early 1970s gas phase infrared studies of molecules were performed at resolutions of between 0.1 and 2.0 cm^{-1}. This of course is well outside the Doppler widths for these molecules typically of the order of 0.001 cm^{-1}. In the context of such studies[1], the term " high resolution" simply meant the maximum spectral resolution which could be achieved experimentally at the time.

In recent years, the development of tunable laser sources has led to experiments conducted at resolutions even below the Doppler width of a typical line[2].

For our purposes, "high resolution" infrared rovibration spectra will be defined to be those obtained at resolutions of approximately 0.06 cm^{-1} in the mid-infrared region, that is between 500 - 4000 cm^{-1}. That was the resolution that was in practice available at UCL.

In most cases the most important piece of information that can be obtained from the rovibrational structure in the gas phase spectra of polyatomic molecules relates to the characterisation of intramolecular potential energy surfaces. This is achieved by the determination of certain spectroscopic constants which subsequently leads to the

calculation of harmonic force constants. Even anharmonic force constants have been obtained from studies of vibrational resonances and from certain rovibrational constants, in favourable cases.

Apart from this, the molecular constants obtained from the analysis of rovibrational spectra may be of use in other problems in physical chemistry such as:

α. The empirical mapping of potential energy surfaces in the kinetic studies;

β. The utilisation of anharmonic force constants in the interpretation of X-ray and electron diffraction data;

γ. The calculation of certain thermodynamic functions.

In theory, the prediction of the rovibrational spectrum of a polyatomic molecule is possible with a knowledge of:

α. The equilibriun structure of the molecule under investigation;

β. The force field and the atomic masses in the molecule;

γ. The formulae for the energy levels, the selection rules and the rovibrational line intensities.

In practice, problems arise when one attempts to calculate the equilibrium structure and the harmonic and

anharmonic force constants from the observed spectrum due to indeterminacy.

To overcome this problem, it is necessary to obtain as complete a set of rovibrational data as is possible. For simple aromatic molecules such investigations are at an early stage of development in comparison to simpler molecules like the methyl halides.

This is a direct consequence of the relatively large size of this kind of molecule which results in a very high number of transitions contributing to the overall structure of a single rovibrational band.

In the infrared spectra of even simple molecules the observed rotational structure is highly complicated consisting of peaks which are superpositions of many lines. It has been found that in this particular region the experimental problems associated with obtaining Doppler limited resolution can be considerable.

Obviously, in order to obtain accurate rovibrational data, there is a need for very high instrumental resolving power. This need has been satisfied with the advent of recent developments in the use of:

α. Tunable infrared laser sources;

β. Fourier transform spectroscopy;

γ. Powerful data handling systems.

Finally, the Doppler and sub-Doppler infrared studies of the smaller polyatomic molecules which have been reported so far indicate that usually there are complex perturbations in rovibrational spectra.

In such cases, it is necessary to perform highly

accurate frequency and intensity calculations for a very large number of transitions. Such operation can only be accomplished with the use of fast digital computers. Their increased capabilities have now facilitated the interpretation of a large number of previously unaccounted for infrared observations.

1.2 Fourier Transform Infrared Spectroscopy

The concept of this technique was originated in the beginning of this century by Michelson's first attempts at interferometric spectroscopy.

However, it was not until the late 1950's and early 1960's that the practical benefits were realised. Then, in the late 1960's with the introduction of He-Ne lasers, Tryglycine Sulphate (TGS) detectors and completely self-contained computerised instrumentation the use of Fourier Transform infrared spectroscopy became widespread.

A review of commercial instrumental developments in FTIR has been written by Griffiths[3] . This covers the history of this field up to 1983.

The present generation of FTIR spectrometers have the following advantages over their predecessors:

α) They have data systems which are faster.

β) They are more reliable.

γ) They have more versatile operating systems.

δ) They have much greater available memory capacity.

Because of these developments the problems associated with

large scale data processing are rapidly diminishing. Besides, a number of computer programs have been developed to assist in the interpretation of the spectra. For example, computer programs have been developed to assist the rotational assignment of complicated spectra[4,5].

The improved performance of FTIR spectrometers over dispersion monochromators is based mainly on two advantages[6]:

α) The Fellgett advantage: Around 1950, Fellgett recognised that information from all spectral elements is measured simultaneously with an interferometer. This so called multiplex advantage is the fundamental theoretical advantage of all Fourier Transform spectrometers.

β) The Jacquinot advantage: Around that time, Jacquinot realised the fact that the maximum allowed solid angle of the collimated beam passing through an interferometer is greater than the solid angle of a beam of the same cross-sectional area at the prism or grating of a monochromator measuring at the same resolution.

Other advantages include built-in callibration and the possibility of improving the signal to noise ratio by co-adding a large number of scans.

The incorporation of a built-in minicomputer makes the elimination of any reproducible error source, if its existence and laws are known, relatively easy. The following catalogue lists error sources, correction procedures and the software to apply them[7]:

a) Interference Fringes: The appearance of interference fringes in the spectrum is caused by a thin sample with parallel sides. These fringes tend to obscure the baseline, obstruct detection of relatively

weak peaks and generally cause distortions in their intensities.

These fringes being sinusoidal, they give a single spike in the interferogram. This spike can be recognised because of its shift in location when the sample is tilted. These fringes can be eliminated using several techniques[6]:

α) The region in the interferogram that contains the spikes can be replaced with zeros. The problem is that zero filling an interferogram within the data introduces a discontinuity in the interferogram. This effect is distributed over the entire spectrum and effectively increases the noise slightly. However, in most cases its effect is less severe than the interference fringes unless the sample is very thin.

β) Two interferograms of the same sample but each one with the sample tilted slightly in the beam path with the respect to the other, are collected. This causes the spike in the interferogram to be displaced. Only one interferogram is necessary for calculating the spectrum, so its spike is effectively removed by grafting corresponding interferogram points from the other interferogram into the first interferogram.

γ) The sinusoidal fringe can be simulated and then subtracted.

δ) The sample is held at Brewster's angle to the beam. Techniques γ) and δ) include the assumption that the refraction index does not vary with wavenumber which is not true in practice. This leads to inaccurate quantitative measurements.

ε) The sample can be wedged. In this case the sample does not have parallel sides and interference fringes can not occur. The problem is that this too can lead to photometric errors. The effects of sample wedging are small but observable.

b) Resolution errors[7]: It can be shown that a substantial deviation from Beer's law exists when the resolution of the measurement approaches the width of the sample bands. In this case[8], the tolerance improves when using boxcar apodization over the common triangular apodization. The problem is the generation of apparent negative absorbances due to the Fourier transform process when the real absorbances are, of course, positive. An alternative apodization function is the trapezoidal one which avoids this phenomenon, at the expense of some loss in resolution.

In some of our measurements, the Blackmann-Harris 3 term apodisation function was found to give good results. The problem is that the resolution is decreased slightly more than with triangular apodization, but the calculated spectrum looks more satisfactory.

c) Interpolation by zero-filling[6]: In general, $(2^m-1)/N$ zeros are added to an interferogram, where m > 1. The bandwidth after the complex FFT (FFT = Fast FT is an algorithm in which the number of computations is reduced when compared with the classical FT) will contain $2^{(m-1)}N$ points of which 1/2 N are linearly independent and the rest are interpolated. The result is a far smoother spectrum. For good photometric precision at least 8 output points per resolution element are necessary, for which m=3. Problems with this method are the increase in computation time and/or the excessive requirement for storage of data.

1.3 The Band Contour Method

In general, the appearance of a rovibrational band is a function of some or all of the following parameters[9]:

α) Selection rules

β) Transition probabilities

γ) Moments of inertia

δ) Temperature

ε) Coriolis interactions

στ) Various perturbations such as l-type resonance, Fermi resonance etc.

ζ) Resolution with which the spectrum is observed.

The 'Band Contour Method' is the name widely used referring to the computer calculation of gas phase molecular band spectra. The main objectives of the 'Band Contour Method'when it is used in the analysis of the vibrational spectra of polyatomic molecules are:

α) The determination of band type leading to vibrational symmetry.

β) The estimation of various molecular constants.

The synthesis of a rovibrational band under study is achieved by calculating the frequencies and the intensities

of the lines which are thought to contribute to the observed band and the application of appropriate selection rules. Then, the calculated lines are integrated so as to build up a realistic band contour. In the next stage, the calculated spectrum is compared with the observed one. The parameters which affect the appearance of the calculated spectrum can then be varied until there is an agreement between the observed and the calculated band contours. In general, two criteria must be satisfied:

α) Agreement between observed and calculated frequencies of the various features in a band.

β) Agreement between observed and calculated intensities of various features in a band.

The first criterion may often be satisfied with the use of analytical expressions to estimate coincidences of lines. The second criterion depends on:

α) The theoretical intensity expressions which are used in the simulations.

β) The experimental conditions.

The resulting line profiles are generally fall into two categories:

α) Those which are described by a Gaussian function, that is, the case when the Doppler broadening is the dominant effect and collision broadening is negligible.

β) Those which are described by a Lorentzian function, that is, the case when collision broadening is the dominant effect and Doppler broadening is negligible.

There are however cases when intermediate situations may arise. It should also pointed out that the Lorentzian function can still contribute to the wings of the line profile even though the Lorentzian halfwidth is small when compared with the Doppler halfwidth. This comes from the fact that the Lorentzian function decays as ν^{-2} while the Gaussian function has an exponential decay. Benedict et al[10] estimated that for a 2 : 1 ratio of Doppler to Lorentzian halfwidths, the Doppler contribution to the total linewidth can be < 10%. This is a consequence of the relatively slow decay of the Lorentzian function in the wings.

Additionally there are problems in relation to the correct use of intensity scales and lineshape functions to simulate appropriate instrumental lineshape functions.

However, one of the great advantages of band contour simulations of spectra over other more conventional analytical techniques lies in the possibility of characterising specific interactions which cause perturbations in the intensities of the observed spectra.

One type of such a perturbation, which we have observed in the present study, is the l-type resonance which is responsible for a prominent and frequently observed intensity perturbation producing a split Q-branch in many symmetric rotors. The theory behind this type of perturbation was thoroughly discussed by Cartwright and Mills[11]. In general, the l-doubling of energy levels in a symmetric rotor arises from the vibrational angular momentum in a degenerate mode. It is observed only in the K = 1←0 sub-band since the splitting of the sub-levels decreases

with increasing K . The splitting arises because the ^{r}Q branch and the ^{r}P and ^{r}R branches terminate in different components of the l-doubled levels. Its effect is only observed at high resolution. The effect of the resonance is to cause a distinct hole near the Q branch region of a perpendicular band. This effect is analysed in more detail in the second Chapter of this thesis.

Another type of perturbation which is important in the present study is the interaction between B and C type of bands in prolate asymmetric rotors which is analysed in detail in the fifth Chapter.

1.4 Population Distribution Of Vibrational Levels

One of the more serious problems encountered in the analysis of vibrational absorption spectra are complications due to transitions from vibrationally excited states. The levels which are usually involved are the relatively highly populated low frequency out- of-plane bending modes. These bands are called 'hot bands' due to the fact that they are temperature dependent and can be reduced in intensity by cooling the sample. The relative intensities of the 'hot bands' with respect to the cold bands are functions of the relative populations of the energy levels. This occupation probability can be calculated from the Maxwell-Boltzmann equation:

$$\frac{N_i}{N} = \frac{g_i\, e^{-\varepsilon_i/kT}}{\sum_i g_i e^{-\varepsilon_i/kT}} \qquad (1.1)$$

where N_i / N is the relative population of energy level ε_i

g_i is the degeneracy of this particular energy level

N is the total population.

If one assumes harmonic oscillator functions, the denominator can be written as:

$$\sum_i g_i e^{-\varepsilon_i/kT} = \prod_\nu (\text{partition function})_\nu \qquad (1.2)$$

which is either $\left[1-e^{-h\omega c/kT} \right]^{-1}$ for non-degenerate a modes

or $\left[1-e^{-h\omega c/kT} \right]^{-2}$ for doubly degenerate e modes.

ω is the vibrational frequency in wavenumbers

and the product is taken over all the vibrational modes of the molecule. The individual partition functions for each vibrational mode together with the total product at various temperatures are listed in Table 1.1 for s-trifluorobenzene-h_3. The relative percentage populations of levels below 750 cm^{-1}, at room temperature, are listed in Table 1.2.

It can be seen that prominent hot bands will be observed for several levels, three of which have a population of at least 30% of ground state population.

Table 1.1

Partition Functions Of The Vibrational Modes Of s-Trifluorobenzene-h_3

Freq/cm^{-1}	Mode	Symmetry	g_i	p.f./ 293 K
207	ν_{17}	a_2''	1	1.568
246	ν_{20}	e''	2	2.037
324	ν_{14}	e'	2	1.577
502	ν_{13}	e'	2	1.194
~ 557	ν_7	a_2'	1	1.069
580	ν_4	a_1'	1	1.062
598	ν_{19}	e''	2	1.115
663	ν_{16}	a_2''	1	1.040
792	ν_{18}	e''	2	1.042
847	ν_{15}	a_2''	1	1.016
998	ν_{12}	e'	2	1.015
1012	ν_3	a_1'	1	1.007
1128	ν_{11}	e'	2	1.008
~ 1178	ν_6	a_2'	1	1.003
~ 1300	ν_5	a_2'	1	1.002
1363	ν_2	a_1'	1	1.001
1475	ν_{10}	e'	2	1.001
1629	ν_9	e'	2	1.001
3076	ν_1	a_1'	1	1.000
3113	ν_8	e'	2	1.001

$\prod_{\nu}(p.f.)_{\nu} = 8.705$

Table 1.2

Relative Populations Of Vibrational Energy Levels Below ~ 750 cm^{-1} For s-Trifluorobenzene-h_3

Level	Freq/cm^{-1}	Γ	g_i	% Population at 293 K
Ground	0	a_1'	1	11.49
ν_{20}	245.8	e''	2	6.88
ν_{14}	324.2	e'	2	4.68
ν_{17}	207.0	a_2''	1	4.16
$2\nu_{20}$	491.6	$(e'')^2$	3	3.09
$\nu_{14}+\nu_{20}$	569.9	$e'xe''$	4	2.80
$\nu_{17}+\nu_{20}$	452.8	$a_2''xe''$	2	2.50
ν_{13}	502.4	e'	2	1.95
$\nu_{14}+\nu_{17}$	531.2	$a_2''xe'$	2	1.69
$2\nu_{17}$	414.0	$(a_2'')^2$	1	1.51
$2\nu_{14}$	648.4	$(e')^2$	3	1.43
$3\nu_{20}$	737.0	$(e'')^3$	4	1.23
ν_{19}	598.0	e''	2	1.22

Chapter 2

Theory Of Vibration-Rotation Transitions For Symmetric Rotors

2.1 Rovibrational Term Values

The empirical rovibrational formulae which follow arise from the block diagonalisation of the Hamiltonian matrix, using perturbation theory. The Hamiltonian matrix is set up as a product of a rigid rotor contribution multiplied by a harmonic oscillator contribution. In the transformed Hamiltonian all the off-diagonal elements connecting different vibrational states are removed, leading to:

$$T(v,J) = G(v) + F_v(J) \qquad (2.1)$$

where G(v) is the vibration term value which can be expressed as follows:

$$\begin{aligned} G(v) &= G(v_s,\ldots,v_t,l_t\ldots) = \\ &= \sum_s \omega_s(v_s+1/2) + \sum_t \omega_t(v_t+1) + \sum_{s\geq s'} x_{ss'}(v_s+1/2)(v_{s'}+1/2) + \\ &+ \sum_{s,t} x_{st}(v_s+1/2)(v_t+1) + \sum_{t\geq t'} x_{tt'}(v_t+1)(v_{t'}+1) + \\ &+ \sum_{t\geq t'} g_{tt'}l_t l_{t'} \end{aligned} \qquad (2.2)$$

the rotation term value F_v for an oblate rotor is given as follows:

$$F_v(J) = B_vJ(J+1) + (C_v-B_v)K^2 - \sum_t 2(C\zeta^z_t)_v kl_t -$$
$$- (D_J)_vJ^2(J+1)^2 - (D_{JK})_v(J+1)JK^2 - (D_K)_vK^4 +$$
$$+ \{ \sum_t (\eta_{tj})_vJ(J+1)kl_t + \sum_t (\eta_{tk})_vk^3l_t\} \qquad (2.3)$$

v is the vibrational quantum number of a molecule

l is the vibrational quantum number of angular momentum

J is the rotational quantum number of angular momentum

k is the signed quantum number associated with the component of J directed along the z-axis

$K = |k|$

ω represents the vibration wavenumber

x,g represent the anharmonicity constants

D,η represent the centrifugal distortion constants

$$B_v = B_e - \sum_r \alpha^B_r(v_r+d_r/2) + \ldots \qquad (2.4)$$

$$C_v = C_e - \sum_r \alpha^C_r(v_r+d_r/2) + \ldots \qquad (2.5)$$

$$(C\zeta^z_t)_v = (C\zeta^z_t)_e - \sum_r \alpha^C_r\zeta^z_t(v_r+d_r/2) + \ldots \qquad (2.6)$$

d_r is the degeneracy of the rth normal mode
v is the subscript used to indicate vibrational dependance
s is the subscript used to denote a non-degenerate mode
t is the subscript used to denote a degenerate mode
and r is the subscript used to denote either a degenerate or a non-degenerate mode.

The third term in equation (2.3) is a consequence of the first

order Coriolis correction to the rotational energies for a degenerate vibrational state of a symmetric rotor. ζ_t^z is considered to be characteristic of a degenerate vibration as a measure of the degree of coupling along the symmetric rotor axis between the rotational and vibrational angular momentum components.

The quartic terms in angular momenta in equation (2.3) are expected to demonstrate a vibrational dependance, but this effect is often neglected[12].

The terms in η's in the third row of equation (2.3) are small and they have been neglected in this study.

As far as the theory of the zeta constants is concerned there are two classical papers. The first one by Boyd and Longuet-Higgins[13] is on the effect of Coriolis perturbation on the perpendicular IR bands of symmetric rotors.

The second paper, by Meal and Polo[14] is on the zeta sum rules which relate ζ's for degenerate pairs of vibrations.

In a paper by Oka[15] the coefficients of the quantum numbers have been classified according to their orders of magnitude, which is very useful in the interpretation of observed spectra.

Cartwright and Mills[11] have classified in orders of magnitude these coefficients in terms of the vibrational wavenumber ω and the parameter $\varkappa$:

$$\varkappa = (m_e/M_n)^{1/4} \approx 0.1$$

where m_e = electron mass

M_n = typical nuclear mass

These coefficients are listed in Table 2.1.

2.2 Selection Rules And (Effective) First Order Coriolis Constants

In Chapter 3, we shall be concerned with observed first order Coriolis constants for the fundamentals and effective first order Coriolis constants for the overtones and combinations. A brief discussion is given here sufficient for the understanding of the conventions used in the experimental part for s-trifluorobenzene-h_3.

In order to compare calculated Coriolis constants with those from computer simulations, one must be consistent with regards to classification of the following quantities:

α. Vibrational wavefunctions.

β. Normal Coordinates.

γ. Transition moment operators.

The rotational selection rules used in the band contour simulation programs were consistent with the simple diagramatic method developed by Mills[16]. In the following treatment it is assumed that:

α. The molecule is in its ground electronic state.

β. There is no change of the electronic state during the transitions.

The degenerate coordinates are represented as:

$$C_3(Q_{ta}+iQ_{tb}) = e^{(-i\theta)}\ (Q_{ta}+iQ_{tb}) \qquad (2.7)$$

where $\theta = 2\pi/n$ where n is the order of the principal axis of the molecule. Since for s-trifluorobenzene the principal axis is C_3 , n=3 in this case.
Q_{ta}, Q_{tb} are the normal coordinates.

The vibrational wavefunctions ~~of a~~ in the D_{3h} point group are characterised by the value of θ as follows:

$$C_3|v_r\rangle = e^{-i\theta} |v_r\rangle \qquad (2.8)$$

where $|v_r\rangle$ is a way of representing a rovibrational wavefunction.

If $\theta = 0$, $|v_r\rangle$ spans a non-degenerate species.

If $\theta = \pm (2\pi/n)$, where n=3 in this case, $|v_r(a)\rangle$ and $|v_r(b)\rangle$ span a degenerate species with $\theta = +(2\pi/3)$ and $-(2\pi/3)$ respectively.

θ is determined by the vibrational quantum numbers of the state as can be seen from the following relation:

$$\theta = \sum_j \theta_j = (2\pi/3) \sum_j l_j \text{ (modulo } 2\pi) \qquad (2.9)$$

The selection rules can be expressed as follows:

$$\langle v_r'' | \mu_x \pm i\mu_y | v_r' \rangle \neq 0 \qquad (2.10)$$

where the + sign applies when $\Delta K=-1$ and vice versa.

$$\langle v_r'' | \mu_z | v_r' \rangle \neq 0 \qquad (2.11)$$

when $\Delta K = 0$.

In the above expressions μ represents the electric dipole moment along a particular direction.

Following Herzberg's classification[17] of rovibrational levels we get:

$(+1)$ level $\Rightarrow |v_r(a)\rangle$; $k>0$

or $|v_r(b)\rangle$; $k<0$

(-1) level $\Rightarrow |v_r(b)\rangle$; $k>0$

or $|v_r(a)\rangle$; $k<0$

The energy difference between the two (a,b) states can be written as follows:

$$\pm 2Ck\zeta^z_{eff} \quad \text{for e(b)/e(a) states} \tag{2.12}$$

$$\pm 2CK\zeta^z_{eff} \quad \text{for (-1)/(+1) states} \tag{2.13}$$

$$\text{where } \zeta^z_{eff} = \sum_j l_j(a)\zeta_j = -\sum_j l_j(b)\zeta_j \tag{2.14}$$

According to the above notation, when $\zeta^z_{eff} > 0$ the (-1) energy level is of higher energy than the $(+1)$ one.

After taking the sum of the θ values for the 3 factors in (2.10) and (2.11) integrals to be 0, the $(\pm 1)\Leftrightarrow(\pm 1)$ selection rules may be obtained. Therefore, the operators transform under C_3 as follows:

$(\mu_x \pm \mu_y)$ with $\theta = \pm(2\pi/3)$

μ_z with $\theta = \emptyset$

and the rovibrational wavefunctions transform as follows:

$|v_r'\rangle$ with $\theta = +\theta$

$|v_r''\rangle$ with $\theta = -\theta$

Thus,

$\Delta K = K'-K'' = \pm 1$, $\Delta\theta = \theta'-\theta'' = \pm(2\pi/3)$

$\Delta K = \emptyset$, $\Delta\theta = \emptyset$

A summary of the selection rules for the D_{3h} symmetry species can be found in Table 2.2.

To calculate a value for ζ^z_{eff} for a given vibrational state, it is necessary to take the following steps:

α. Determine which set of quantum numbers l_j is associated with $|v_r(a)\rangle$ and $|v_r(b)\rangle$ from equation (2.9)

β. Use equation (2.14) to calculate ζ^z_{eff}.

2.3 l-Resonance Perturbations

l-resonance perturbations are seen in some of the bands of s-trifluorobenzene-h_3. A brief discussion of the theory behind such perturbations is given here.

l-resonance perturbations are considered to be the most important of the resonances which are off-diagonal only in the rotational quantum numbers. l-resonance refers to the coupling of symmetric rotor rotational levels by means of the following matrix elements:

$$\langle v_t, l_t; J, k\pm1 | H | v_t, l_{t-1}; J, k\mp1\rangle =$$

$$= (\rho/4) q_t^{(\pm)} [(v_t+1)^2 - l_t^2]^{1/2} \cdot$$

$$\cdot [\{J(J+1)-k(k+1)\}\{J(J+1)-k(k-1)\}]^{1/2} \qquad (2.15)$$

$$\langle v_t, l_t; J, k | H | v_t, l_t \mp 2; J, k\pm1\rangle =$$

$$= \rho r_t [(v_t+1)^2 - (l_t+1)^2]^{1/2} \cdot$$

$$\cdot [J(J+1)-k(k+1)]^{1/2} (2k\pm1) \qquad (2.16)$$

where $q_t^{(+)}$, $q_t^{(-)}$, r_t are the l-doubling constants for the degenerate vibrational state and are associated with the off-diagonal elements connecting ($\Delta l_t = \pm2, \Delta k = \pm2$), ($\Delta l_t = \pm2, \Delta k = \mp2$) and ($\Delta l_t = \pm2, \Delta k = \mp1$) respectively, and $\rho = \pm1$.

There are symmetry restrictions on the species of the degenerate vibrations (Q_{t1},Q_{t2}) for which each type of interaction can occur.

$q_t^{(+)}$ interactions occur for all E_1(or E) species vibrations in all symmetric rotor point groups. In the v_t=1 fundamental levels of such vibrations the matrix elements due to $q_t^{(+)}$ give rise to a doubling of the $k=l_t=\pm 1$ pair of levels. This is the familiar l-type doubling effect and $q_t^{(+)}$ is the familiar l-doubling constant.

Another important point of discussion refers to the choice of the signs of l-doubling constants. Due to the fact that the sign of the $q_t^{(+)}$ l-doubling constants is an observable quantity, a convention devised by Cartwright and Mills[11] has been used to relate the experimental observations to the theoretical expressions for the l-doubling constants in terms of the rovibrational interaction parameters and the anharmonic force constants.

Following the Cartwright and Mills[11] phase convention together with the sign convention for the l-doubling constant $q_t^{(+)}$ it can be shown that ρ=-1 for $q_t^{(+)}$ for all IR active species of all symmetric rotor point groups. The detailed expression of the $q_t^{(+)}$ constant for all symmetric rotor molecules was derived by Oka[15] and Grenier-Besson[18].

The first two terms of the expression for $q_t^{(+)}$ which arise from second order XY plane Coriolis interactions contain a resonance denominator. Hence, the perturbation treatment upon which that expression is given may fail in the case of such strong interactions.

Besides the l-doubling effect due to $q_t^{(+)}$ type interactions in the $k=l_t=\pm 1$ levels, it is also possible to have an accidental resonance due to $q_t^{(+)}$. This depends on the values that the rotational constants have, such

that the interacting levels happen to be nearly degenerate. The condition for accidental l-type resonance in an oblate rotor with $C \approx (1/2)B$ is $\zeta_t \approx -1$.

For the case when the degenerate normal coordinates (Q_{t1}, Q_{t2}) are IR active the resonance will be largest for high J and low K values. From that it follows that the biggest perturbation will occur for the high J lines in the central sub-bands.

The effect of $q_t^{(+)}$ resonance can be calculated by diagonalising a typical (2x2) block of the Hamiltonian matrix involving two levels coupled by l-resonance in the following form:

$$\begin{array}{c} \\ |\psi_1\rangle \\ |\psi_2\rangle \end{array} \begin{array}{c} \begin{array}{cc} |\psi_1\rangle & |\psi_2\rangle \end{array} \\ \begin{bmatrix} H_{11} & H_{12} \\ H_{12} & H_{22} \end{bmatrix} \end{array}$$

This can be done as follows:

$$\begin{bmatrix} a & \sigma b \\ -\sigma b & a \end{bmatrix} \cdot \begin{bmatrix} H_{11} & H_{12} \\ H_{12} & H_{22} \end{bmatrix} \cdot \begin{bmatrix} a & -\sigma b \\ \sigma b & a \end{bmatrix}$$

$$= \begin{bmatrix} E^+ & \emptyset \\ \emptyset & E^- \end{bmatrix}$$

$$\therefore E^{\pm} = (1/2)(H_{11}+H_{22}) \pm (1/2)\Delta \qquad (2.17)$$

where $\Delta = [\delta^2 + 4H_{12}^2]^{1/2}$

H_{12} is defined by expression (2.15)

$\delta = H_{11}-H_{22}$

δ for the $q_t^{(+)}$ interaction can be given as follows:

$|1\rangle = |l_t=+1, k+1\rangle$, $|2\rangle = |l_t=-1, k-1\rangle$:

$$H_{11}-H_{22} = B[J(J+1)-(k+1)^2] + C(k+1)^2 -$$

$$- 2(C\zeta)(k+1)-B[J(J+1)-(k-1)^2] -$$

$$- C(k-1)^2- 2(C\zeta)(k-1)$$

$$= 4k[C-(C\zeta)-B] \qquad (2.18)$$

The above expression does not include the centrifugal distortion terms in equation (2.3).

Assuming H_{12} is real it follows that:

$E^+ \geq E^-$

The eigenvectors are given by the following expressions:

$a = [(\Delta+\delta)/2\Delta]^{1/2}$ and $b = [(\Delta-\delta)/2\Delta]^{1/2}$

Assuming that the square root $> 0 \Rightarrow a,b > 0$.

$\therefore$ $a>b$ when $\delta>0$ and $a<b$ when $\delta<0$

Also, $\sigma=+1$ when $H_{12}>0$ and $\sigma=-1$ when $H_{12}<0$.

By using the explicit equations for the eigenvalues

of a (2x2) matrix given above we can obtain explicit formulae for the perturbed line positions.

The two interacting basis functions in the excited vibrational state are denoted by (J′,K+1,+1) and (J′,K-1,-1). The eigenfunctions resulting from the interaction are denoted by (J′,K+) and (J′,K-), where K+ denotes the upper and K- the lower of the resulting eigenstates. Transitions to these states obey the usual selection rules i.e. from a (J,K) level of the ground state according to $\Delta J = J'-J = -1,0,1$ for a P,Q or R branch line respectively.

The wavenumbers of the lines resulting from the perturbation are given by the following formula:

$$\nu\{(v_t=1,J',K\pm) - (v_t=0,J,K)\} =$$

$$= \nu_o + B'J'(J'+1) - B''J(J+1) + C'-2(C\zeta_t)'-B' +$$

$$+ [(C'-C'')-(B'-B'')]K^2 \pm 2K\{[C'-(C\zeta_t)'-B']^2 +$$

$$+(q_t^{(+)}/4K)^2 [J'(J'+1) - K(K+1)].[J'(J'+1) - K(K-1)]\}^{1/2} \quad (2.19)$$

This formula simplifies to the usual one when $q_t^{(+)} = 0$. The l-resonance perturbations are accompanied by intensity perturbations. A discussion of the treatment of such perturbations is given by Cartwright and Mills[11] and is not repeated here.

The effect of $q_t^{(+)}$ l-resonance perturbations on P,Q and R lines is represented diagramatically in Figure 2.1.

2.4 Computer Simulation Of Band Contours

As it was indicated in the introduction, the aim of the band contour calculations is to identify the major influences which are thought to contribute to the observed spectrum. So this method can be used to assist assignments of the individual lines and hence help with the determination of the main spectroscopic constants which influence the structure of a particular band.

In most cases the energies of the combining states and intensities of the lines can be satisfactory calculated using:

α. The appropriate analytical expressions for the energies.

β. The electric dipole selection rules which control these transitions.

The general procedure can be summarised as follows:

α. Input of data

β. Calculation of line frequencies and intensities

γ. Formation of basic intensity distribution

δ. Processing of intensity distribution for output of synthetic spectrum.

A more detailed discussion of these four steps follows.

First step : The program which was used in the majority of the calculations in this thesis is a modified version of

the PLLBAND program first described by Barnard[19]. The PLLBAND program calculates and plots parallel and perpendicular band spectra for a symmetric rotor molecule. The selection rules are calculated using the method of Mills[16]. The general description of the PLLBAND program is given in Appendix 3.

Second step: α. Parallel Bands: The selection rules for parallel bands are:

$K \neq 0$; $\Delta J = 0, \pm 1$, $\Delta K = 0$

$K = 0$; $\Delta J = \pm 1$, $\Delta K = 0$

The parallel band contours were computed from combinations between energy levels given in standard text books[17].

β. Perpendicular Bands: The selection rules for the perpendicular bands are:

$\Delta J = 0, \pm 1$

$\Delta K = \pm 1$

The formulae for the calculation of the frequencies for the Q-branches, neglecting the effects of centrifugal distortion are again given in standard textbooks[20].

γ. 1-Resonance Perturbations:

The modified subroutine PEBAND, part of the PLLBAND program is given in Appendix 1. The theory behind this kind of perturbation is discussed earlier in this Chapter. The procedure which was adopted may be summarised

as follows:

For the l resonance perturbation we have[11]:

$$\pm 2K\{[C' - (C\zeta)' - B']^2 + (q^{(+)}/4K)^2[J'(J'+1) -$$

$$-K(K+1)].[J'(J'+1) - K(K-1)]\}^{1/2}$$

If we put $a = C' - (C\zeta)' - B'$

$b = q^{(+)}/4K$

$c = [J'(J'+1) - K(K+1)].[J'(J'+1) - K(K-1)]$

the above expression transforms as follows:

$$\pm 2K\{a^2+b^2c\}^{1/2} = \pm 2Ka/a\{a^2+b^2c\}^{1/2} =$$

$$\pm 2Ka\{(a^2+b^2c)/a^2\}^{1/2} = \pm 2Ka\{\ 1 + (b^2/a^2)c\ \}^{1/2}$$

If we put $x = (b^2/a^2)c$, we have

$$\pm 2Ka\{\ 1 + x\ \}^{1/2} \approx 2Ka\{\ 1 + x/2 - x^2/8 + \ldots\}$$

provided x is small.

∴ We end up with the following expression:

$$\pm 2Ka \pm Kax \mp Kax^2/4....$$

where the first part of the expression is the unperturbed expression.

If

$(C'-(C\zeta)'-B') > 0$

$\Delta K = +1$; r-type transition
positive sign

$\Delta K = -1$; p-type transition
negative sign

if

$(C'-(C\zeta)'-B') < 0$

$\Delta K = +1$; r-type transition
negative sign

$\Delta K = -1$; p-type transition
positive sign.

$\therefore$ The perturbation term = $\pm Kax(1-x/4...)$

Assuming $(C'-(C\zeta)'-B') < 0$ we have

$$\{\pm K[q^{(+)}/4K)^2/\ [(C'-B')-(C\zeta)']\}[J(J-1) -$$

$$- K(K+1)][J(J-1)-K(K-1)][1-\{(q^{(+)}/4K)^2/4[C'-B'-(C\zeta)']^2\}$$

$$[J(J-1) - K(K+1)][J(J-1) - K(K-1)]]$$

where the positive sign refers to a p-branch while the negative one refers to an r-branch.

Third Step: The intensities of the rovibrational transitions are calculated using the Hönl-London formulae[17]:

$$I_{JK} = C\nu A_{JK} g_{JK} e^{-F''(J,K) / kT}$$

where C is a constant

ν is the frequency of the transition

g_{JK} is the statistical weight of the lower state:

$g_{Jk} = (2J+1)g_N$ for $K = \emptyset$

$g_{JK} = 2(2J+1)g_N$ for $K \neq \emptyset$

where g_N is the nuclear spin statistical weight

$e^{-F''(J,K) / kT}$ is the Boltzmann factor

and A_{JK} is the line strength factor. The A_{JK} factors are given in standard textbooks[17].

The constant C in the Hönl-London formula is set in the computer program when the computed contour is normalised with respect to the most intense feature in the spectrum.

Fourth Step: The processing of the intensity distribution for the output of the synthetic spectrum can be divided into the following number of steps:

α. The individual lines are broadened using a chosen lineshape function (Lorenzian in our case). The choice is important in high resolution work[11].

β. The intensities of the individual lines are partitioned about the line frequency among a number of frequency elements of an array.

γ. The total intensity of each element of the array is summed and stored in an array for further processing.

δ. The frequency interval for the raw intensity contour is usualy chosen to be about an order of magnitude lower than the desired convoluted linewidth.

ε. The raw intensity array can then be prepared for plotting on one of a number of hardware devices. For plotting purposes the intensities are normalised to the most intense line in the spectrum. Then, they are scaled so that the final output at the digital plotter represents frequency versus linear or logarithmic scale in intensity.

Table 2.1

Terms In Rovibrational Hamiltonian Classified By Order Of Magnitude

	Constant	Magnitude
ω	vibration wavenumbers	ω
$x_{rr'}$, $g_{tt'}$	anharmonicity constants	$\varkappa^2\omega$
$B_v, C_v, (C\zeta^z_t)_v$	rotational constants	$\varkappa^2\omega$
$\alpha^B, \alpha^C, \alpha^{(C\zeta^z_t)}$	vibrational dependance of rotational constants	$\varkappa^4\omega$
$q_t^{(+)}$	l-doubling constants	$\varkappa^4\omega$
D_J, D_{JK}, D_K η_{tj}, η_{tk}	centrifugal distortion constants	$\varkappa^6\omega$

Note: $\varkappa \approx 0.1$ and ω = typical vibration wavenumber

Table 2.2

Selection Rules For Rovibrational Transitions For The D_{3h} Point Group

Transition Γ		Selection Rules ΔK = K′-K′′		
Upper State	Lower State	+1(⊥)	-1(⊥)	Ø(∥)
E	$A_{1,2}$	(+1)⇔(Ø)	(-1)⇔(Ø)	
$A_{1,2}$	E	(Ø)⇔(-1)	(Ø)⇔(+1)	
E	E	(-1)⇔(+1)	(+1)⇔(-1)	(+1)⇔(+1) (-1)⇔(-1)

Note: The requirement (′′)⇔(′) on ΔK = Ø transitions and (′′)⇔(′′) or (′)⇔(′) for ΔK = ±1 transitions is assumed for the D_{3h} point group.

Figure 2.1

The Effect Of $q^{(+)}$ l-resonance On P,Q, And R-Branch Lines

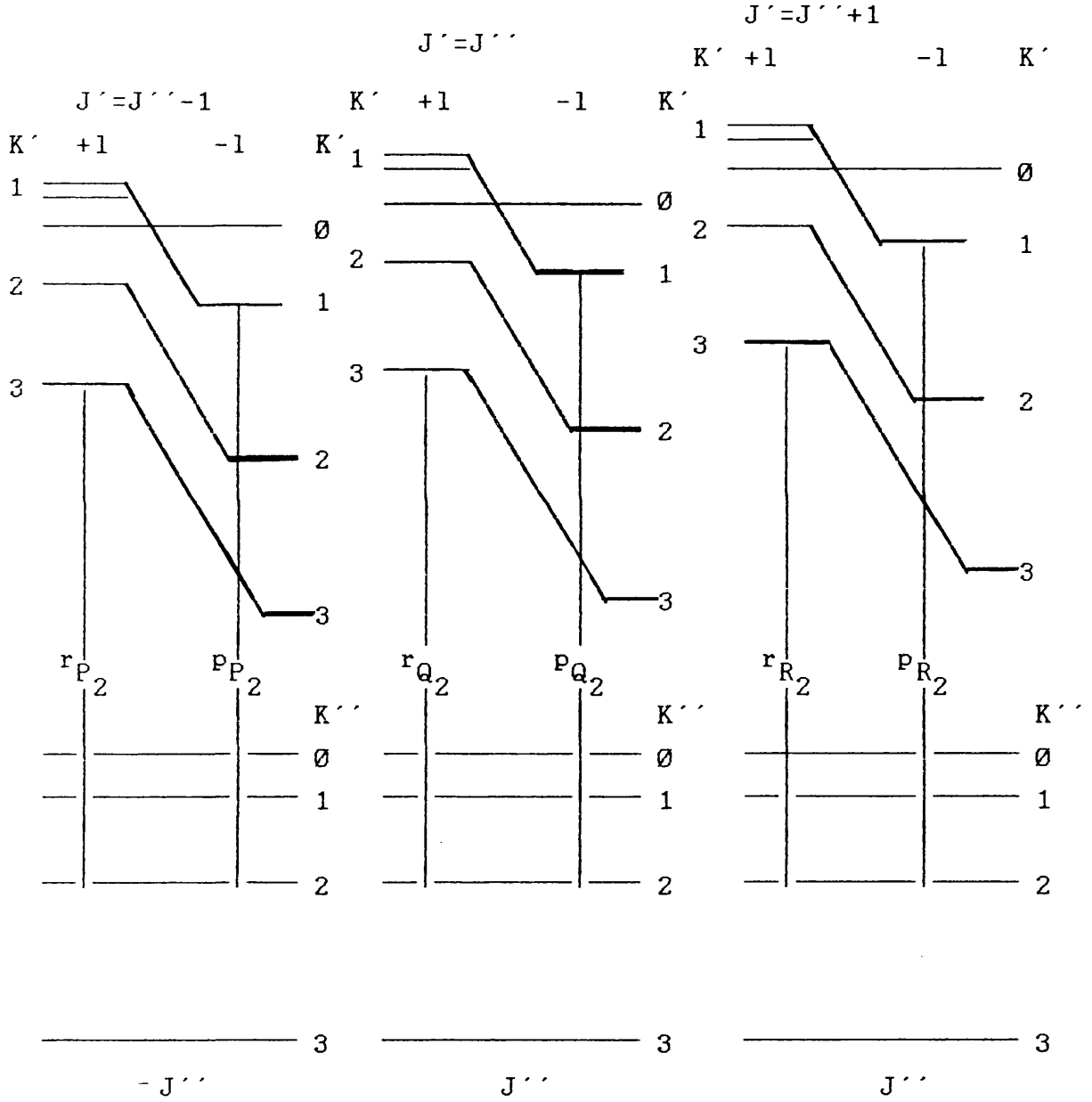

Notation: $^{\Delta K}\Delta J_{K''}$ where $\Delta K = K'-K''$; $\Delta J = J'-J''$.

Chapter 3

Investigation Of The Mid-IR Spectrum Of s-Trifluorobenzene-h_3 Using FTIR Spectroscopy

3.1 The Infrared Spectroscopy Of s-Trifluorobenzene

The 3Ø normal vibrations of s-trifluorobenzene are distributed among the irreducible representations of D_{3h} as follows:

$$\Gamma(Q_v) = 4a_1' + 3a_2' + 7e' + 3a_2'' + 3e''$$

The $a_1'(\nu_1-\nu_4)$, $e''(\nu_{18}-\nu_{2Ø})$ modes are Raman active, the $a_2''(\nu_{15}-\nu_{17})$ modes are infrared active, the $e'(\nu_8-\nu_{14})$ modes are both Raman and infrared active and finally the a_2' modes are inactive according to the dipole selection rules. Furthermore, the planar vibrations of s-trifluorobenzene are of symmetry species a_1', a_2' and e' while its out-of-plane vibrations are of symmetry species a_2'' and e''.

Throughout this report the numbering of normal modes follows Herzberg's[17] recommendation which is consistent with that adopted in previous vibrational studies.

There have been a number of experimental and theoretical studies relating to s-trifluorobenzene since the early infrared and Raman study of Nielsen, Liang and Smith[21], in 195Ø. In their work, the infrared spectrum of s-trifluorobenzene in the gaseous and liquid states together with its Raman spectrum in the liquid state was investigated.

In 1953, a normal coordinate analysis of the out-of-plane vibations of s-trifluorobenzene was carried out by Ferguson[22]. His study furnished support for Nielsen et al's tentative assignment of the lowest a_2'' fundamental but concluded that the value of the e'' fundamental was too high.

In 1962, a Modified Urey-Bradley force field calculation was performed by Scherer, Evans and Muelder[23]. Their report also included a valence force field calculation for the out-of-plane vibrations.

In 1973, Schlupf and Weber[24] performed the first high resolution rotational Raman study of the molecule, using a single mode Ar laser. Their experiment led to the determination of the B_o'' rotational constant and the D_J'' centrifugal distortion constant.

In the same year, Eaton and Steele[25] presented a study of the planar vibrations of benzene and fluorobenzenes including s-trifluorobenzene. In their study, 36 and 39 parameter force fields were used. Two years later, the same two researchers[25] tried to investigate the effect that the removal of the Kekule' assumption would have on the force field.

In 1976, Eaton, Pearce, Steele and Tindle[26] recorded the low frequency absorption spectrum between 400 and 50 cm^{-1}.

Three years later, the gas phase contours of the infrared active fundamentals and some overtones and combination bands were recorded at about 0.5 cm^{-1} resolution by Shurvell et al[27]. Their experiment led to the determination of first order Coriolis constants for the e' fundamentals together with 'effective' Coriolis constants of some overtones and combination bands of the same symmetry species.

Finally, in 1981 Korppi-Tommola et al[28], recorded the gas phase Raman band contours of s-trifluorobenzene-h_3 and the infrared and Raman band contours of its fully deuterated isotope at about 0.5 cm^{-1} resolution. They also did computer simulation of the band contours of the e' modes to determine the first order Coriolis coupling constants for both isotopes.

In an attempt to upgrade the various data for s-trifluorobenzene, we have re-recorded the mid-infrared spectrum between 550-3500 at a resolution of about 0.06 cm^{-1} using the Bruker IFS113 Fourier Transform spectrometer with

the MCT detector cooled down to 77K. Commercially available s-trifluorobenzene-h_3 was used without further purification. Path lengths of 10 cm and 4 m were used. The survey spectra at a resolution of about 0.5 cm^{-1} with a sample pressure of ca 10 Torr are shown in Figures 3.1 and 3.2. They were recorded without use of computer subtraction of CO_2 and H_2O absorptions. The fundamental wavenumbers obtained from the literature[27,28] and the present investigation are collected in Table 3.1.

3.2 The Parallel Bands Of s-Trifluorobenzene-h_3

3.2.1 The $\nu_{15}(a_2'')$ Parallel Fundamental Band

The $\nu_{15}(a_2'')$ parallel fundamental was re-recorded at a resolution of ca. 0.06 cm^{-1} using the Blackmann-Harris 3-term apodization function instead of Sellors[12] trapezoidal one. The apodization function which was used here is described in Chapter 1 and it gives an improved line shape at the expense of a slight decrease in the resolution. Also, we have completed a computer simulation of the partially resolved rotational structure.

ν_{15} is a very strong band which was recorded using a 10 cm cell fitted with KBr windows. The pressure of the sample was ca. 2 Torr. In the absence of any strong Fermi or Coriolis resonances this a_2'' mode was expected to give rise to a parallel band with a relatively simple rotational structure.

The computer simulation was carried out as described in Section 2.4 using the closed term expressions for an oblate symmetric rotor molecule and the appropriate selection rules for a parallel band. Assuming that the distortion

constants are the same in both states, the P and R branches are expected to have a coarse J structure determined primarily by the constants $\overline{\nu}_0$, B′′, α_s^B= B′′-B′ and D_J. When J manifolds are observed at high resolution they would have a fine K structure determined mainly by α_s^C= C′′-C′, α_s^B and D_{JK} . The assumption that for a planar oblate symmetric rotor C = B/2 was found to be sufficient. Finally, the following relations were assumed to exist between the centrifugal distortion constants of a planar symmetric rotor molecule:

$$2D_J + 3D_{JK} + 4D_K = \emptyset \qquad (3.1)$$

$$D_{JK} = 2D_J\{(C_e/B_e)^4 - 1\} \approx -1.875\ D_J \qquad (3.2)$$

The first relation was originally derived by Dowling[30] while the second approximate one is due to Aliev, Subbotin and Tyulin[31]. A more detailed analysis of these two relationships is given in Chapter 4 where the harmonic force field calculations are discussed.

The region of the observed ν_{15} band from 835.5 to 861.42 cm^{-1} with the band centre at 848.13 $cm^{-1}$is shown in compressed form in Figure 3.4. From that Figure it can be seen that the observed structure is complicated by the presence of at least another strong band and several other medium to weak bands. After considering the relative populations of the vibrational levels at room temperature, it seems that there are at least three relative intense 'hot bands' involving low frequency fundamentals. These are the following:

	Γ	Type Of Vibration	% Total Population
Ground	a_1'		11.49
ν_{17}	a_2''	out-of-plane	4.16
ν_{14}	e′	planar	4.68
$\nu_{2\emptyset}$	e′′	out-of-plane	6.88

Therefore, the primary candidate for the assignment of the second strongest peak at 847.6Ø cm^{-1} seems to be a 'sequence band' of the type ($\nu_{15}+\nu_{2Ø}-\nu_{2Ø}$). Another relatively strong peak at 847.1Ø cm^{-1} could be due either to ($\nu_{15}+\nu_{17}-\nu_{17}$) or ($\nu_{15}+\nu_{14}-\nu_{14}$).

The analysis of the main band can be divided into the following steps:

α. Initially, a series of computations was performed to determine the K value of the J lines. It was found that the various ^{q}P and ^{q}R peaks coincide with low K transitions (i.e. K ≈ Ø). An example of such a calculation is given in Figure 3.3.

β. The observed J structure was fitted into a polynomial of the following form:

$$\bar{\nu}_m \; P,R = a + bm + cm^2 + dm^3 + \ldots \qquad (3.4)$$

where: m = -J for a P-branch, m = J+1 for an R-branch

$$a = \bar{\nu}_o + [(C'-B')-(C''-B'')]K^2 =$$

$$= \bar{\nu}_o + (\alpha_s^B - \alpha_s^C)K^2 \qquad (3.5)$$

$$b = (B' + B'') - 2D_{JK}K^2 \qquad (3.6)$$

$$c = B' - B'' = -\alpha_s^B \qquad (3.7)$$

$$d = -4D_J \qquad (3.8)$$

Assuming K ≈ Ø we have:

$$a = \bar{\nu}_o$$

$b = B' + B''$

$c = -\alpha_s^B$

$d = -4D_J$

So from the above relations values for $\bar{\nu}_o$, B'', α_{15}^B and D_J were derived.

γ. The values derived from the previous step were used for a computer simulation of the observed band using the PLLBAND program.

The standard deviation in the residuals $\{\nu_{(obs)}-\nu_{(calc)}\}$ was σ = Ø.ØØ3 which is consistent with the estimated uncertainty in the peak positions. The value for B'' differs slightly from the ones quoted by Schlupf[24] and Sellors[12]. The discrepancy with the value obtained by the rotational Raman analysis[24] is expected due to the effects of 'hot bands' which are different in each case. The problem tends to become more important towards the bottom of Table 3.2 which lists the observed and calculated peak positions. At the relatively high temperatures at which the rotational Raman spectra are photographed, there are several low lying vibrational states which are appreciably populated. So it is likely that the analysis of the spectrum yields a value for B'' which is not quite equal to the true value of B'' but a weighted average of B over these vibrational states.

The peak assignments, together with the differences between observed and calculated peak wavenumbers are listed in Table 3.2. The parameters which were used in the computer simulation of the band are listed in Table 3.3. The observed and calculated band contours are given in Figure 3.4.

3.2.2 The $\nu_{16}(a_2'')$ Parallel Fundamental Band

The $\nu_{16}(a_2'')$ band was investigated at a resolution of ca. Ø.Ø6 cm^{-1} using the same apodization function as in the case of the $\nu_{15}(a_2'')$ band. The experimental conditions were the same as in the case of the $\nu_{15}(a_2'')$ band.

The region of the observed ν_{16} band from 65Ø.Ø to 68Ø.Ø cm^{-1} is shown in a compressed form in Figure 3.5. From that Figure, it can be seen that there are several quite strong peaks in the central region. As in the case of the ν_{15} band, the most intense of them was assumed to be the ^{q}Q branch of the ν_{16} band at ca. 664.7cm^{-1}. The second most intense peak was at ca. 664.4 cm^{-1}. Once again the primary candidate for the second strongest peak would seem to be a 'sequence band' of the type $(\nu_{16}+\nu_{2Ø}-\nu_{2Ø})$. Also, another two slightly weaker peaks were present at ca. 664.5 cm^{-1} and ca. 664.Ø cm^{-1}. These are probably due to the 'sequence bands' $(\nu_{16}+\nu_{17}-\nu_{17})$ and $(\nu_{16}+\nu_{14}-\nu_{14})$ respectively.

For the main band, a similar type of analysis was carried out as in the case of the ν_{15} band which led to a simulated spectrum which reproduced the partially resolved rotational structure satisfactorily. The effects of 'hot bands' in the central region of the band were not taken into account in the simulation of the band.

A regular J structure in the P and R branch can be seen more clearly in some places than in others. The central Q sructure was once again completely unresolved. The J and ΔJ values may be assigned to about 1ØØ P and R branch peaks of the main band though at not such a high accuracy as in the ν_{15} band. As in the case of the ν_{15} band, it was assumed that the ^{q}P and ^{q}R peaks coincide with low K transitions (i.e. $K\approx Ø$).

The standard deviation in the residuals $\{\nu_{(obs)}-\nu_{(calc)}\}$

is σ = Ø.Ø1 which is well outside the expected uncertainty in the peak positions of ca. Ø.ØØ6 cm^{-1} (for a resolution of Ø.Ø6 cm^{-1}). So it is expected that the value of B'' rotational constant will not be so accurate. In fact, it was found to be Ø.Ø57Ø33 cm^{-1} compared with a value of Ø.Ø58742 cm^{-1} from the analysis of the ν_{15} band. This is due to the two following reasons:

α. A decrease in the signal to noise ratio in this particular region gives rise to a relatively noisy spectrum. This leads to a higher uncertainty in the observed line positions.

β. The usual presence of several peaks due to 'hot bands' which leads to a perturbation in the positions of the individual peaks in the P and R branches. This effect is difficult to be measured due to the fact that the individual peaks are not so well resolved.

The line positions are, therefore, quoted to three decimal places instead of four decimal places as in the ν_{15} band.

In the simulation of the band the values for $\bar{\nu}_o$, B'' and α^B_{16} were taken from the least squares analysis. The usual relationship between the rotational constants of a planar oblate molecule were assumed to hold. The distortion constants were transferred from the analysis of the ν_{15} band.

The observed and calculated lines for the $\nu_{16}(a_2'')$ fundamental band are given in Table 3.4. The derived constants for the same band are given in Table 3.5. The observed and calculated band contours are given in Figure 3.5

3.3 The Perpendicular Bands of s-Trifluorobenzene-h_3.

Shurvell et al[27] estimated the Coriolis constants for the perpendicular bands of s-trifluorobenzene-h_3 for the first time. One of the methods used in their analysis of partially resolved bands is the so-called 'P-R-separation' method by Hoskins[32]. This method can be used only to obtain approximate values of Coriolis constants for symmetric rotor molecules according to the following formula:

$$\Delta\nu_{PR} = 4.0(AkT/hc)^{1/2}(1-\zeta_t^z) \qquad (3.9)$$

where $\Delta\nu_{PR}$ indicates the separation between the P and R branches in a band,
ζ_t^z is the first order Coriolis coupling constant,
A is the rotational constant and the rest of the parameters have their usual meaning.

The problem with this method is that relatively small errors in the determination of P-R maxima separations can lead to large errors in the Coriolis constants, particularly when P-R maxima become less well defined as $\zeta_t^z \Rightarrow \mp 1.0$. Such values of ζ_t^z for planar oblate symmetric rotor molecules cause the subband origins to give rise to a 'pseudo-parallel' band appearance in the overall band profile with sharp coalesced Q branch structures which are usually distorted by 'hot bands'. This could lead to errors in ζ_t^z values of between ±0.05 to ±0.20.

Another method which is considered to be more accurate is to match the observed and calculated spectra. This method was employed by Shurvell et al[27] but they did not take into account the following effects which contribute

to the overall band profile:

α. Overlap of combination or overtone bands.

β. Hot bands of the type $(\nu_s+\nu_t)-\nu_t$ discussed in the analysis of the parallel fundamental bands.

γ. Differences in rotational constants between the ground and excited states.

δ. l-resonance perturbations.

In this study, the second method of analysis was used taking into account the factors γ and δ.

It was found that at the resolution used, l-resonance effects were observable in a number of perpendicular fundamental bands.

3.3.1 The $\nu_{12}(e')$ Perpendicular Fundamental Band

The $\nu_{12}(e')$ band extends from about 977 cm^{-1} to about 1014 cm^{-1} with the band centre at 996.25 cm^{-1} and can be seen in Figure 3.6. The band exhibits a PQR structure with an obvious l-resonance perturbation affecting the central Q branch.

In the computer simulation of the $\nu_{12}(e')$ band, the ground state rotational and centrifugal distortion constants taken from the least squares analysis of the $\nu_{15}(a_2'')$ parallel fundamental band, were used. Once again, it was assumed that the vibrational dependance of the centrifugal distortion constants could be neglected and the usual

relationship C=B/2 applied for the planar e´ vibrations. The synthetic spectrum was calculated using the PLLBAND program. Maximum values of J and K were taken as 17Ø with synthetic spectral line widths usually at slightly lower than the observed experimental resolution.

In preliminary calculations the l-resonance ($q_t^{(+)}$) parameter was not included. It was found that the best fit was achieved when α_{12}^B = Ø.ØØØØ62 cm^{-1} and ζ_{12}^z = -Ø.35. The value quoted by Shurvell et al[29] for ζ_{12}^z is -Ø.47.

After optimising these two parameters, the $q_{12}^{(+)}$ was allowed to vary. It was found that the best fit was achieved with $q_{12}^{(+)}$ = +Ø.ØØØ12 cm^{-1}.

The best fit parameters for the ν_{12}(e´) perpendicular band are listed in Table 3.6. The observed and calculated spectra ,in compressed form, are given in Figure 3.6.

3.3.2 The ν_{11}(e´) Perpendicular Fundamental Band

The ν_{11}(e´) band extends from about 1112 cm^{-1} to 1142 cm^{-1} with the band centre at 1127.6Ø cm^{-1}, as can be seen in Figure 3.7. The band exhibits a PQR srtucture. A weak l-resonance effect was observed perturbing the central Q branch of the band.

The band was investigated using the method of matching observed with calculated spectra. In the simulation of the observed band the maximum J and K values were taken as 15Ø. Once again the ground state rotational constants and centrifugal distortion constants were taken from the analysis of the $\nu_{15}(a_2'')$ parallel fundamental band. The same assumptions as in the ν_{12}(e´) case were applied.

In the initial calculations the l-resonance $q_t^{(+)}$ parameter was not included. After several trial and error attempts, it was found that the best fit was achieved with α_{11}^B = 0.000062 cm^{-1} and ζ_{11}^z = 0.05. The value obtained by the present study for the Coriolis constant is the same as the one quoted by Shurvell et al[27].

After optimising these two parameters, the $q_{11}^{(+)}$ l-resonance parameter was allowed to vary. It was found that the best fit was achieved with $q_{11}^{(+)}$ = +0.00013 cm^{-1}.

The best fit parameters for the $\nu_{11}(e')$ perpendicular band are listed in Table 3.7. The observed and calculated spectra, in compressed form, are given in Figure 3.7.

3.3.3 The $\nu_{10}(e')$ Perpendicular Fundamental Band

The $\nu_{10}(e')$ band extends from about 1460 cm^{-1} to 1490 cm^{-1} with the band centre at 1475.40 cm^{-1} as can be seen in Figure 3.8. The $\nu_{10}(e')$ band exhibits a PQR structure. The central region has a somewhat unusual feature in the form of a dip at ca. 1476 cm^{-1}. Although l-resonance perturbation was taken into account in the simulation of the band, this particular feature could not be reproduced completely satisfactorily. Another relatively minor problem was due to the presence of trace H_2O lines which obscured parts of the spectrum but not enough to affect the general shape of the band.

In the computer simulation of the observed band, the maximum J and K values were taken as 170. The usual assumptions were made as in the $\nu_{12}(e')$ case.

It was found that the best fit was achieved with α_{10}^B = 0.000132 cm^{-1}, ζ_{10}^z = -0.40 and $q_{10}^{(+)}$ = +0.00020 cm^{-1}.

The value quoted by Shurvell et al[27] for the Coriolis constant is -Ø.55.

The best fit parameters are given in Table 3.8 and the observed and calculated spectra are given, in compressed form, in Figure 3.8.

3.3.4 The $\nu_9(e')$ Perpendicular Fundamental Band.

The $\nu_9(e')$ fundamental band extends from about 1623 cm^{-1} to about 1648 cm^{-1} with the band centre at 1629 cm^{-1}, as can be seen in Figure 3.9. The spectrum in this region is complicated due to the presence of another combination band. This combination band has been found to affect the low wavenumber part of the band which exhibits a slightly distorted PQR structure. Another problem is that the central region has been found to be slightly complicated by the presence of some trace H_2O lines. However, it is obvious that the central peak of the band exhibits an l-resonance perturbation.

The exact position of the band centre can not be measured very accurately due to Fermi resonance between the ν_9 band and the combination band. (Fermi resonance is the phenomenon, when in a polyatomic molecule two vibrational levels belonging to different vibrations have nearly the same energy, so as to be accidentally near degenerate.)

In the computer simulation of the observed band the maximum J and K values were taken as 17Ø. The usual assumptions were made as in the $\nu_{12}(e')$ case.

Following the usual procedure for the perpendicular fundamental bands described earlier in this chapter, it was found that the best fit was achieved with

α_s^B = Ø.ØØØØ62 cm^{-1}, ζ_9^z = Ø.Ø5 and $q_9^{(+)}$ = +Ø.ØØØ1Ø cm^{-1}. The value quoted by Shurvell et al[27] for the Coriolis constant did not contradict the one obtained from the present study.

The best fit parameters are given in Table 3.9 and the observed and calculated spectra are given, in compressed form, in Figure 3.9.

3.3.5 The $\nu_8(e')$ Perpendicular Fundamental Band.

The $\nu_8(e')$ perpendicular fundamental band was recorded using a multi-pass cell with a total path length of about 4m. The pressure of the sample was ca. 2 Torr.

The $\nu_8(e')$ fundamental band is a very weak band which extends from about 3Ø8Ø cm^{-1} to about 3135 cm^{-1} with the band centre at 3113 cm^{-1}, as can be seen in Figure 3.1Ø.

This perpendicular band is a very weak and distorted one, so a satisfactory computer simulation is almost impossible. Another problem arises from the presence of trace H_2O lines which obscure parts of the band contour. Finally, in the region that the $\nu_8(e')$ band lies, the detector power drops dramatically which leads to an increase in the noise level.

It has been speculated[27], that there is a combination band in this region in Fermi resonance with $\nu_8(e')$ band which leads to the observed distorted feature but nothing really conclusive could be observed at this relatively high resolution.

The calculated contour was not expected to fit satisfactorily with the observed band due to the reasons discussed earlier. Under these circumstances, the best

possible fit was achieved with α_8^B = Ø.ØØØØ82 and ζ_8^z = -Ø.ØØ2. The value derived for ζ_8^z did not contradict the one quoted by Shurvell et al[27].

Not any l-resonance effect could be observed so the $q_8^{(+)}$ l-resonance parameter was assumed to be Ø.

The best fit parameters for the $v_8(e')$ perpendicular band are listed in Table 3.1Ø and the observed and calculated spectrum, in compressed form, are given in Figure 3.1Ø.

3.3.6 The ζ Sum Rule.

According to the ζ sum rule[16] we have the following expression:

$$\sum \zeta_t = -1 \qquad (3.1Ø)$$

Therefore, by adding the five ζ_t's which were obtained from the present study and the two ζ_t's from the literature[27], we get:

$$\zeta_8+\zeta_9+\ldots+\zeta_{14} = Ø.ØØ+Ø.Ø5-\ldots-Ø.2Ø= -1.25$$

After taking into account the relative uncertainties in each of the Coriolis constants the value obtained for $\sum \zeta_t$ is considered satisfactory.

3.4 Overtone And Combination Bands Of s-$C_6H_3F_3$.

In this study, the overtone and combination bands of s-$C_6H_3F_3$ were recorded at the same resolution as before using the same multipass cell which was used for the recording of the $\nu_8(e')$ fundamental band. The total path length was again 3m and the pressure of the sample was ca. 2 Torr. A common problem in the recording of all the combinations and overtones was a dramatic decrease in the signal to noise ratio which was caused by the decreased signal from a larger number of traversals in the multipass cell.

The analysis which was employed was the same as in the case of the perpendicular fundamental bands. In general, the results of such an analysis can be used as a check for the first order Coriolis constants obtained from the analysis of the fundamentals. Furthermore, first order Coriolis constants obtained from the analysis of combination bands can then be used to provide useful supplementary force field data.

The profile shapes of the combination and overtone band contours are determined primarily by the effective Coriolis constants ζ^z_{eff} which under the harmonic vibrations assumption are formed from certain linear combinations[16] of the ζ^z_t values.

For the combination of two degenerate e' modes ν_s and ν_t, the effective Coriolis constant, denoted as ζ^z_{eff}, is equal to the following expression:

$$\zeta^z_{eff} = -(\zeta^z_s + \zeta^z_t) \qquad (3.10)$$

For the combination of a non-degenerate a mode with a degenerate e' mode ν_t the effective Coriolis constant is as follows:

$$\zeta^{z}_{eff} = \zeta^{z}_{t} \qquad (3.11)$$

The ζ^{z}_{eff} constant for the first overtone of degenerate e´ mode ν_t is given by the following relationship:

$$\zeta^{z}_{eff} = -2\zeta^{z}_{t} \qquad (3.12)$$

Finally, following the analysis of Korppi-Tommola et al[28] for the gas phase Raman band contours of s-trifluorobenzene-h_3 the ζ^{z}_{t} constants of the e´´ degenerate modes were set to Ø.

In the analysis, l-resonance effects were ignored due to the lower quality of the spectra. The best fit values for the observed and calculated ζ^{z}_{eff} values together with the proposed assignments of the combinations and overtones obtained from the present analysis are given in Table 3.11. The observed ζ^{z}_{eff} values were taken from the computer simulation analysis of each band and compared with the calculated ζ^{z}_{eff} values from expressions (3.1Ø)-(3.12).

The α^{B}, J_{max} ,K_{max} values which were used are of the same order as the ones in the analysis of the perpendicular fundamental bands.

3.4.1 The $\nu_{1Ø}$+ ν_{11} (e´x e´) Combination Band.

The $\nu_{1Ø}$ + ν_{11} band extends from about 259Ø cm^{-1} to about 261Ø cm^{-1} with the band centre at 26Ø1 cm^{-1} as can be seen in Figure 3.11.

The ζ^{z}_{eff}(obs.) value obtained from the computer simulation analysis of the band was Ø.45 the same as the ζ^{z}_{eff}(calc.) one.

The corresponding values given by Shurvell et al[27] are Ø.57 and Ø.47 respectively. (At this point it was realised that the calculated ζ^z_{eff} values in the above mentioned paper do not correspond to the values obtained using expressions like (3.1Ø) with values for ζ^z_s and ζ^z_t for the appropriate fundamentals. By using the values for $\zeta^z_s$and ζ^z_t for the appropriate fundamentals in each case from the same paper, new corrected values for the ζ^z_{eff} constants were derived. So, for example, in the present case the corrected ζ^z_{eff}(calc.) constant has a value of Ø.6Ø using $\zeta^z_{1Ø}$and ζ^z_{11} values from the paper by Shurvell et al[27] instead of Ø.47 quoted in the same paper. From now on, only the corrected ζ^z_{eff} constants will be used as a comparison with the values obtained from the present study).

The observed and calculated band contours for the $\nu_{1Ø}$+ ν_{11} combination band are given in Figure 3.11.

3.4.2 The ν_2+ ν_{11}(a′xe′) Combination Band.

This band extends from about 246Ø cm^{-1} to 25ØØ $cm^{-1}$with the band centre at 2483 cm^{-1} as can be seen in Figure 3.12.

The ζ^z_{eff}(obs.) value was Ø.Ø5 while the ζ^z_{eff}(calc.) one was -Ø.Ø5. After taking into account that the Coriolis constant is almost Ø, the agreement between the two values is satisfactory.

The corresponding values obtained by Shurvell et al[27]are Ø.1Ø and -Ø.Ø5 respectively.

The observed and calculated band contours are given in Figure 3.12.

3.4.3 The $\nu_5+\nu_{11}(a_2'xe')$ Combination Band.

This band extends from ca. 2415 cm^{-1} to ca. 2431 cm^{-1} with the band centre at 2425 cm^{-1} as can be seen in Figure 3.13.

The ζ^z_{eff}(obs.) value was Ø.Ø5 whereas the ζ^z_{eff}(calc.) one obtained from expression (3.11) was again -Ø.Ø5. The agreement between the two values is satisfactory due to the fact that the Coriolis constant is close to zero.

The corresponding values for these constants given by Shurvell et al[29] are -Ø.Ø3 and -Ø.Ø5 respectively.

The observed and calculated band contours are given in Figure 3.13.

3.4.4 The $\nu_2+\nu_{12}(a_1'xe')$ Combination Band.

The $\nu_2+\nu_{12}$ combination band extends from about 2330 cm^{-1} to 2370 cm^{-1} with the band centre at 2355 cm^{-1}as can be seen in Figure 3.14. The band is obscured by the presence of trace CO_2 lines which were identified and ignored. Their positions are denoted with small dots in Figure 3.14.

The ζ^z_{eff} (obs.) value was found to be -Ø.15 while the ζ^z_{eff}(calc.) one was -Ø.35. The agreement between the two values is not satisfactory.

The corresponding values in the literature[27] are -Ø.48 and -Ø.47 respectively.

The observed and calculated band contours are given in Figure 3.14.

3.4.5 The $2\nu_{11}(e')^2$ Overtone Band.

The $2\nu_{11}$ overtone band extends from about 2240 cm^{-1} to 2265 cm^{-1} with the band centre at 2252 cm^{-1} as can be seen in Figure 3.15.

The ζ^z_{eff}(obs.) and ζ^z_{eff}(calc.) values were found to be -0.1 and 0.1 respectively. The agreement between the two values is satisfactory due to the fact that the Coriolis constant is close to zero.

The corresponding values in the literature[27] are -0.2 and 0.1 respectively.

The observed and calculated band contours are given in Figure 3.15.

3.4.6 The $\nu_{11}+\nu_{12}(e'xe')$ Combination Band.

This combination band extends from ca 2110 cm^{-1} to ca. 2130 cm^{-1} with the band centre at 2121 cm^{-1} as can be seen in Figure 3.16.

The ζ^z_{eff}(obs.) and ζ^z_{eff}(calc.) constants were found to be 0.5 and 0.4 respectively. The agreement between the two values is satisfactory.

The corresponding values given by Shurvell[27] are 0.32 and 0.52.

The observed and calculated band contours are given in Figure 3.16.

3.4.7 The $\nu_3+\nu_{12}$ ($a_1'xe'$) Combination Band.

The $\nu_3+\nu_{12}$ combination band extends from about 1995 cm^{-1} to

2015 cm^{-1} with the band centre at 2007 cm^{-1} as can be seen in Figure 3.17.

The ζ^{z}_{eff}(obs.) and (calc.) constants were found to be -0.25 and -0.35 respectively. The agreement between the two values is satisfactory.

In Shurvell's[27] paper the coresponding values are -0.43 and -0.47 respectively.

The observed and calculated band contours of this combination band are given in Figure 3.17.

3.4.8 The $\nu_{10}+\nu_{14}(e'xe')$ Combination Band.

This combination band extends from ca. 1790 cm^{-1} to ca. 1810 cm^{-1} with the band centre at 1802 cm^{-1}as can be seen in Figure 3.18. The band is partially obscured by the presence of trace H_2O lines which were identified and ignored. Their positions are denoted by small dots in Figure 3.18.

The ζ^{z}_{eff}(obs.) and (calc.) constants were found to be 1.0 and 0.6. respectively. The agreement between the two values is satisfactory due to the fact that the Coriolis constant is close to 1 and also due to the lower quality of the spectrum.

In the literature[27], the corresponding values are 0.95 and 0.75.

The observed and calculated spectra are given in Figure 3.18.

3.4.9 The $\nu_{4}+\nu_{11}(a_1'xe')$ Combination Band.

The $\nu_{4}+\nu_{11}$ combination band extends from ca 1690 cm^{-1} to ca 1715 cm^{-1} with the band centre at 1705 cm^{-1} as can be

seen in Figure 3.19. Here again the band is partially obscured by the presence of trace H_2O lines which were identified and removed.

The ζ^z_{eff}(obs.) and (calc.) constants were found both to be Ø.1.

Shurvell[27] quotes ζ^z_{eff}(obs.) and (calc.) as -Ø.Ø4 and -Ø.Ø5 respectively.

The observed and calculated band contours are given in Figure 3.19.

3.4.1Ø The $\nu_{12}+\nu_{14}$ (e´xe´) Combination Band.

The $\nu_{12}+\nu_{14}$ combination band extends from ca. 131Ø cm^{-1} to 1325 cm^{-1} with the band centre at 132Ø cm^{-1} as can be seen in Figure 3.2Ø. The band was again partly obscured by trace H_2O lines.

The ζ^z_{eff}(obs.) and (calc.) constants were found to be Ø.75 and Ø.55 respectively. The agreement between the two values is satisfactory.

In the literature[27] they are quoted as Ø.72 and Ø.67.

The observed and calculated band contours are given in Figure 3.2Ø.

3.4.11 The $\nu_{16}+\nu_{19}$($a_2^{''}$xe´´) Combination Band.

This combination band extends from ca 125Ø cm^{-1} to ca. 127Ø cm^{-1} with the band centre at 1261 cm^{-1} as can be seen in Figure 3.21. It is again partly obscured by H_2O lines though not to a great extent.

The ζ^z_{eff}(obs.) value was found to be -Ø.Ø5 whereas the

calculated value was set to Ø. The agreement between the two values is satisfactory.

The ζ^{z}_{eff}(obs.) value given by Shurvell[27] is Ø.

The observed and calculated band contours are given in Figure 3.19.

3.4.12 Other Combination Bands In The Mid-Infrared Spectrum Of s-Trifluorobenzene-h_3.

There are several other bands in the s-$C_6H_3F_3$ mid-infrared spectrum which can not be assigned with a great certainty. However, possible assignments will be discussed in this section and in some cases first order Coriolis constants will be given.

In the 2700-3000 cm^{-1} region there are four relatively weak bands. One at ca 2921 cm^{-1} could be due to $2\nu_{10}(e')^2$ in which case the ζ^{z}_{eff}(calc.) value would be Ø.8. Due to the low quality of the spectrum, no computer simulation of this band was performed.

The other three features in the same region are found at ca. 2831 cm^{-1}, 2801 cm^{-1} and 2770 cm^{-1}. The first one could be either due to $\nu_2+\nu_{10}$ ($a_1'xe'$) with ζ^{z}_{eff}(calc.) = -Ø.4 or $\nu_9+2\nu_{19}(e'x(e'')^2)$ with ζ^{z}_{eff}(calc.) = Ø.Ø5. The second one could be due to $\nu_9+2\nu_{19}(e'x(e'')^2)$. Finally, the third one could be due to $\nu_5+\nu_{10}(a_2'xe')$ with ζ^{z}_{eff}(calc.) = -Ø.4. Again a better quality spectrum is needed to confirm these assignments. The region is shown in Figure 3.22.

Another band which extends from ca. 2650 cm^{-1} to ca. 2680 cm^{-1} could be attributed to $\nu_{10}+2\nu_{19}(e'x(e'')^2)$ with

ζ^z_{eff} (calc.) = -Ø.4Ø. The band in this region was simulated with ζ^z_{eff}(obs.) = -Ø.2 and is shown in Figure 3.23 with the experimental one.

The band which extends from ca. 22ØØ cm^{-1} to 222Ø cm^{-1} could be either due to $\nu_4+\nu_9(a_1'xe')$ with ζ^z_{eff}(calc.) = Ø.Ø5 or $\nu_9+\nu_{19}(e'xe'')$ with the same ζ^z_{eff}(calc.). It was simulated with a ζ^z_{eff}(obs.) = Ø.2 and is shown in Figure 3.24.

Another band which extends from ca. 118Ø $cm^{-1}$to ca. 124Ø cm^{-1} with an irregular feature at ca.122Ø cm^{-1} is partially obscured by H_2O lines. This feature could be due to either $\nu_3+\nu_{17}(a_1'xa_2'')$ or $\nu_{1Ø}-\nu_{2Ø}(e'xe'')$ with a ζ^z_{eff}(calc.) = -Ø.4Ø. Here it was reproduced with ζ^z_{eff}(obs.) = -Ø.15 and is shown in Figure 3.25 with the simulated one.

There is another band at ca. 1155 cm^{-1} which is shown in Figure 3.24 which could be due to $\nu_{1Ø}-\nu_{14}(e'xe')$ with a ζ^z_{eff}(calc.) = Ø.6Ø. This band was not simulated due to the lower quality of the spectrum.

Another prominent band extends from ca. 1Ø7Ø cm^{-1} to 11ØØ cm^{-1} and could be due to $\nu_4+\nu_{13}(a_1'xe')$ with a ζ^z_{eff}(calc.) = -Ø.3. Here it is simulated with a ζ^z_{eff}(obs.)= -Ø.4 and is shown in Figure 3.27 together with the experimental one.

Finally, in the region between ca. 78Ø cm^{-1} and ca. 885 cm^{-1} there are another three features at ca. 881 cm^{-1}, 8Ø5 cm^{-1} and 785 cm^{-1} which could be due to $\nu_{1Ø}+\nu_{19}(e'xe'')$ with a ζ^z_{eff}(calc.) = -Ø.4Ø, $\nu_{17}+\nu_{19}(a_2''xe'')$ with a ζ^z_{eff}(calc.) = Ø and $\nu_4+\nu_{17}(a_1'xa_2'')$ respectively. These are shown in Figures 3.28 and 3.29. These bands were not simulated due to the lower quality of the spectrum.

Table 3.1

Fundamental Wavenumbers/in cm^{-1} Of s-Trifluorobenzene-h_3 and -d_3

Γ	ν_r	$\bar{\nu}$ $C_6H_3F_3$	$\bar{\nu}$ $C_6D_3F_3$
a_1'	ν_1	3076[27]	2319[28]
	ν_2	1363[27]	1360[28]
	ν_3	1012[27]	969[28]
	ν_4	580[27]	577[28]
a_2'	ν_5	1304.6	1261.3
	ν_6	1173.8	947.7
	ν_7	553.7	509.8
e'	ν_8	3113	2314[28]
	ν_9	1629	1617[28]
	ν_{10}	1475.4	1425[28]
	ν_{11}	1127.6	1054[28]
	ν_{12}	996.25	792[28]
	ν_{13}	502[27]	487[28]
	ν_{14}	324[27]	322[28]
a_2''	ν_{15}	848.130	777[28]
	ν_{16}	664.693	522[28]
	ν_{17}	207[27]	206[28]
e''	ν_{18}	792[27]	646[28]
	ν_{19}	598[27]	538[28]
	ν_{20}	246[27]	231[28]

Note: The a_2' fundamentals were derived from our force field calculations.

Table 3.2

Observed And Calculated Lines For $\nu_{15}(a_2'')$ Fundamental Band Of s-$C_6H_3F_3$.

P(J'');ΔJ=-1	Obs.Wavenumber	(Obs.-Calc.)Wavenumber
P(20)	845.7720	-0.0035
P(22)	845.5388	-0.0007
P(23)	845.4258	0.0043
P(24)	845.3049	0.0015
P(25)	845.1838	-0.0016
P(26)	845.0640	-0.0033
P(27)	844.9509	0.0018
P(28)	844.8298	-0.0012
P(29)	844.7100	-0.0028
P(30)	844.5969	0.0023
P(31)	844.4758	-0.0006
P(32)	844.3560	-0.0022
P(33)	844.2429	0.0030
P(34)	844.1218	0.0001
P(35)	844.0020	-0.0014
P(36)	843.8889	0.0039
P(37)	843.7678	0.0011
P(38)	843.6479	-0.0004
P(39)	843.5269	-0.0030
P(40)	843.4138	0.0023
P(41)	843.2939	0.0008
P(42)	843.1729	-0.0017
P(43)	843.0598	0.0036
P(44)	842.9390	0.0013
P(45)	842.8188	-0.0004
P(46)	842.6980	-0.0026
P(47)	842.5850	0.0029
P(48)	842.4648	0.0013
P(49)	842.3440	-0.0009
P(51)	842.1108	0.0031
P(52)	841.9900	0.0010
P(53)	841.8699	-0.0004
P(54)	841.7488	-0.0028
P(55)	841.6360	0.0031
P(56)	841.5159	0.0017
P(57)	841.3948	-0.0006
P(58)	841.2749	-0.0018
P(59)	841.1619	0.0040
P(60)	841.0408	0.0017
P(61)	840.9199	-0.0003
P(62)	840.7998	-0.0016

P(J´´);ΔJ=-1	Obs.Wavenumber	(Obs.-Calc.)Wavenumber
P(63)	840.6790	-0.0035
P(64)	840.5659	0.0022
P(65)	840.4458	0.0010
P(66)	840.3250	-0.0008
P(67)	840.2048	-0.0021
P(68)	840.0840	-0.0039

R(J´´);ΔJ=+1	Obs.Wavenumber	(Obs.-Calc.)Wavenumber
R(11)	849.5388	0.0011
R(12)	849.6519	-0.0029
R(13)	849.7649	-0.0070
R(14)	849.8848	-0.0042
R(15)	849.9978	-0.0083
R(16)	850.1189	-0.0042
R(17)	850.2468	0.0067
R(18)	850.3599	0.0029
R(19)	850.4729	-0.0011
R(20)	850.5940	0.0031
R(21)	850.6990	-0.0088
R(22)	850.8198	-0.0048
R(23)	850.9480	0.0066
R(24)	851.0608	0.0026
R(25)	851.1738	-0.0017
R(26)	851.2939	0.0022
R(27)	851.4148	0.0064
R(28)	851.5198	-0.0053
R(29)	851.6409	-0.0008
R(30)	851.7610	0.0027
R(31)	851.8738	-0.0011
R(32)	851.9949	0.0035
R(33)	852.1079	0.0001
R(34)	852.2209	-0.0036
R(35)	852.3408	-0.0001
R(36)	852.4619	0.0046
R(37)	852.5750	0.0013
R(38)	852.6958	0.0057
R(39)	852.8088	0.0024
R(40)	852.9219	-0.0008
R(41)	853.0420	0.0029
R(42)	853.1548	-0.0005
R(43)	853.2759	0.0044

R(J´´);ΔJ=+1	Obs.Wavenumber	(Obs.-Calc.)Wavenumber
R(44)	853.3889	Ø.ØØ13
R(45)	853.5Ø2Ø	-Ø.ØØ18
R(46)	853.6218	Ø.ØØ19
R(47)	853.7349	-Ø.ØØ11
R(48)	853.856Ø	Ø.ØØ39
R(49)	853.969Ø	Ø.ØØØ9
R(5Ø)	854.Ø818	-Ø.ØØ22
R(51)	854.2Ø19	Ø.ØØ19
R(52)	854.3149	-Ø.ØØØ1
R(53)	854.428Ø	-Ø.ØØ38
R(54)	854.5488	Ø.ØØ12
R(55)	854.6619	-Ø.ØØ15
R(56)	854.7749	-Ø.ØØ43
R(57)	854.8948	-Ø.ØØØ2
R(58)	855.ØØ78	-Ø.ØØ29
R(59)	855.1289	Ø.ØØ25
R(6Ø)	855.2419	-Ø.ØØØ1
R(61)	855.3550	-Ø.ØØ26

Table 3.3

Derived Constants For $\nu_{15}(a_2'')$ Fundamental Band

Of $s\text{-}C_6H_3F_3$.

Parameter	Derived Value
$\bar{\nu}_o/cm^{-1}$	848.130
B''/cm^{-1}	0.058742
α_{15}^B $/cm^{-1}$	0.000013
C''/cm^{-1}	0.029371
α_{15}^C $/cm^{-1}$	0.000006
D_J $/cm^{-1}$	5.3×10^{-9}
D_{JK} / cm^{-1}	-9.9×10^{-9}
D_K / cm^{-1}	4.8×10^{-9}
σ / cm^{-1}	0.003

Note: $\alpha^B = B''-B'$, $\alpha^C = C''-C'$

Table 3.4

Observed And Calculated Lines For $\nu_{16}(a_2'')$ Fundamental Band Of s-$C_6H_3F_3$.

P(J'');ΔJ=-1	Obs.Wavenumber	(Obs.-Calc.)Wavenumber
P(29)	661.394	0.017
P(30)	661.281	0.020
P(31)	661.175	0.029
P(32)	661.055	0.024
P(33)	660.942	0.027
P(34)	660.828	0.028
P(35)	660.701	0.017
P(36)	660.580	0.012
P(37)	660.460	0.007
P(38)	660.347	0.010
P(39)	660.218	-0.003
P(40)	660.105	-0.000
P(41)	559.992	0.003
P(42)	559.856	-0.017
P(43)	559.759	0.002
P(44)	559.638	-0.002
P(45)	559.533	0.009
P(46)	559.405	-0.002
P(47)	559.284	-0.007
P(48)	559.164	-0.010
P(49)	559.043	-0.014
P(50)	558.930	-0.010
P(51)	558.817	-0.006
P(52)	558.697	-0.009
P(53)	558.569	-0.020
P(54)	558.456	-0.015
P(55)	558.343	-0.011
P(56)	558.245	0.009
P(57)	558.101	-0.017
P(58)	557.988	-0.013
P(59)	557.868	-0.015
P(60)	557.747	-0.017
P(61)	557.653	0.007
P(62)	557.514	-0.014
P(63)	557.401	-0.008
P(64)	557.280	-0.011
P(65)	557.167	-0.005

P(J´´);ΔJ=-1	Obs.Wavenumber	(Obs.-Calc.)Wavenumber
P(66)	557.039	-0.014
P(67)	556.937	0.003
P(68)	556.813	-0.002
P(69)	556.685	-0.011
P(70)	556.587	0.011
P(71)	556.470	0.013
P(72)	556.331	-0.006
P(73)	556.237	0.020
P(74)	556.120	0.023
P(75)	556.000	0.023

R(J´´);ΔJ=+1	Obs.Wavenumber	(Obs.-Calc.)Wavenumber
R(28)	667.858	-0.035
R(29)	667.978	-0.029
R(30)	668.091	-0.031
R(31)	668.204	-0.033
R(32)	668.340	-0.012
R(33)	668.468	0.001
R(34)	668.588	0.007
R(35)	668.679	-0.017
R(36)	668.807	-0.004
R(37)	668.912	-0.014
R(38)	669.025	-0.016
R(39)	669.153	-0.004
R(40)	669.270	-0.002
R(41)	669.390	0.003
R(42)	669.492	-0.010
R(43)	669.620	0.002
R(44)	669.749	0.016
R(45)	669.862	0.013
R(46)	669.974	0.010
R(47)	670.080	-0.000
R(48)	670.193	-0.003
R(49)	670.336	0.024
R(50)	670.438	0.010
R(51)	670.540	-0.004
R(52)	670.668	0.008
R(53)	670.788	0.012
R(54)	670.901	0.008

R(J´´);ΔJ=+1	Obs.Wavenumber	(Obs.-Calc.)Wavenumber
R(55)	671.014	0.005
R(56)	671.135	0.009
R(57)	671.248	0.006
R(58)	671.372	0.013
R(59)	671.496	0.020
R(60)	671.602	0.009
R(61)	671.707	-0.003
R(62)	671.843	0.016
R(63)	671.956	0.012
R(64)	672.076	0.014
R(65)	672.182	0.003
R(66)	672.302	0.005
R(67)	672.423	0.009
R(68)	672.536	0.004
R(69)	672.641	-0.009
R(70)	672.777	0.009
R(71)	672.882	-0.005
R(72)	672.996	-0.009
R(73)	673.124	0.000
R(74)	673.237	-0.005
R(75)	673.357	-0.004
R(76)	673.470	-0.010
R(77)	673.591	-0.008
R(78)	673.696	-0.022
R(79)	673.824	-0.013

Table 3.5

Derived Constants For $\nu_{16}(a_2'')$ Fundamental Band

Of s-$C_6H_3F_3$.

Parameter	Derived Value
$\bar{\nu}_o/cm^{-1}$	664.693
B''/cm^{-1}	Ø.Ø57Ø33
α_{16}^B $/cm^{-1}$	Ø.ØØØØØ5
C''/cm^{-1}	Ø.Ø28517
α_{16}^C $/cm^{-1}$	Ø.ØØØØØ3
σ $/cm^{-1}$	Ø.Ø14

Note: See note at the bottom of Table 3.3

Table 3.6

Best Fit Constants For $\nu_{12}(e')$ Fundamental Band

Of s-$C_6H_3F_3$.

Parameter	Best Fit Value ± Uncertainty
$\bar{\nu}_o$ / cm^{-1}	996.25 ± Ø.Ø1
α^B_{12} / cm^{-1}	Ø.ØØØØ62 ± Ø.ØØØØ3Ø
ζ^z_{12}	-Ø.35 ± Ø.Ø5
$q^{(+)}_{12}$ / cm^{-1}	+Ø.ØØØ12 ± Ø.ØØØ1Ø
J,K = 17Ø	

Note: See note at the bottom of Table 3.3.

Table 3.7

Best Fit Constants For $\nu_{11}(e')$ Fundamental Band

Of s-$C_6H_3F_3$.

Parameter	Best Fit Value ± Uncertainty
$\bar{\nu}_o$/ cm^{-1}	1127.60 ± 0.01
α^B_{11}/ cm^{-1}	0.000062 ± 0.000020
ζ^z_{11}	-0.05 ± 0.02
$q^{(+)}_{11}$/ cm^{-1}	+0.00013 ± 0.00005
J,K = 150	

Note: See note at the bottom of Table 3.3.

Table 3.8

Best Fit Constants For $\nu_{10}(e')$ Fundamental Band

Of s-$C_6H_3F_3$.

Parameter	Best Fit Value ± Uncertainty
$\bar{\nu}_o$ / cm^{-1}	1475.40 ± 0.05
α^B_{10} / cm^{-1}	0.000132 ± 0.000040
ζ^z_{10}	-0.40 ± 0.15
$q^{(+)}_{10}$ / cm^{-1}	+0.00020 ± 0.00010
J,K = 170	

Note: See note at the bottom of Table 3.3.

Table 3.9

Best Fit Constants For $\nu_9(e')$ Fundamental Band Of s-$C_6H_3F_3$.

Parameter	Best Fit Value ± Uncertainty
$\bar{\nu}_o$ / cm^{-1}	1629.Ø ± Fermi Resonance
α_9^B / cm^{-1}	Ø.ØØØØ62 ± Ø.ØØØØ3Ø
ζ_9^z	Ø.Ø5 + Ø.Ø2
$q_9^{(+)}$ / cm^{-1}	+Ø.ØØØ1Ø ± Ø.ØØØØ5
J,K = 17Ø	

Note: See note at the bottom of Table 3.3.

Table 3.10

Best Fit Constants For $\nu_8(e')$ Fundamental Band Of $s\text{-}C_6H_3F_3$.

Parameter	Best Fit Value ± Uncertainty
$\bar{\nu}_o$ / cm^{-1}	3113.0 ± Fermi Resonance(?)
α_8^B / cm^{-1}	0.000082 ± 0.000040
ζ_8^z	-0.002 ± 0.001
$q_8^{(+)}$ / cm^{-1}	(0)
J,K = 170	

Note: See note at the bottom of Table 3.3.

Table 3.11

Overtone And Combination Bands Of s-$C_6F_3H_3$.

Wavenumber/cm^{-1}	ζ^z_{eff}(obs.)	ζ^z_{eff}(calc.)	Assignment
2920	-	0.80	$2\nu_{10}$ (?)
2830	-	-0.40	$\nu_2+\nu_{10}$ (??)
		0.05	$\nu_9+2\nu_{19}$ (??)
2801	-	0.05	$\nu_9+2\nu_{19}$ (??)
2770	-	-0.40	$\nu_5+\nu_{10}$ (??)
2668	-0.20	-0.40	$\nu_{10}+2\nu_{19}$
2601	0.45	0.45	$\nu_{10}+\nu_{11}$
2483	0.05	-0.05	$\nu_2+\nu_{11}$
2425	0.05	-0.05	$\nu_5+\nu_{11}$
2355	-0.15	-0.35	$\nu_2+\nu_{12}$
2252	-0.10	0.10	$2\nu_{11}$
2210	0.20	0.05	$\nu_4+\nu_9$ (?)
		0.05	$\nu_9+\nu_{19}$ (?)
2121	0.50	0.40	$\nu_{11}+\nu_{12}$
2007	-0.25	-0.35	$\nu_3+\nu_{12}$
1802	1.00	0.60	$\nu_{10}+\nu_{14}$
1705	0.10	0.10	$\nu_4+\nu_{11}$
1320	0.75	0.55	$\nu_{12}+\nu_{14}$
1261	-0.05	0.0	$\nu_{16}+\nu_{19}$
1218	-0.15	0.0	$\nu_3+\nu_{19}$ (?)
		-0.40	$\nu_{10}-\nu_{20}$ (?)
1155	-	0.60	$\nu_{10}-\nu_{14}$ (??)
1087	-0.40	-0.30	$\nu_4+\nu_{13}$
881	-	-0.40	$\nu_{10}+\nu_{19}$ (??)
805	-	0.0	$\nu_{17}+\nu_{19}$ (??)
785	-	0.0	$\nu_4+\nu_{17}$ (??)

Figures

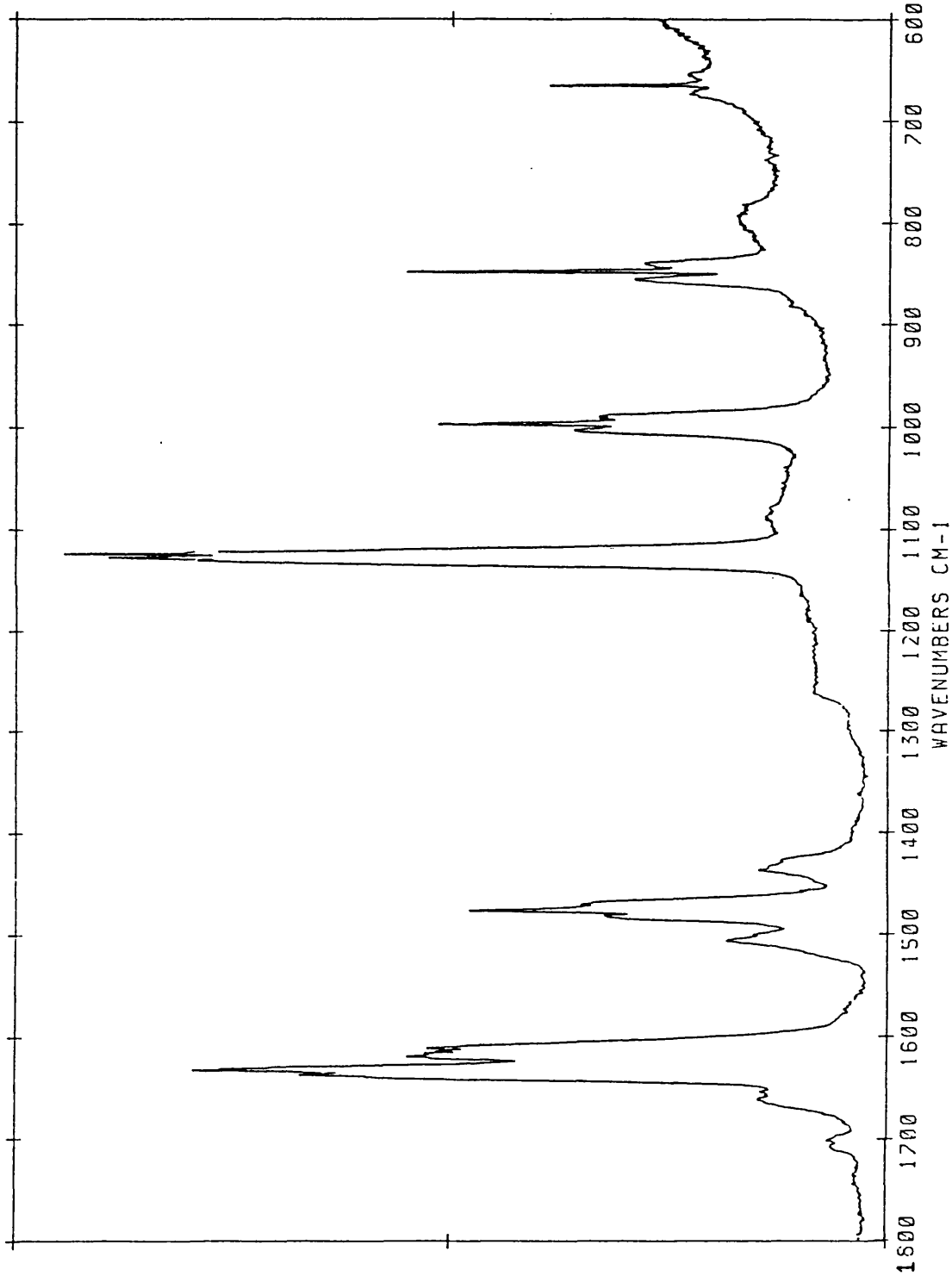
1800
1700
1600
1500
1400
1300
1200
1100
1000
900
800
700
600
WAVENUMBERS CM-1

Figure 3.1

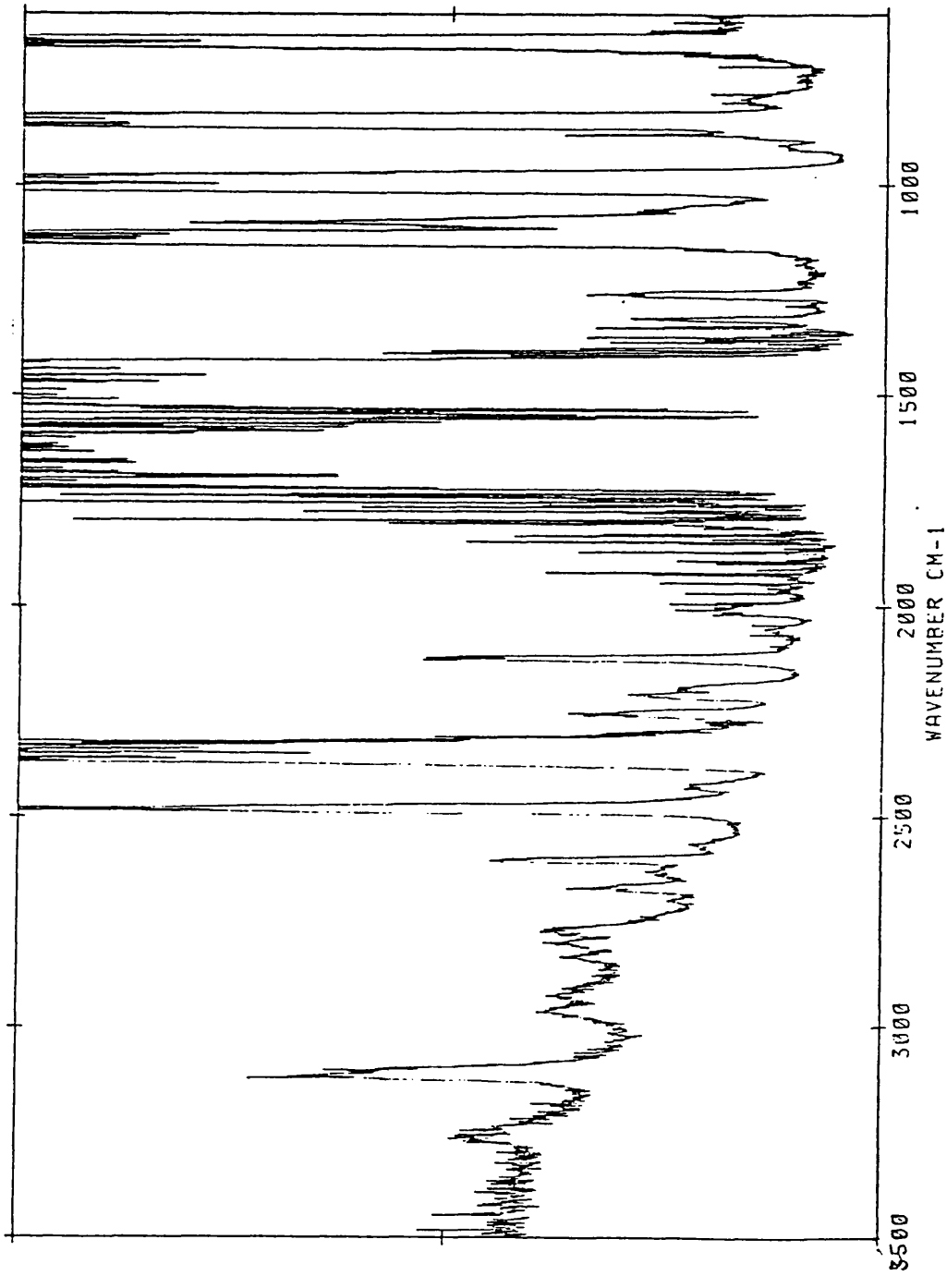

Figure 3.2

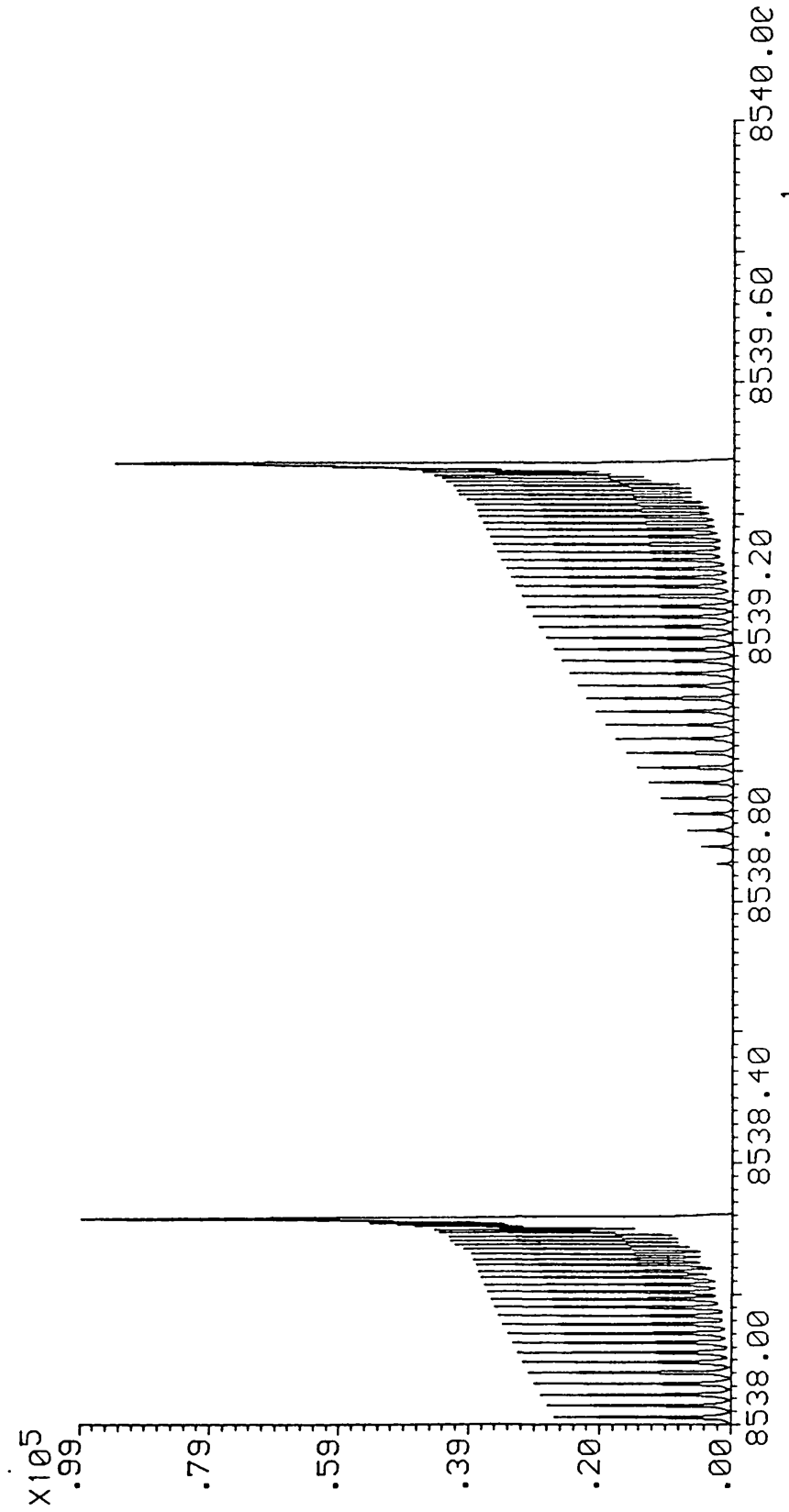
X10^5
.99
.79
.59
.39
.20
.00
8538.00
8538.40
8538.80
8539.20
8539.60
8540.00
X10^-1

Figure 3.3

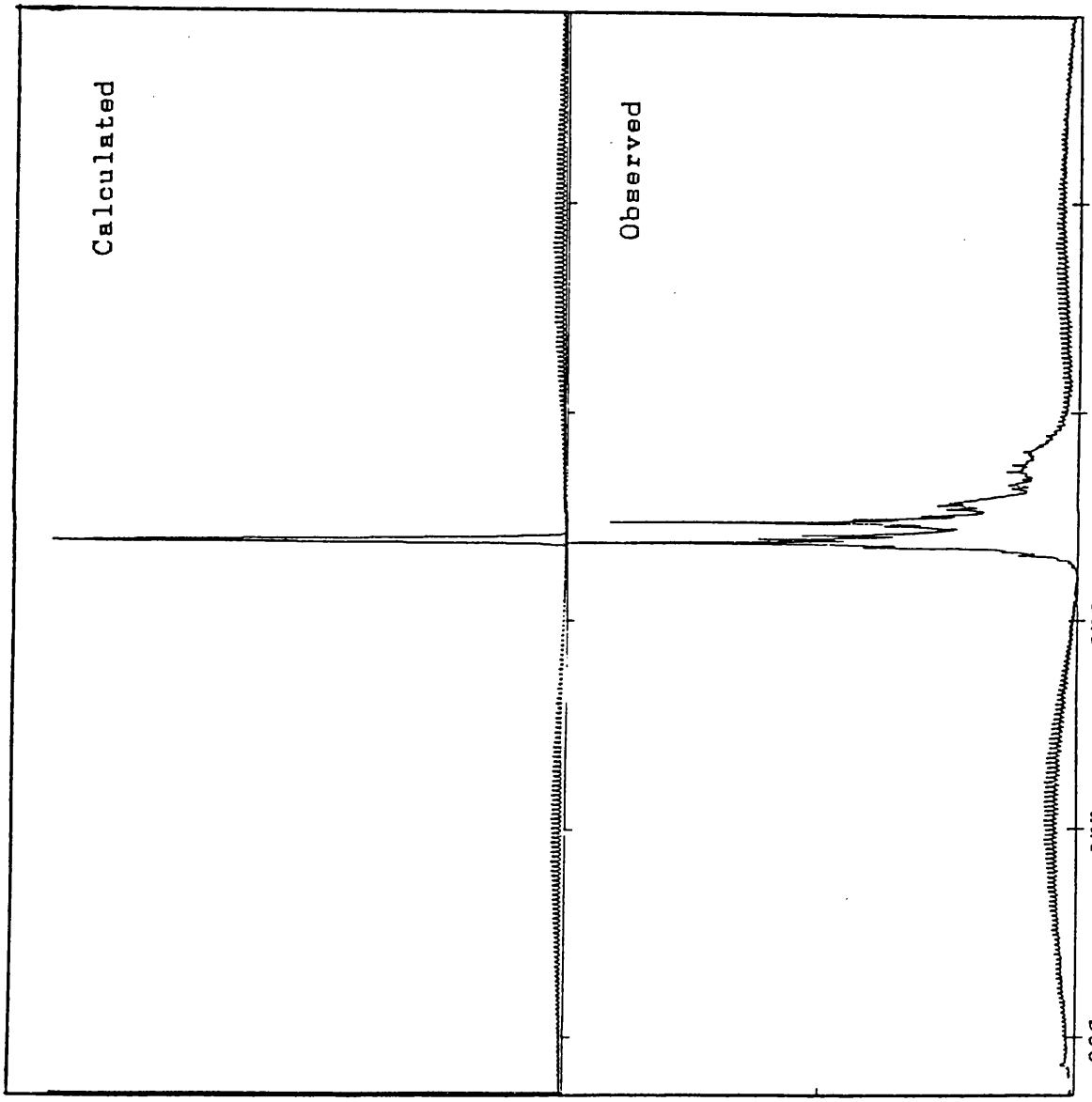

Figure 3.4

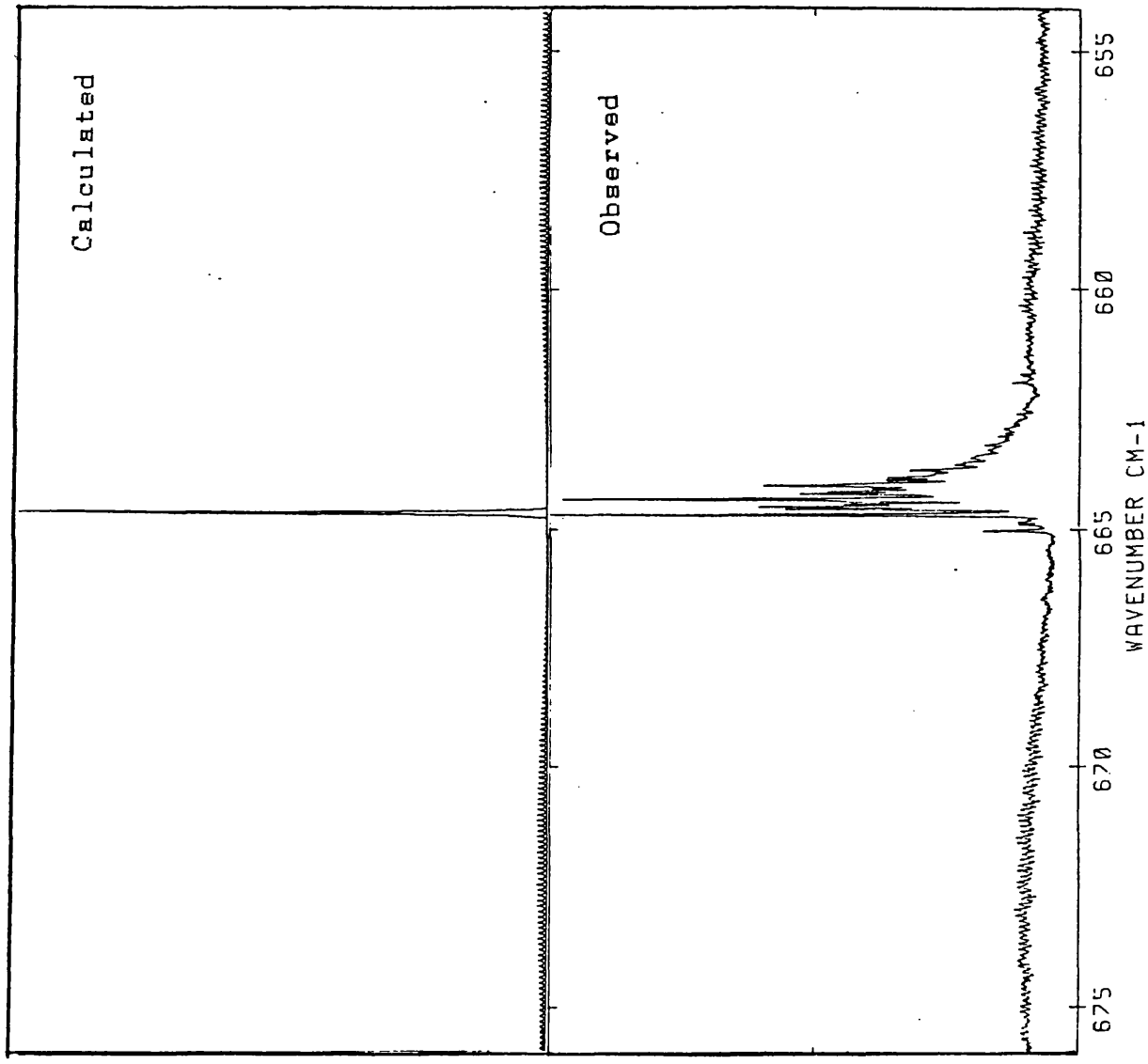

Figure 3.5

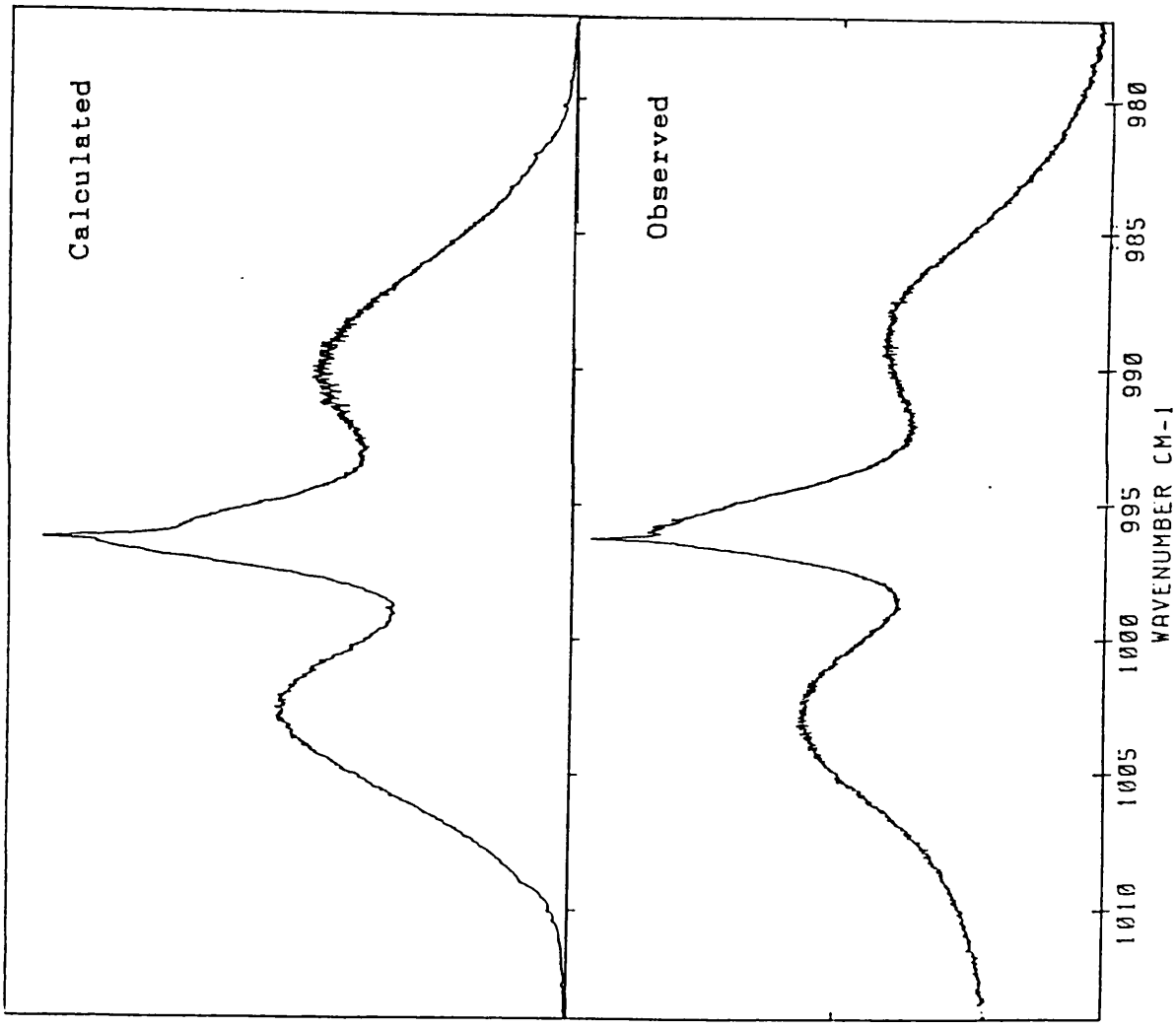
Calculated
Observed
1010
1005
1000
995
990
985
980
WAVENUMBER CM-1

Figure 3.6

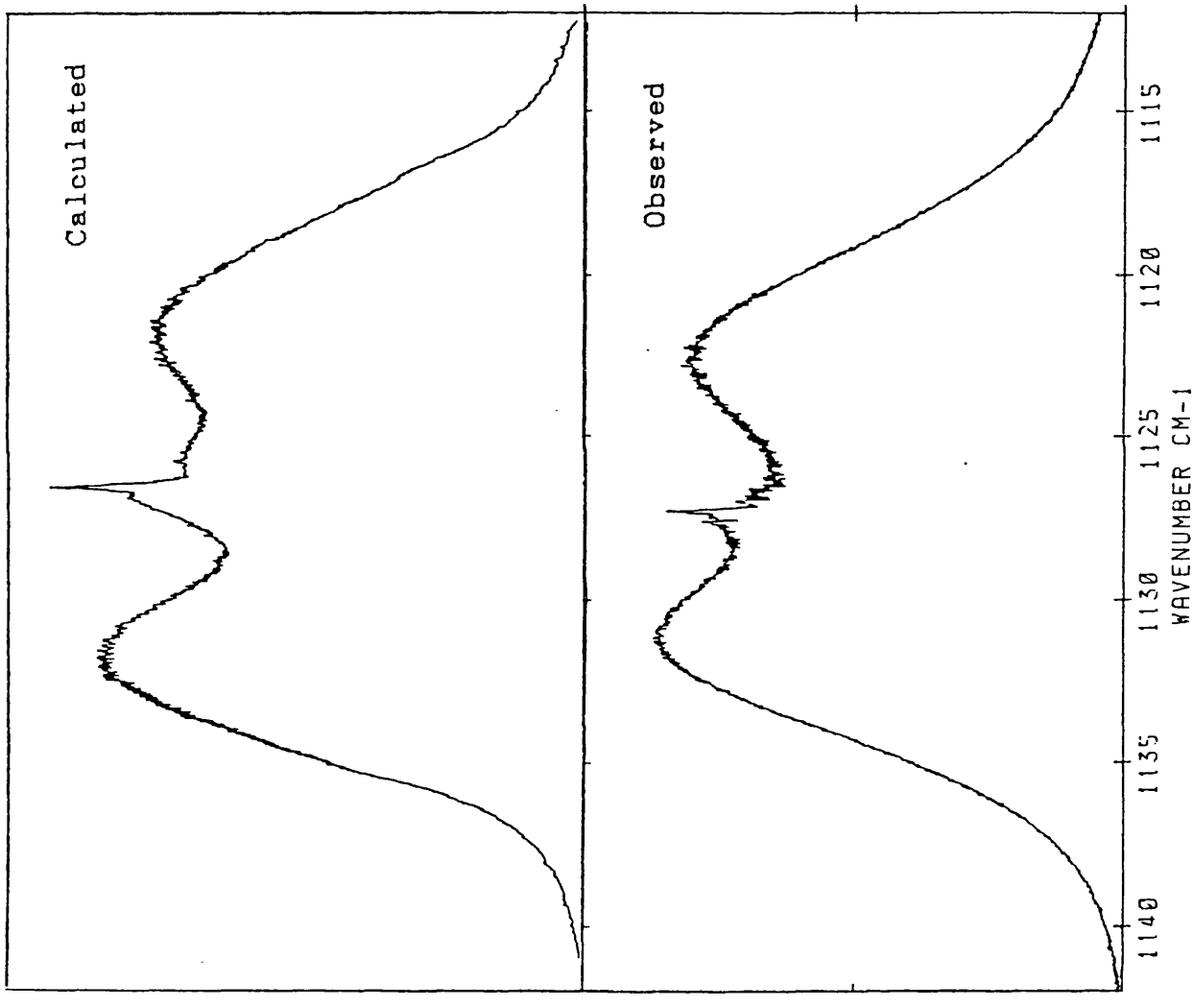
Calculated
Observed
1140
1135
1130
1125
1120
1115
WAVENUMBER CM-1

Figure 3.7

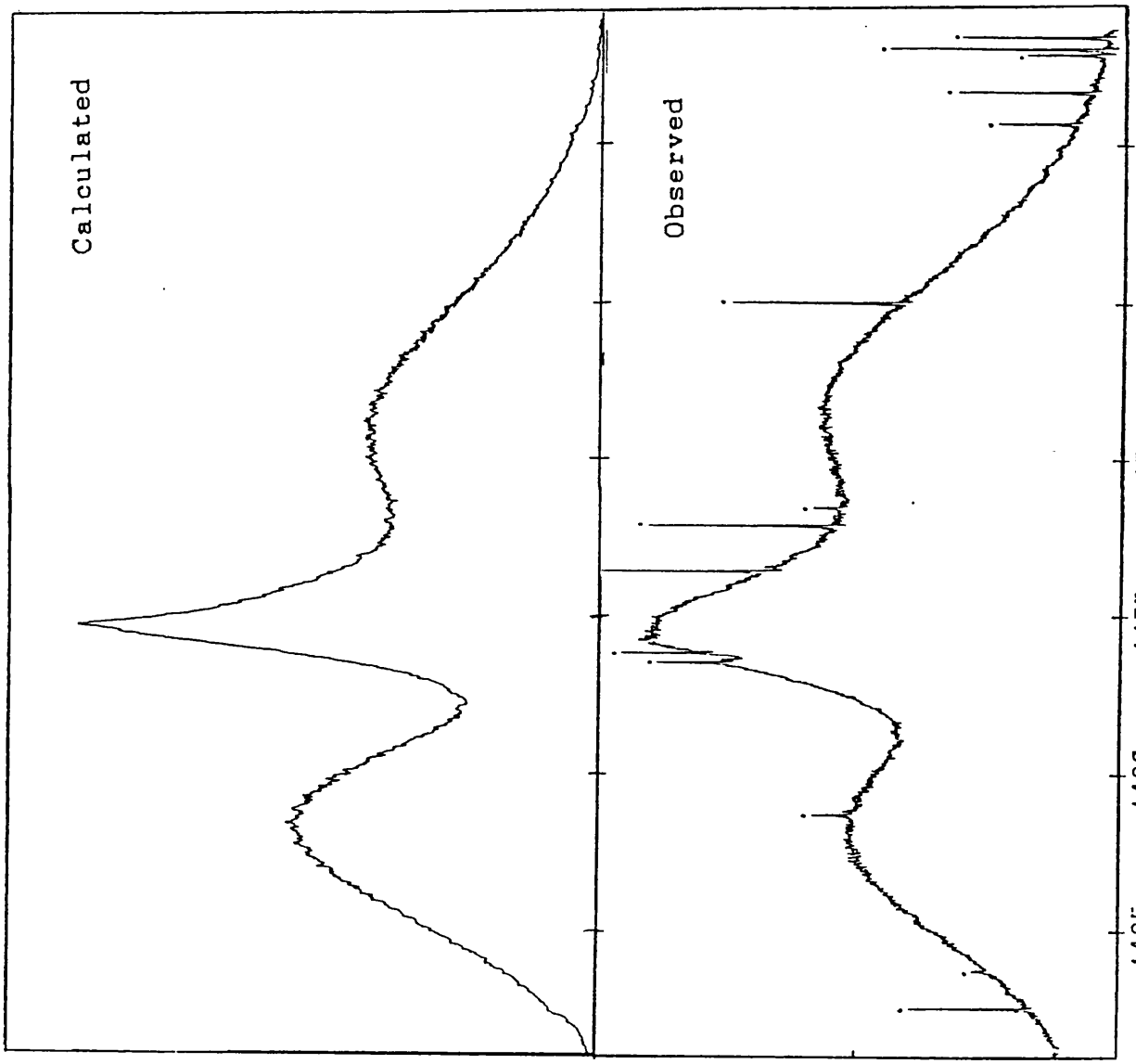
Calculated
Observed
1485
1480
1475
1470
1465
1460
WAVENUMBER CM-1

Figure 3.8

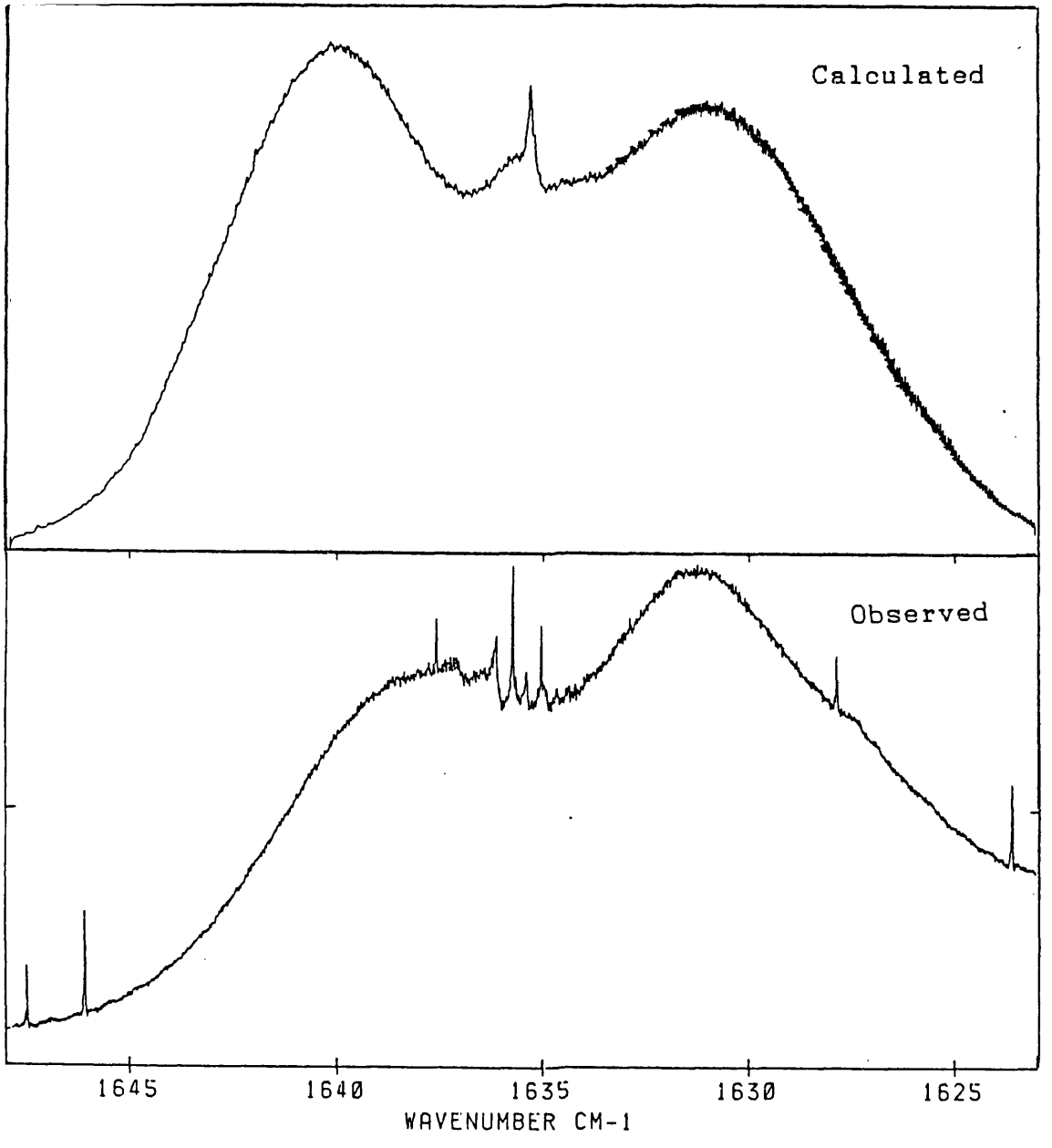
Calculated
Observed
1645
1640
1635
1630
1625
WAVENUMBER CM-1

Figure 3.9

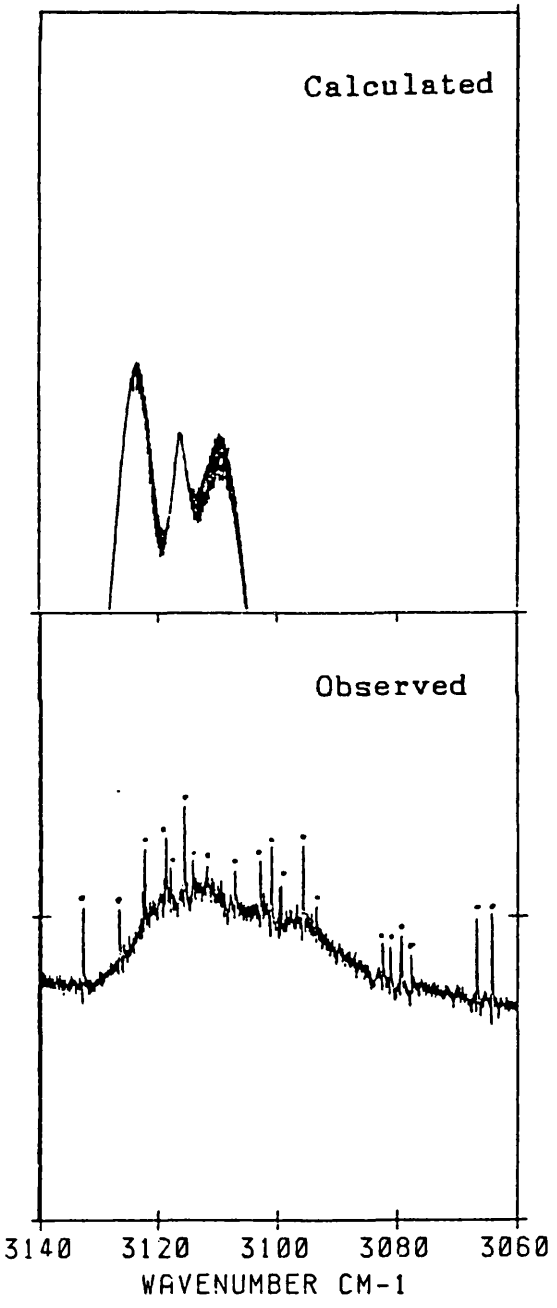

Figure 3.10

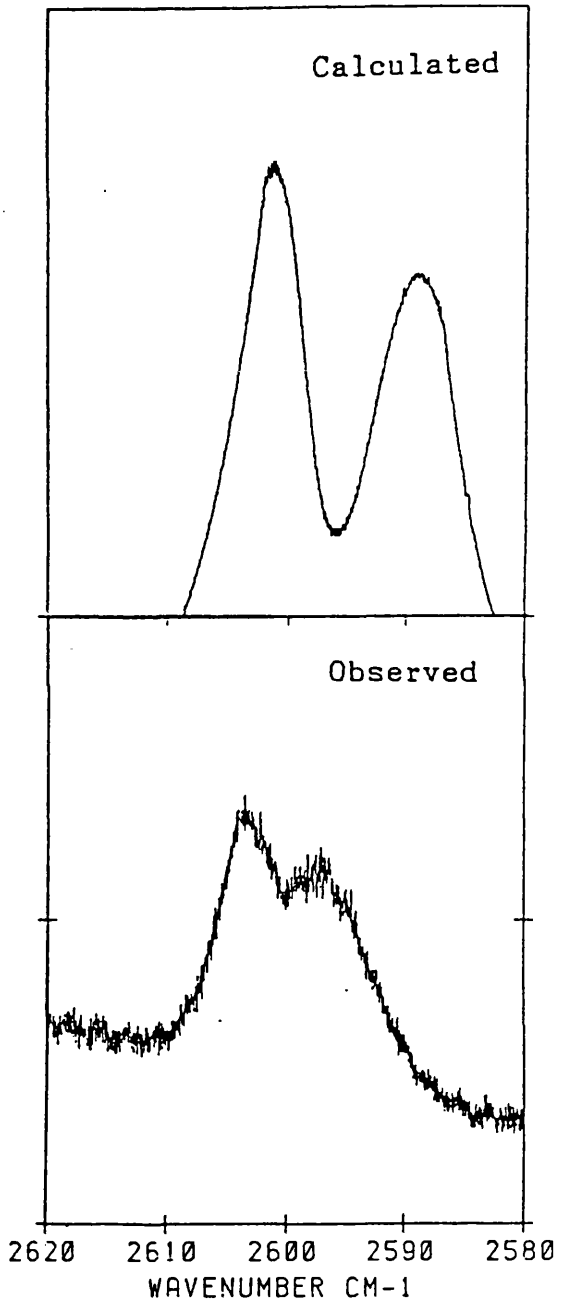

Figure 3.11

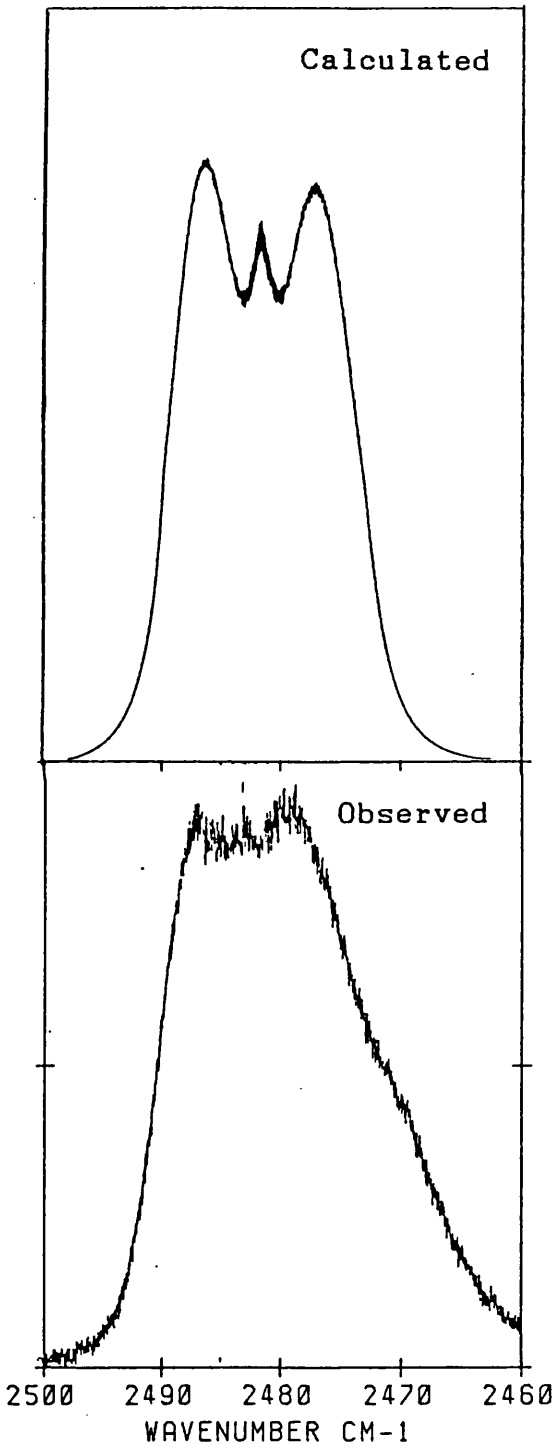

Figure 3.12

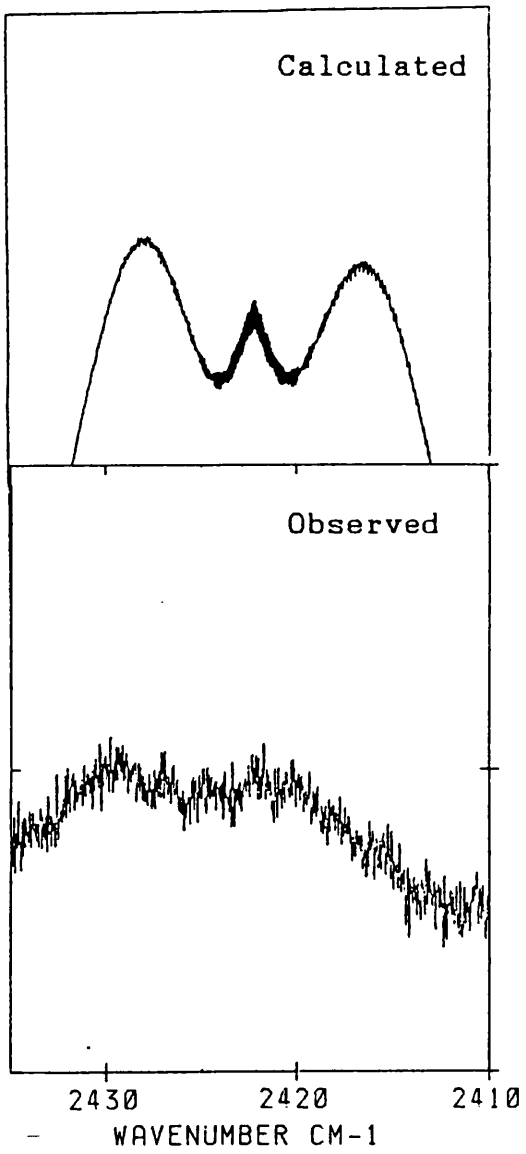

Figure 3.13

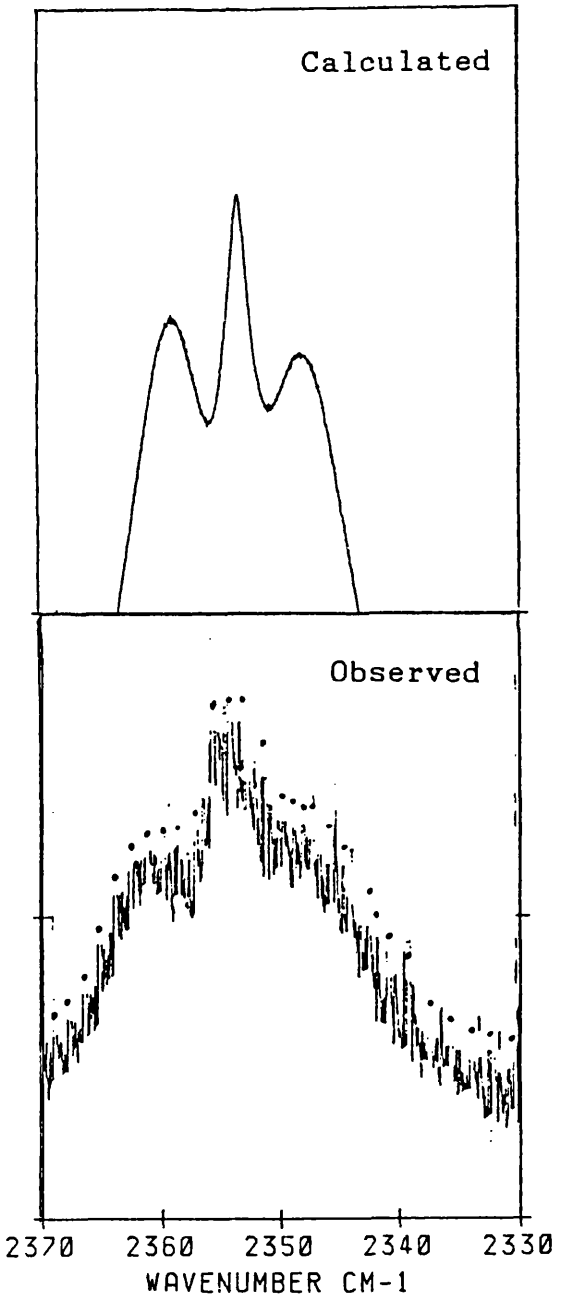

Figure 3.14

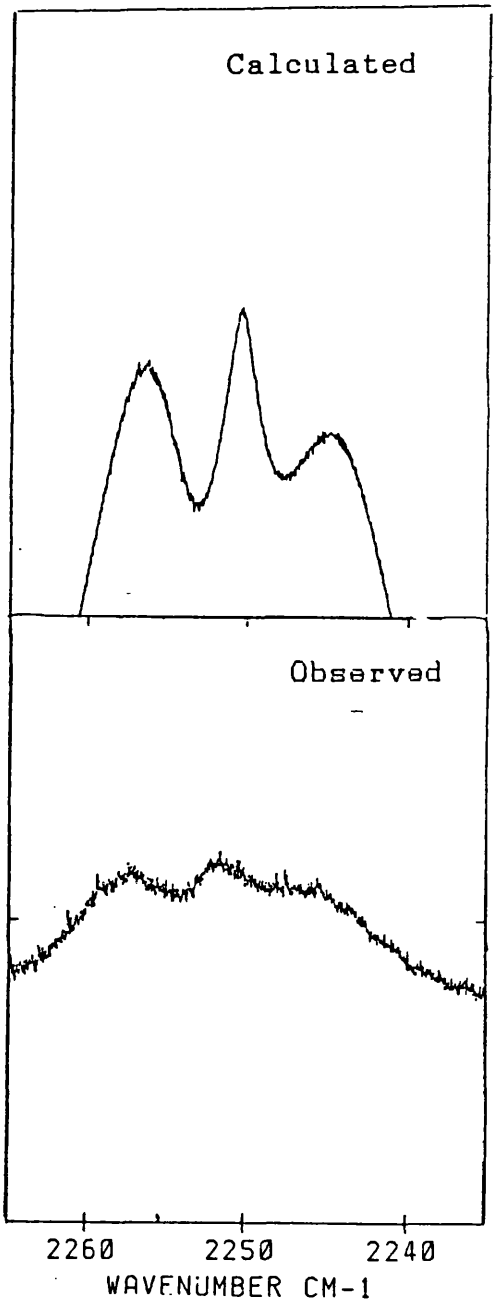

Figure 3.15

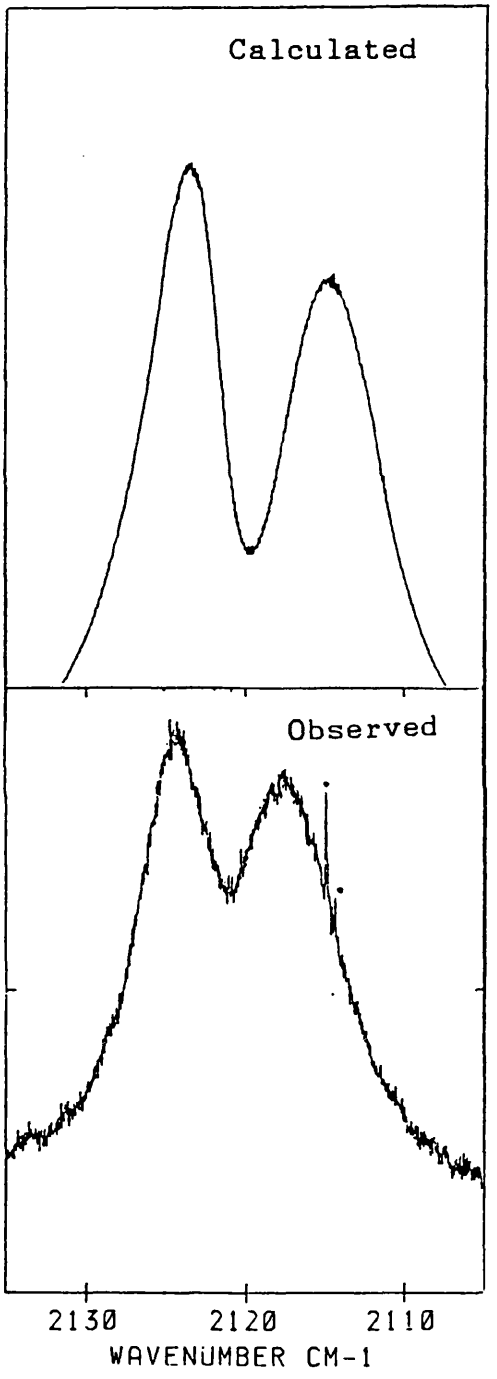

Figure 3.16

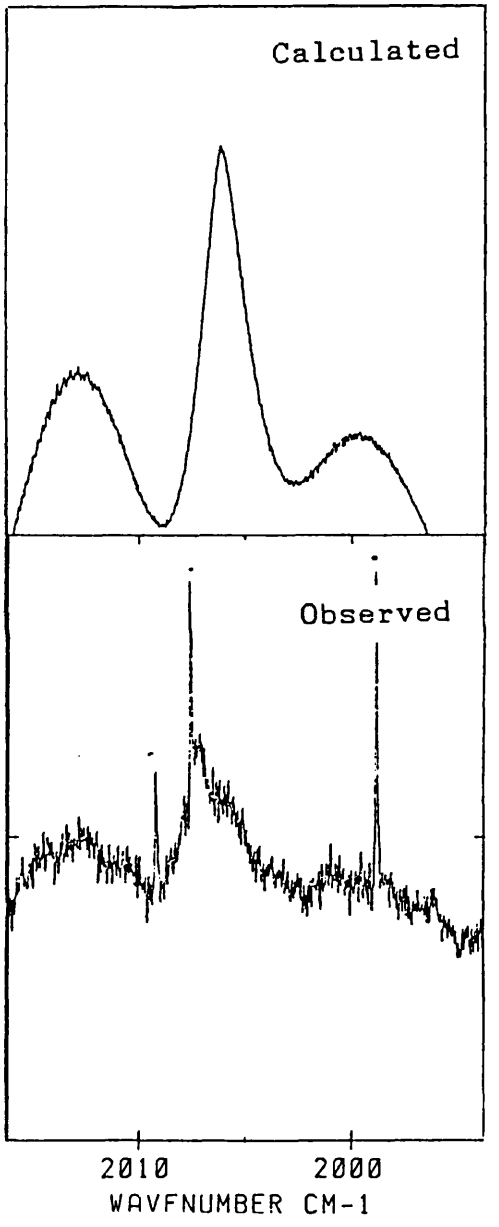

Figure 3.17

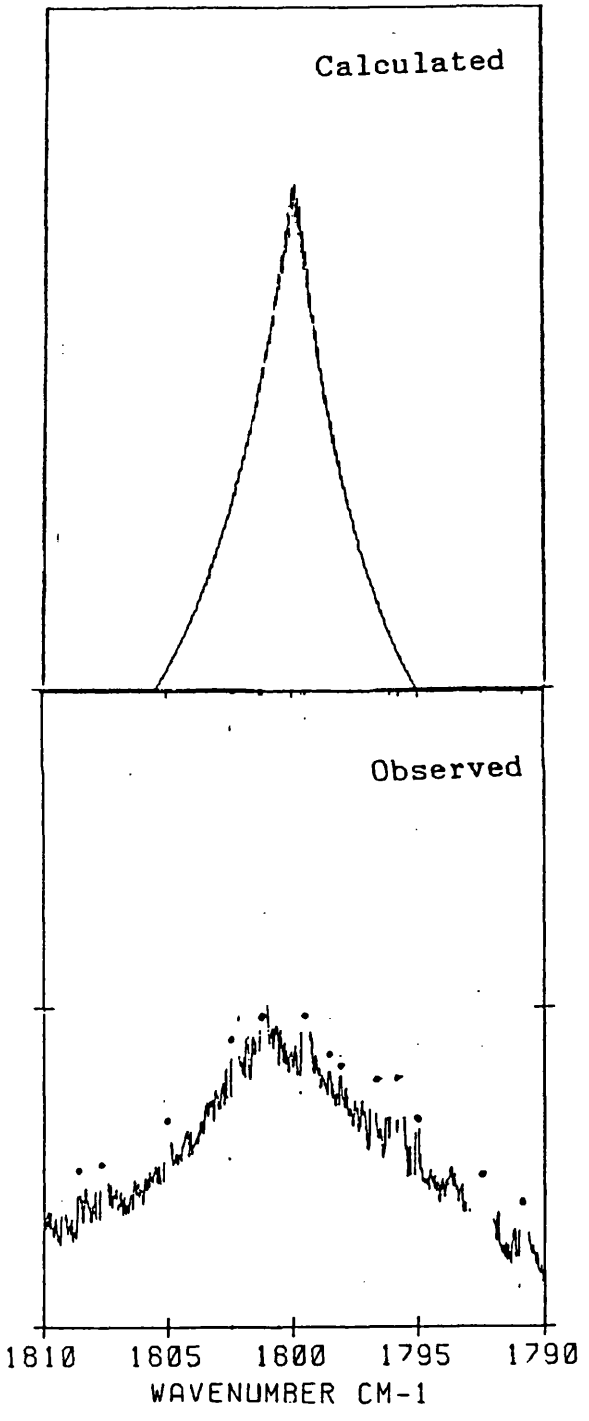

Figure 3.18

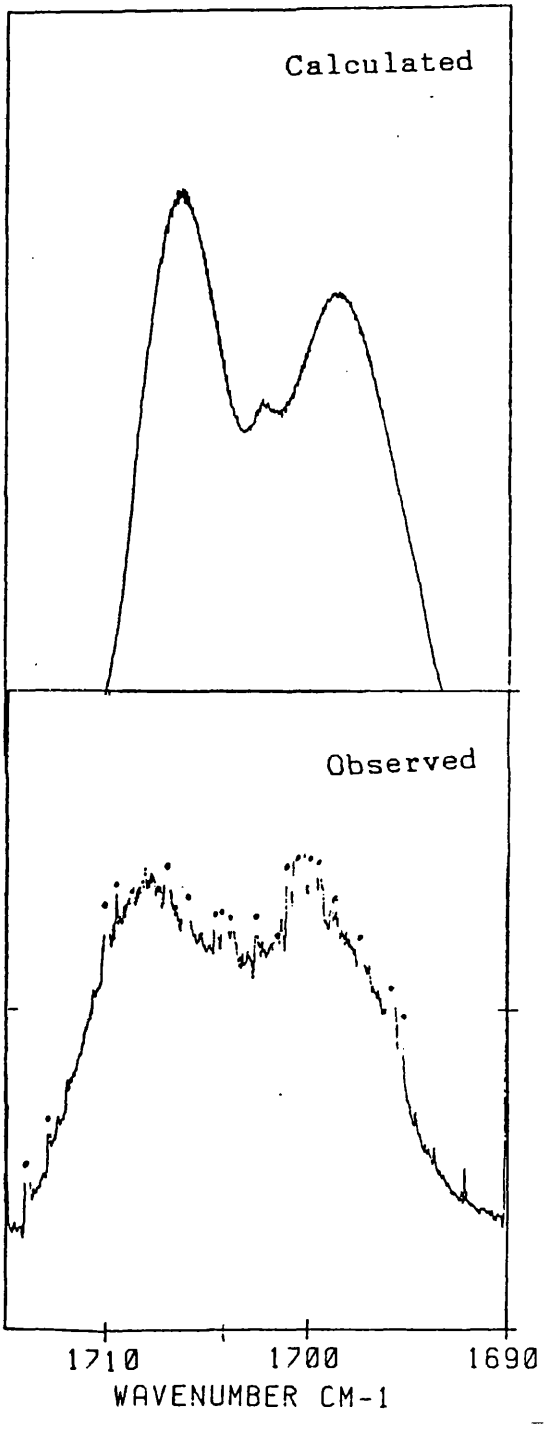

Figure 3.19

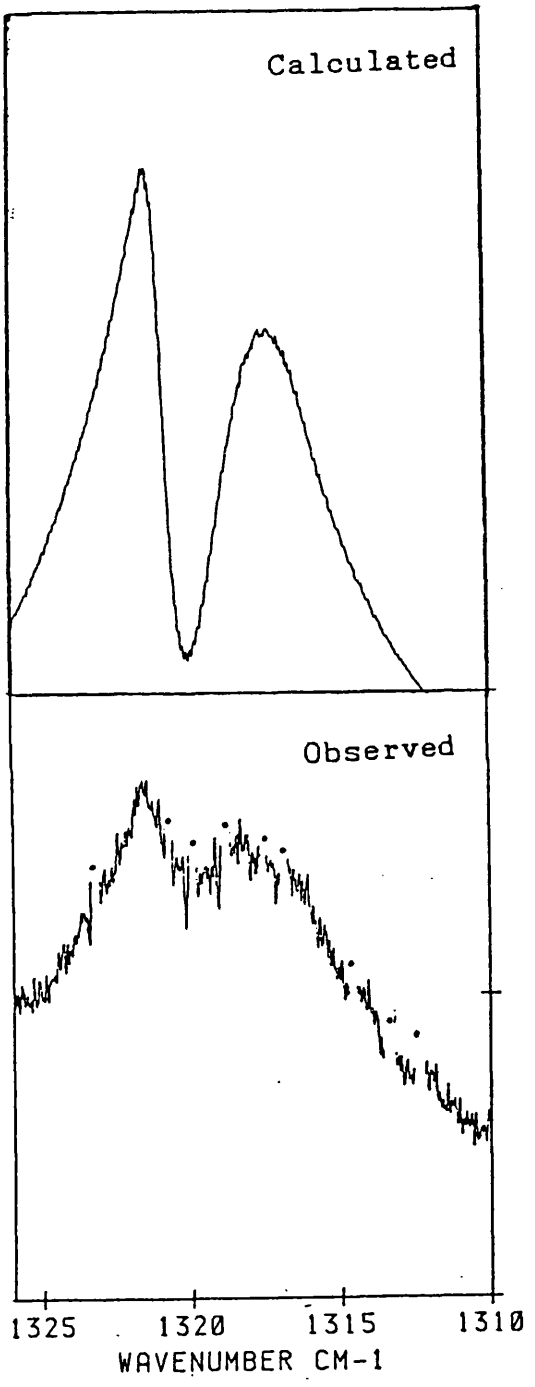

Figure 3.20

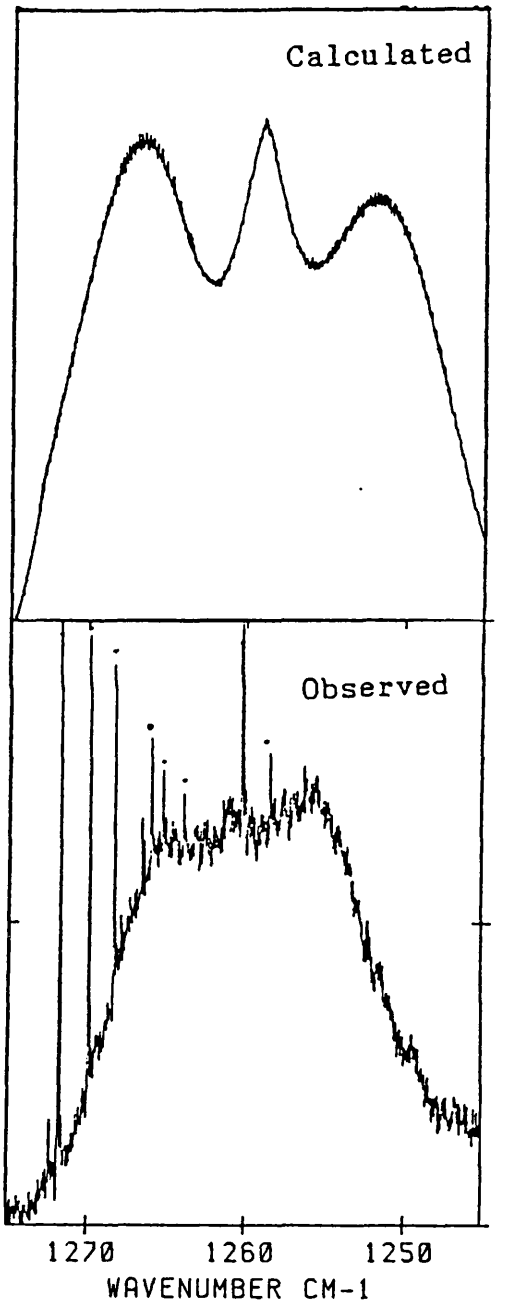

Figure 3.21

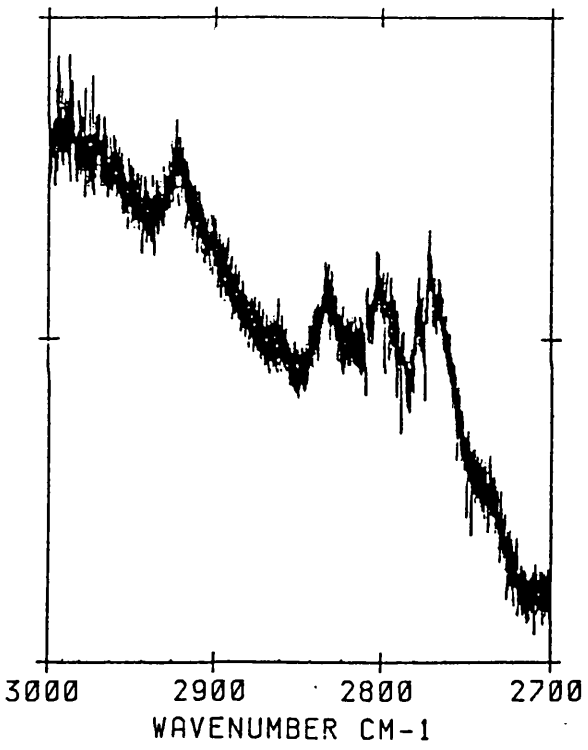

Figure 3.22

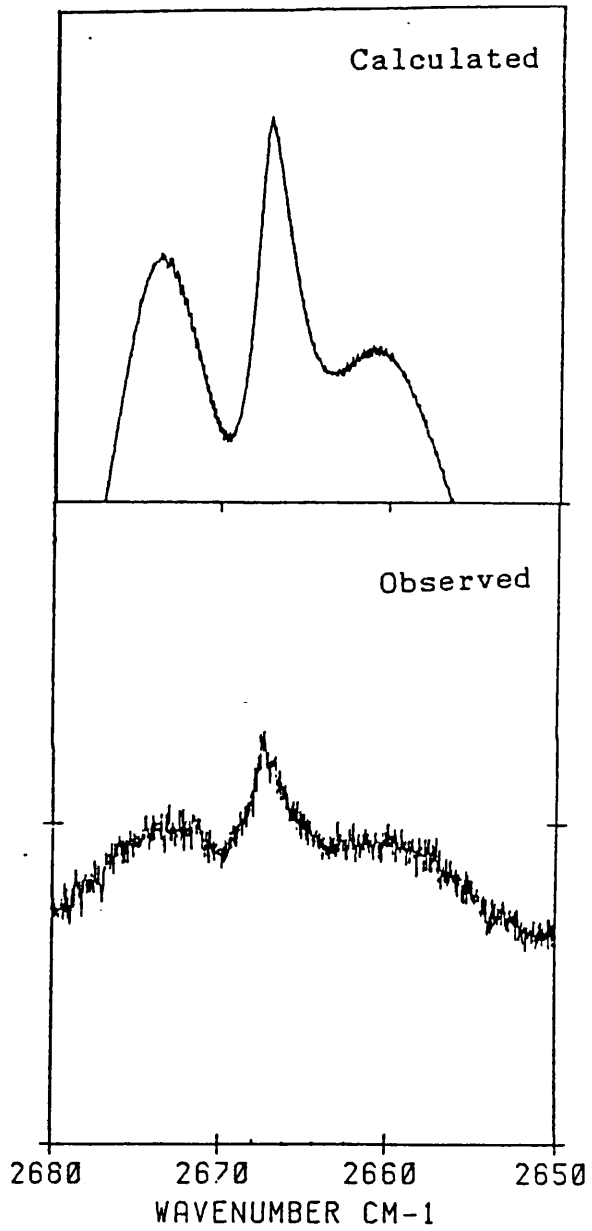

Figure 3.23

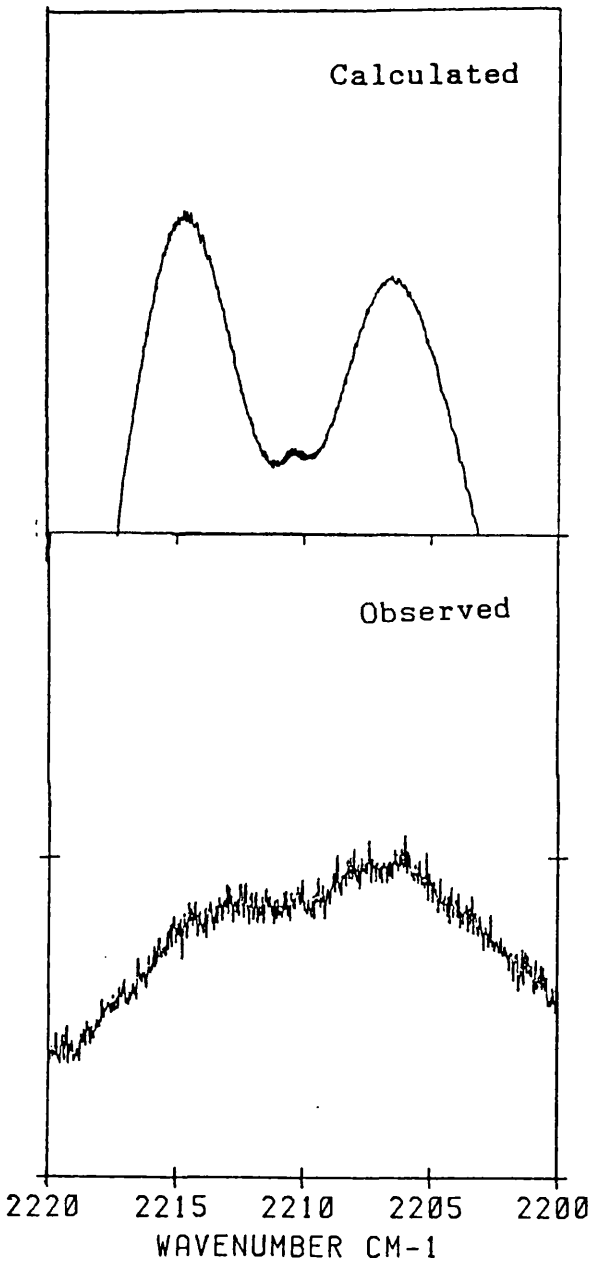

Figure 3.24

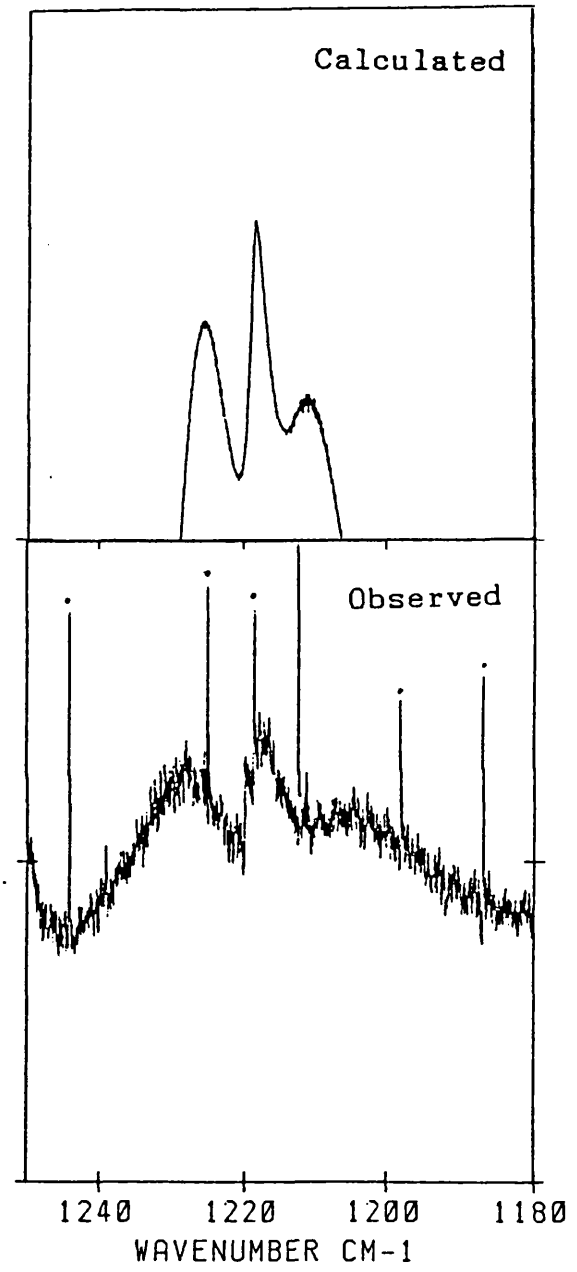

Figure 3.25

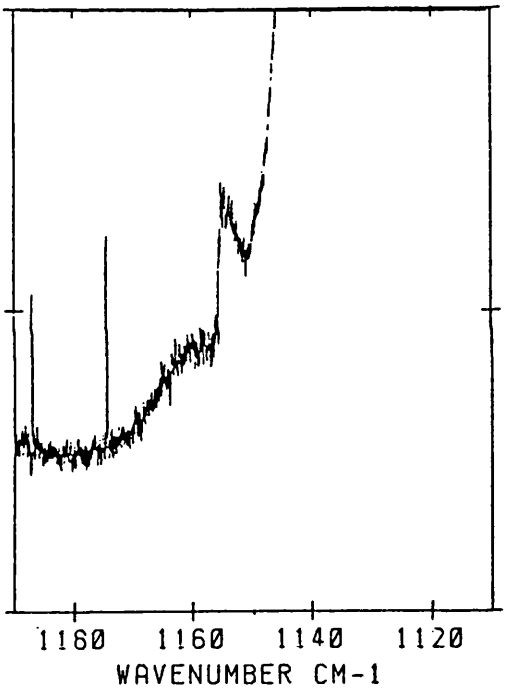

Figure 3.26

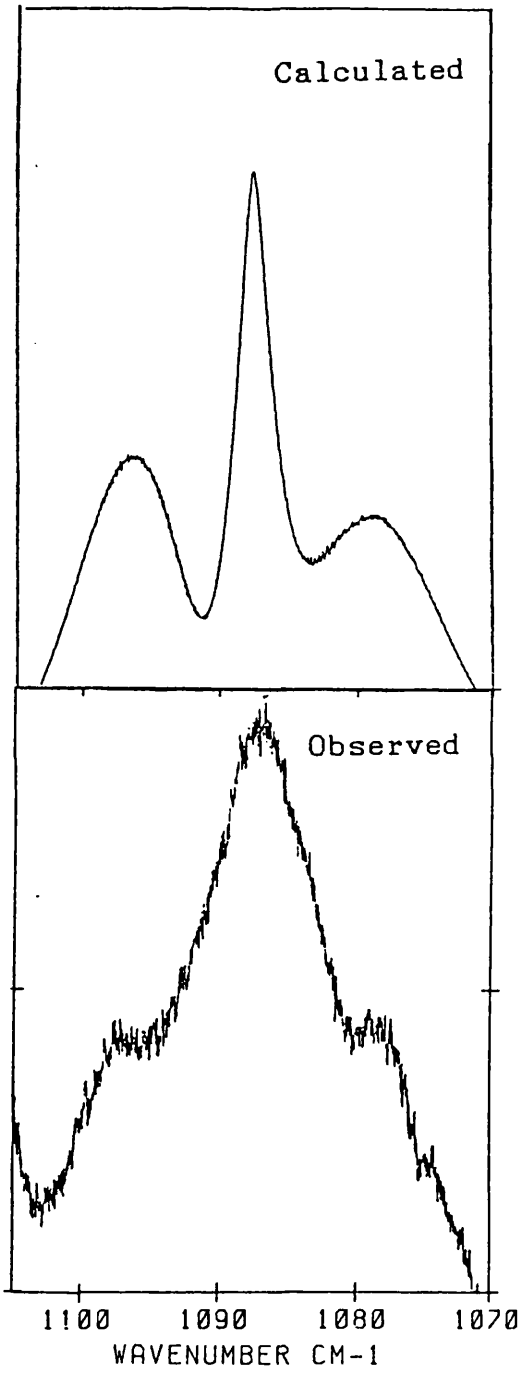

Figure 3.27

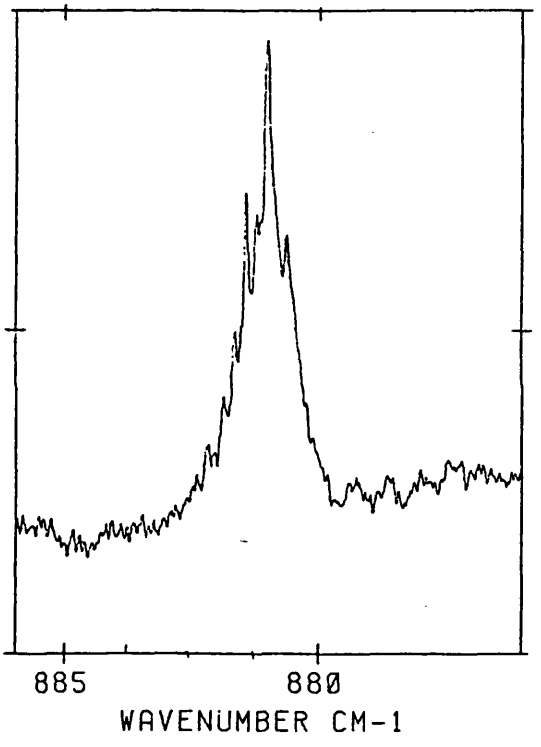

Figure 3.28

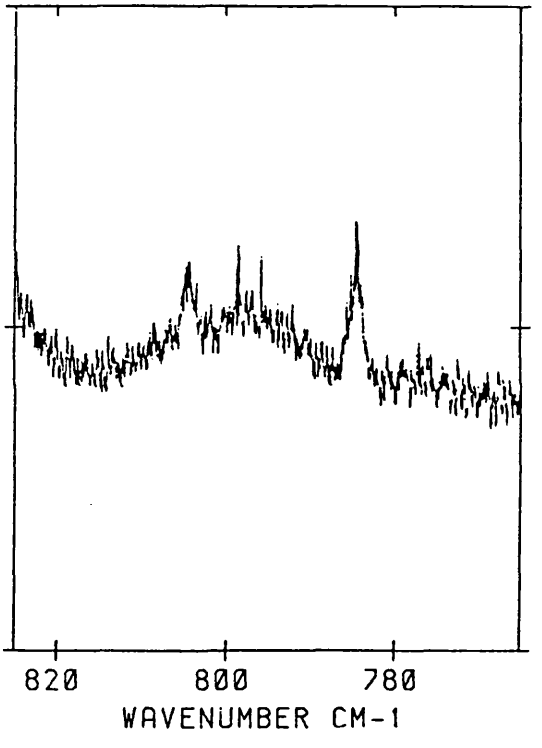

Figure 3.29

Chapter 4

Harmonic Force Field Calculations

For s-Trifluorobenzene

4.1 Introduction

Several reviews of calculations which seek to establish the force fields controlling the normal vibrations of polyatomic molecules have appeared in the literature[33-36]. In these reviews the types of observed data that are needed to determine the force constants as well as the mathematical and computational methods which are used to simpify calculations are included.

The greatest difficulty which is usually encountered in this type of calculations is that the number of force constants is larger than the number of observed data available for their determination. Consequently, the force constants are not well determined by the data. As one might expect, the problem becomes worse with increasing size and decreasing symmetry of a particular molecule. To overcome this problem a number of approximate force fields containing fewer force constants than the General Force Field (G.F.F.) have been proposed. Some of the more important ones are listed below:

α. The Valence Force Field (V.F.F.),
β. The General Valence Force Field (G.V.F.F.),
γ. Several Modified Valence Force Fields(M.V.F.F.),
δ. The Central Force Field (C.F.F.),
ε. The Urey-Bradley Force Field (U.B.F.F.),
$\sigma\tau$.The Local Symmetry Force Field (L.S.F.F.),
ζ. The Hybrid Orbital Force Field (H.O.F.F.).

4.2 The Calculation Of Force Constants

The vibrational secular equation is solved using the so called GF method[37]. There are several textbooks[38] which describe the detailed method involved in the force constant calculations. The whole procedure may be divided into the following steps:

First step: The choice of internal coordinates (e.g. stretching, bending etc.) is made. Usually the number of internal coordinates is different from the number of internal degrees of freedom. This leads to a number of redundancies which increases as the molecular dimension increases.

Second step: The G matrix (the kinetic energy matrix) which has a mxm dimension (where m is the number of internal coordinates) is constructed. This can be done using several standard procedures which are widely available. If redundancies are included, then the G matrix is singular (i.e. G^{-1} does not exist). This leads to m-(3N-6) zero roots in the secular equation. N of course is the number of atoms in the molecule.

Third step: The F matrix, the potential energy matrix, also of dimension mxm, is constructed. For the case of an approximate force field, a new vector $\bar{F}$ is constructed which consists of the elements of the upper triangular part of the F matrix. This can be accomplished using the following relationship:

$$\bar{F} = Z.\Phi \qquad (4.1)$$

where Z is a matrix with non-zero elements only in the rows corresponding to non-zero F matrix elements
and Φ is a vector of the non-zero force constants required by the chosen approximate force field.

Fourth step: The F and G matrices are symmetrized to reduce computational time using the symmetry coordinates. The transformation from internal to symmetry coordinates may be expressed as follows:

$$S = U.s \qquad (4.2)$$

where S is the symmetry coordinates vector,
U is a unitary matrix
and s is the internal coordinates vector.
Then, the F and G matrices are symmetrized as follows:

$$F = U.F.U^{T}$$

$$G = U.G.U^{T} \qquad (4.3)$$

This leads to the factorization of the secular equation in internal coordinates into a number of secular equations of smaller dimension, which can be expressed as:

$$G^{a}.F^{a}.L^{a} = L^{a}.\Lambda^{a} \qquad (4.4)$$

where G^{a} is the block of the G matrix which belongs to the Γ^{a} irreducible representation,
F^{a} is the corresponding F matrix block,
L^{a} is the eigenvector matrix which belongs to the same representation
and Λ^{a} is the corresponding eigenvalue matrix.

Fifth step: The secular equation is solved using some numerical method available for the calculation of the eigenvectors and eigenvalues of a matrix.

Sixth step: The Potential Energy Distribution (P.E.D.) can be calculated. This gives information on the contribution of each force constant to the normal frequencies of vibrations. This can be done using the following relatioship:

$$P.E.D. = \Lambda^{-1}.J.F \qquad (4.5)$$

where J is the Jacobian matrix whose form is widely available in the literature.

Seventh step: The cartesian displacements of the atoms of a molecule in a normal vibration are calculated. They are given by the following relationship:

$$T = M^{-1}.\tilde{B}.F.L.\Lambda^{-1} \qquad (4.6)$$

where B is the matrix used to transform the internal coordinates to the cartesian ones.

The ith coordinate of the T matrix gives the atomic displacements for a unit displacement of the normal coordinate Q_i.

Eighth step: The Coriolis constants are calculated using the following relationship:

$$\zeta^{\alpha} = T^{T}.M^{1/2}.M^{\alpha}.M^{1/2}.T \qquad (4.7)$$

where σ = x,y,z,
ζ^{σ} are the Coriolis constants,
T is the diagonal matrix of the eigenvalues of G,
M is a diagonal matrix whose elements are the atomic masses
and M^{σ} are auxiliary matrices[14].

Ninth step: The centrifugal distortion constants are calculated. In general, the observed distortion constants are related to the so called τ constants which are in turn directly related to the elements of the inverse F matrix. These constants are calculated as follows:

$$\tau_{\alpha\beta\gamma\delta} = \frac{1}{2I^{o}_{\alpha\alpha}I^{o}_{\beta\beta}I^{o}_{\gamma\gamma}I^{o}_{\delta\delta}} \sum_{k,l} J^{k}_{\alpha\beta}(F^{-1})_{kl}J^{l}_{\gamma\delta} \qquad (4.8)$$

where $I_{\alpha\alpha} = \sum_i m_i(\beta^2+\gamma^2)$ etc. , $I_{\alpha\beta} = -\sum_i m_i\alpha_i\beta_i$ etc.

$$J^{k}_{\alpha\alpha} = \left(\frac{dI_{\alpha\alpha}}{ds_k} \right)_o = 2 \sum_i m_i \left(\beta_i \frac{d\beta_i}{ds_k} + \gamma_i \frac{d\gamma_i}{ds_k} \right)$$

$$J^{k}_{\alpha\beta} = \left(\frac{dI_{\alpha\beta}}{ds_k} \right)_o = - \sum_i m_i \left(\alpha_i \frac{d\beta_i}{ds_k} + \beta_i \frac{d\alpha_i}{ds_k} \right)$$

$$\left(F^{-1}\right)_{kl} = \sum_i \lambda_i^{-1} L_{ki} L_{ir}$$

s_k, s_l denote internal or symmetry coordinates
and α, β, γ, δ, are the cartesian coordinates.

For planar symmetric rotor molecules, the three centrifugal distortion constants D_J, D_{JK}, D_K are linear combinations of only four τ's, namely τ_{xxxx}, τ_{zzzz}, τ_{xxyy}, τ_{xzxz}[30]. This can be simplified further to yield the following relationships:

$$D_J = -1/4\ \tau_{xxxx}\hbar^4$$

$$D_{JK} = 1/2\ (\tau_{xxxx}-2\tau_{zzzz})\hbar^4$$

$$D_K = -1/4(\tau_{xxxx}-3\tau_{zzzz})\hbar^4 \qquad (4.10)$$

In the above relationships the symmetry axis, which is perpendicular to the plane of the molecule was chosen as the z axis. It has been found[30,31], that the following relationships exist between the centrifugal distortion constants of a planar symmetric rotor molecule:

$$D_{JK} \approx 2D_J\ [(C_e/B_e)^4-1] \approx -1.875D_J$$

$$D_K = -\ [1/2D_J + 3/4D_{JK}] \qquad (4.10)$$

Thus, if one of the three distortion constants for a planar symmetric rotor molecule can be determined, the above equations can be used to find the approximate values of the other two.

Tenth step: The force constants are refined using some iterative method. This step is analysed in more detail in the next section.

4.3 The Refinement Of The Force Constants

The process of the refinement of the force constants can be divided into the following number of steps[39]:

First step: A trial set of force constants is guessed. These are used to calculate the vibrational frequencies, the Coriolis constants and the centrifugal distortion constants. Then, the Jacobian matrix elements of the frequencies, zetas and distortion constants defined as the first term in the Taylor expansion of the calculated data with respect to each force constant, are calculated. These can be defined as follows:

$$J = \begin{bmatrix} J_\lambda \\ J_\zeta \\ J_D \end{bmatrix} \qquad (4.11)$$

Second step: The error vector is formed. This can be denoted as follows:

$$\varepsilon = \begin{bmatrix} \varepsilon_\lambda \\ \varepsilon_\zeta \\ \varepsilon_D \end{bmatrix} \qquad (4.12)$$

Thus, the Jacobian matrix is used to set up linear equations relating the first order changes in the force constants (δF) to the consequent small changes in all the calculated data which

is identified with the error vector, i.e.

$$J.\delta F = \varepsilon \qquad (4.13)$$

Third step: A residual vector is formed which can be expressed as follows:

$$r = J.\delta F - \varepsilon \qquad (4.14)$$

Then, the solution δF which minimises the sum of the weighted squares of residuals is determined. This can be done by forming the normal equations:

$$J'WJ.\delta F = J'W\varepsilon \qquad (4.15)$$

where W is a diagonal matrix of the weights W_i.These are related to the estimated probable error of the observed values by the equation:

$$\sigma_i^2 W_i = \sigma_j^2 W_j = \ldots = \text{constant}\sigma^2 \qquad (4.16)$$

where $\sigma^2$is the variance of an observation of unit weight. The $\sigma^2$is given from the sum of the weighted squares of the residuals:

$$\sigma^2 = r'Wr / (N-M) \qquad (4.17)$$

where N-M is the excess of equations over unknowns. Thus, the solution is obtained as:

$$\delta F = [J'WJ]^{-1}J'W\varepsilon \qquad (4.18)$$

The diagonal elements of $(J'WJ)^{-1}$ give the variance and the best estimates of the force constants:

$$\sigma^2[\bar{F}_i] = [J'WJ]^{-1}_{ii} \cdot \sigma^2 \qquad (4.19)$$

and the off-diagonal elements give the correlation coefficients between the $\bar{F}$s:

$$\rho[\bar{F}_i,\bar{F}_j] = [J'WJ]^{-1}_{ij} \cdot \sigma^2/\sigma_i[F_i]\sigma_j[F_j] \qquad (4.20)$$

In the case where a Φ vector is used, the previous equations are transformed as follows[40]:

$$\delta F = Z\delta\Phi = Z(Z'J'WJZ)^{-1}Z'J'W\varepsilon$$

$$\sigma^2(\Phi_i) = (Z'J'WJZ)^{-1}_{ii} \cdot \sigma^2$$

$$\sigma^2(\bar{F}_i) = [Z(Z'J'WJZ)Z^{-1}]_{ii}\sigma^2 \qquad (4.21)$$

Fourth step: The δFs which are determined from the previous equation are used to form a new set of force constants

$$F(new) = F(old) + \delta F \qquad (4.22)$$

Then, the whole cycle is repeated a preset number of times. Usually 7 to 8 cycles are sufficient for the $\delta F \approx 0$, i.e. for the calculation to have converged.

4.4 Mathematical Difficulties in Force Field Calculations

There are three main mathematical difficulties which arise in force field calculations[39], namely

α. Non-linearity

β. Singularity

γ. Multiple Solutions.

α. Non-linearity: If the initial F matrix is not a good guess, the errors ε and the corrections δF will contain some relatively large elements and the relationship

$$J.\delta F = \varepsilon$$

will not hold. This will also happen if some elements of J are very sensitive to changes in the force constants. This is usually observed as oscillations in the calculation. This can be avoided by adding only 1/2 δF for the first few cycles of the calculation increasing it until it reaches 1 in the final cycle.

β. Singularity: If the matrix $[J'WJ] \approx$ singular large rounding errors may occur in taking its inverse causing corresponding errors in the calculated corrections δF. This in general means that the original data do not suffice to fix the force field. An easy way to detect this is by observing the diagonal elements of the $[J'WJ]^{-1}$ matrix. If at least one diagonal element of the matrix becomes unusually large, it will lead to a corresponding large uncertainty in at least one of the force constants. If this is indeed the case then either further data must be added or the force field must be constrained in some way.

γ. Multiple Solutions: There may be several distinct solutions to the force field which fit all the available data satisfactorily. The likelihood of this occurrence generally decreases with increasing variety in the type of the experimental data used. If two or more solutions are found, it may be necessary to choose between the possible solutions on physical and chemical grounds.

4.5 Planar Normal Coordinates For s-Trifluorobenzene

The planar normal vibrations of s-trifluorobenzene are distributed among the irreducible representation as follows:

$$\Gamma(Q_v, \text{planar}) = 4a_1' + 3a_2' + 7e'$$

It is obvious that the problem is more complicated than the corresponding one for benzene[58-60]. This is mainly due to the fact that the blocks into which the planar vibrational secular determinant factorises are larger than the corresponding ones for benzene. There are 11 ($4a_1'$ + $7e'$) assigned fundamental frequencies and three uncertain ones ($3a_2'$) for each isotopic species. This indicates that the G.F.F. is seriously underdetermined due to the fact that there is a total of 44 independent symmetry force constants controlling the planar vibrations in it. So it is not surprising that there are only two published planar force field calculations. The earlier one[23] was a M.U.B.F.F. calculation published in 1962. In 1973, another force field calculation was published[29] which was a part of a general study of fluoro derivatives of benzene using the overlay technique. The authors of the above calculations did

not evaluate normal coordinates or centrifugal distortion constants from their force fields. However, in more recent papers[27,28], calculated Coriolis constants have been quoted, derived from the second force field.

One of the aims of the present investigation was the derivation of a model force field for the planar vibrations for s-trifluorobenzene and also the computation of normal coordinates and Cartesian displacements, which have not been reported before.

4.6 The Secular Equation

The equilibrium geometry of s-trifluorobenzene has been found to be as follows[29]:

$R_{\emptyset}$ (C-C) = 1.397Å

$r_{\emptyset}$ (C-H) = 1.Ø84Å

$l_{\emptyset}$ (C-F) = 1.327Å

It was also assumed that s-trifluorobenzene is a regular hexagonal ring. The definitions of the internal displacement coordinates are given in Table 4.1. In constructing the planar symmetry coordinates from the given set of internal coordinates, redundancies are introduced into the a_1' and e´ blocks. An explanation of the procedure for removing the redundancies follows:

α. Non-Degenerate species: For the totally symmetric species, the removal of the redundancy is done following

the relationship[37]:

$$\sum_i \alpha_i = \emptyset$$

The primitive symmetry coordinates are:

$$S_4' = (\alpha_1 + \alpha_2 + \alpha_3)$$

$$S_5' = (\gamma_1 + \gamma_2 + \gamma_3)$$

Hence,

$$\begin{bmatrix} S_4 \\ S_R \end{bmatrix} = \begin{bmatrix} -1 & 1 \\ 1 & 1 \end{bmatrix} \cdot \begin{bmatrix} S_4' \\ S_5' \end{bmatrix}$$

Therefore, the redundancy can be removed by the above orthogonal transformation where S_R is the redundant coordinate, identically equal to zero, and S_4 is the symmetry coordinate which is used in Table 4.2.

β. Degenerate species: The removal of the redundancy for the degenerate species is of a very complicated form if one assumes a geometry different from a hexagonal one. But, if 120° bond angles are assumed, the redundancy adopts a much simpler

form. The primitive symmetry coordinates are:

$$S'_{13a} = 6^{-1/2}(-\alpha_1 + 2\alpha_2 - \alpha_3)$$

$$S'_{13b} = 2^{-1/2}(\alpha_1 - \alpha_3)$$

$$S'_{15a} = 6^{-1/2}(2\gamma_1 - \gamma_2 - \gamma_3)$$

$$S'_{15b} = 2^{-1/2}(-\gamma_2 + \gamma_3)$$

Then, the following linear combinations are formed:

$$S_{13a} = S'_{15a} + S'_{13a}$$

$$S''_{15a} = S'_{13a} - S'_{15a}$$

$$S_{13b} = S'_{15b} + S'_{13b}$$

$$S''_{15b} = S'_{13b} - S'_{15b}$$

Then, the usual orthogonal transformation is applied:

$$\begin{bmatrix} S_{14a} \\ S_R \end{bmatrix} = 2^{-1/2} \begin{bmatrix} 1 & -1 \\ 1 & 1 \end{bmatrix} \cdot \begin{bmatrix} S_{12a} \\ S''_{15a} \end{bmatrix}$$

$$\begin{bmatrix} S_{14b} \\ S_R \end{bmatrix} = 2^{-1/2} \begin{bmatrix} 1 & -1 \\ 1 & 1 \end{bmatrix} \cdot \begin{bmatrix} S_{12b} \\ S''_{15b} \end{bmatrix}$$

where the S_R is again the reduntant coordinate. It should also be stressed at this point that the S_{13} symmetry coordinate is a combination of two primitive symmetry coordinates.

The symmetry coordinates, which were constructed specifically for this study but can also be used for related molecules (eg. s-trichlorobenzene etc.), are listed in Table 4.2.

4.7 Symmetry Force Constants

The symmetry force constants were constructed using the method developed by Wilson, Decius and Cross[27] . In general, the rule for the diagonal constants is as follows:

Multiply the force constant in the first row and in the column labelled by a given internal coordinate by the coefficient with which that internal coordinate appears in the symmetry coordinate. Then divide by the coefficient of the first internal coordinate (row label). Do this for each column and all the results.

Whereas, for the off-diagonal constants the rule is as follows:

Multiply the force constant in the first row and in the column labelled by a given internal coordinate by the coefficient with which that internal coordinate appears in the symmetry coordinate. Then divide by the coefficient of the first internal coordinate of the other set (row label). Do this for each column and add.

The internal force constants are listed in Table 4.3. The symmetry force constants derived from the internal force constants are listed in Table 4.4. These were constructed specifically for the present study, but can also be used for related molecules (eg. s-trichlorobenzene etc.).

4.8 Observed Data

The observed data are summarised in Tables 4.5 and 4.6. The fundamental frequencies, Coriolis constants and centrifugal distortion constants were not corrected for any anharmonic effects. It was expected that because of the great variety of data used that there would be an improvement in the possibility of determining an acceptable force field. However, the main problem still remains, namely, that the number of observables is not sufficient to determine a unique solution for the G.F.F. The situation is summarised as follows:

Symmetry Species	Number of independent parameters in G.F.F.	Number of observables
A_1'	F_{11}, F_{21}, F_{22}, F_{31}, F_{32}, F_{33}, F_{41}, F_{42}, F_{43}, F_{44} Total = 10	8 $\bar{\nu}$s Total = 8
A_2'	F_{55}, F_{65}, F_{66}, F_{75}, F_{76}, F_{77} Total = 6	Total = 0
E'	F_{88}, F_{98}, F_{99}, F_{108}, F_{109}, F_{1010}, F_{118}, F_{119}, F_{1110}, F_{1111}, F_{128}, F_{129}, F_{1210}, F_{1211}, F_{1212}, F_{138}, F_{139}, F_{1310}, F_{1311}, F_{1312}, F_{1313}, F_{148}, etc. until F_{1414} Total = 28	14 $\bar{\nu}$s 11 ζs Total = 25
Total	44	(+3Ds)= 36

4.9 Results And Discussion.

A model force field of 19 parameters was used in the case of the planar vibrations of s-trifluorobenzene to see how well the five e´ fundamental modes , four Coriolis coupling constants and centrifugal distortion constants measured in this study, were reproduced.

The calculated values for the observed data, the internal force constants, the symmetry force constants and the normal coordinates are given in Tables 4.5 to 4.11.

The pictorial representation of the Cartesian displacements for each normal mode for s-trifluorobenzene $-h_3$ and $-d_3$ are given in Figures 4.1 and 4.2. The program which was used to construct these pictorial representations is given in Appendix 2. The program ASYM2Ø, which is described in Appendix 3, was used in all our calculations.

The starting values for the internal force constants were taken from the literature[29]. It is obvious, from Tables 4.5 and 4.6 that the observed frequencies, Coriolis coupling constants and centrifugal distortion constants are reproduced reasonably well within the limits of the assumed experimental uncertainties, in almost all of the cases. A more detailed analysis of the individual internal force constants used in the construction of the model force field follows:

D: This corresponds to the carbon stretching diagonal constant. The value that was derived as a result of the refinement procedure in this study is about the same as the one obtained by Eaton and Steele´s 39 parameter force field[29] for the planar vibrations of benzene and various fluorobenzenes. At this point, it should be noted that

slight and in some cases even relatively major discrepancies between the values for the internal force constants in this study and the 39 parameter force field are to be expected due to the following reasons:

α. A different model force field was used.

β. A different variety of observed data was used. That is, only vibrational frequencies from various fluorobenzenes were included. In a later study[27], Coriolis constants calculated from a modified version of the above mentioned force field were quoted , without any indication of the changes that these extra data will have in the independent internal force constants.

E: This refers to the hydrogen stretching diagonal constant. The value that was calculated in this study is of the same order of magnitude as in the 39 parmeter force field[27].

E^F: This corresponds to the fluorine stretching diagonal constant. Once again, the value that was obtained did not contradict the similar one in the 39 parameter force field[29].

F: This is the diagonal constant due to carbon bending where the central carbon atom is attached to a hydrogen atom. This time the value which was obtained is about one third the corresponding one in Eaton and Steele's field[29].

F^F: This diagonal constant corresponds to a carbon bending

where the central carbon atom is attached to a fluorine atom. This time the value which was derived is twice the value of the 39 parameter force field[29].

G: This refers to a carbon-hydrogen bending diagonal constant. The value obtained was about the same as in Eaton and Steele's field[29].

G^F: This corresponds to a carbon-fluorine bending diagonal constant. The value that was obtained was significantly higher than the corresponding one in the 39 parameter force field[29].

d: This is a constant representing the interaction between two carbon stetchings. d can be defined as follows:

$$d = d_o = -d_m = d_p \qquad (4.23)$$

It was introduced by Scherer and Overend[41] and was supported by Duinker and Mills[42]. It is called the 'Kekule' assumption'. The arguments about the sign relationship among the above parameters are basically as follows:

According to the 'Kekule' assumption' a benzene-like molecule exists in the following two forms:

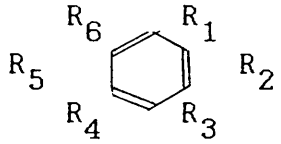

1st form

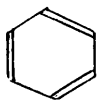

2nd form

A positive displacement in R_1 will tend to localise the π electrons in the 1st 'Kekule' form'. The sign of the interaction constant d_o arises after considering that part of the potential function which depends on R_1^2 and R_2^2 :

$$2V = DR_1^2 + 2d_oR_1R_2 + DR_2^2 \qquad (4.24)$$

After differentiating with respect to R_1 and making the result equal to zero at the new maximum, we have:

$$dV/ dR_1 = 2DR_1 + 2d_oR_2 = 0 \Rightarrow$$

$$d_o = -DR_1/ R_2 \qquad (4.25)$$

From equation (4.25) it follows that $d_o > 0$ since $R_1/ R_2 < 0$. Similar arguments can be employed to show that $d_m < 0$ and $d_p > 0$.

In the 'Kekule' assumption', it is further assumed that these constants are equal in magnitude. That is, on stretching R_1 the induced double bond character in R_2 is the same as that induced in R_4 and energetically equivalent to the increase in single bond character in R_3. There is not any particular reason why this should be true, but, in our case it was assumed that this is indeed the case.

The value obtained in this study is about the same as the corresponding one in the 39 parameter field[29].

h_o^F: This is the constant corresponding to the interaction of carbon stretching and fluorine stretching in the ortho position. The value obtained is about the same as the one obtained from the 39 parameter force field[29].

i_o: This constant corresponds to the interaction between carbon stretching and carbon bending with a hydrogen atom attached to the central carbon atom, in the ortho position. The value derived from the present study was twice the value obtained by Eaton and Steele[29].

j_o: This refers to the interaction between carbon stretching and carbon-hydrogen bending, in the ortho positon. The value produced in this study was again almost twice the value quoted by Eaton and Steele[29].

j_o^F: This refers to the interaction between carbon stretching and carbon-fluorine bending , in the ortho position. Again, our value is about twice the value quoted by Eaton and Steele[29].

j_m^F: This corresponds to the force constant relating to the interaction of the same two coordinates but in the meta position. The constant derived has the same negative sign as the value quoted in the literature but it is three times as large.[29]

k^F: This constant corresponds to the interaction between carbon-fluorine stretching and carbon bending with a fluorine atom attached to the central carbon atom. This time there is complete disagreement between the present field and the 39 parameter force field. In this study a relatively large positive value was obtained while in the 39 parameter force field a large negative value was quoted[29].

n_o^F: This refers to the interaction between carbon bending with a hydrogen atom attached to the central carbon atom and carbon fluorine bending, in the ortho position. The value predicted in the present study is more than twice the one in the literature[29].

$k_o^{F'}$: This corresponds to the interaction between fluorine stretching and carbon bending with a hydrogen atom attached to the central carbon atom. The value predicted in this study is very much larger than the one quoted in the literature[29].

k: This corresponds to the interaction between hydrogen stretching and carbon bending with hydrogen attached to the carbon atom in the central position, in the ortho position. The value calculated here is about four times the one quoted in the literature[29].

g_o^F: This corresponds to the interaction between hydrogen bending and fluorine bending in the ortho position. The value predicted has the opposite sign than the one quoted in the literature[29].

g_p^F: This is the same as above with the two internal coordinates in the para position. This time the negative sign in the internal force constant in this study is the same as the one predicted in the literature[29].

The rest of the internal force constants were constrained to zero. The above internal force constants were chosen because of the relative large values associated with them in the literature[29]. Initially, some of them were constrained to certain plausible values until a satisfactory fit was achieved. In the next stage, all the internal force constants associated with s-trifluorobenzene in the 39 parameter force field were included. This led to the construction of a 27 parameter force field. It is obvious that this number of parameters is too large compared with the number of observed data. Therefore, some of the parameters were constrained to zero beginning with h_o, h_m^F and h_p^F .These three internal force constants were chosen because it had been predicted in the 39 parameter field that their values would be close to zero. This was found to be true in the present analysis.

The removal of the three parameters led to the construction of a 24 parameter force field which was found to be ill-conditioned, when all of the parameters were allowed to vary. After constraining several parameters to zero and allowing the rest to vary, the present 19 parameter force field was constructed. It should be noted that further force constant adjustment calculations were tried applying different constraints to individual parameters in an attempt to find best values for the internal force constants, but a more satisfactory solution could not be found. However, due to the essential complexity and underdeterminacy of this problem, this solution is regarded as a possible solution rather than the best one.

4.10 Out-Of-Plane Normal Coordinates For s-Trifluorobenzene

The out-of-plane normal vibrations of s-trifluorobenzene are distributed among the irreducible representation as follows:

$$\Gamma(Q_v, \text{ non-planar}) = 3a_2'' + 3e''$$

In this case, there are 6 ($3a_2'' + 3e''$) assigned fundamental frequencies for each isotopic species. Because of the fact that there is a total of 12 independent symmetry force constants controlling the out-of-plane vibrations in it, the force field seems to be well behaved even though only a total of seven internal symmetry constants was used.

There are two published out-of-plane force field calculations. In 1952, the earlier one was published[43] which was carried out with the purpose of finding out the value of the highest e'' fundamental. In 1962[23], a 7-parameter V.F.F. calculation similar to ours was carried out. One of the aims of the present investigation was the computation of out-of-plane normal coordinates for s-trifluorobenzene which have not been reported before.

The internal coordinates are defined in Table 4.12. The symmetry coordinates which were essentially the same as the ones used before[43] and also the internal force constants and the symmetry force constants are listed in Tables 4.13, 4.14, 4.15 respectively. A notation consistent with the one used for the planar vibrations problem was adopted. All the calculations were carried out with the ASYM20 program which is described in Appendix 3.

The number of observables compared with the number

of independent parameters of the G.F.F. are summarised next.

Symmetry Species	Number of independent parameters in G.F.F.	Number of observables
A_2''	F_{11}, F_{21}, F_{22}, F_{31} F_{31}, F_{32}, F_{33} Total = 6	6 $\bar{\nu}$s Total = 6
E''	F_{44}, F_{54}, F_{55}, F_{64} F_{64}, F_{65}, F_{66} Total = 6	6 $\bar{\nu}$s Total = 6
Total	12	12

4.11 Results And Discussion

A model force field of 7 parameters was used to see how well our two more accurately measured a_2'' frequencies were reproduced. The calculated values for the frequencies, the internal force constants, the symmetry force constants and the normal coordinates are given in Tables 4.16 to 4.21. The starting values for the internal force constants were taken from the literature[23].

As it is obvious from Tables 4.16 and 4.17, the observed frequencies are reproduced quite well. However, there are some discrepancies between our calculated symmetry force constants and the ones quoted in the literature. The symmetry force constants values attributed to Scherer, Evans and Muelder[23] were calculated using the values for their internal force constants. A more detailed analysis of the situation follows:

H: This corresponds to the fluorine bending diagonal constant. The value that was obtained as a result of our refinement process is about three times the value quoted by Ferguson[43] and twice the value quoted by Scherer [23].

A: This corresponds to the hydrogen bending diagonal constant. Our value is of about the same order of magnitude as the other one quoted in the literature[23]. Ferguson[43] transferred the corresponding force constant from benzene[44].

B: This corresponds to the carbon torsional diagonal constant. Again our value is of about the same order of magnitude as Scherer's[23]. Ferguson[43] did not use any value for the B constant. Instead, he transferred the symmetry force constant in which B is involved from benzene.

$\bar{a}_o$: This internal force constant corresponds to the interaction between a fluorine bending and a hydrogen bending in the ortho position. The values quoted in the literature[23,43] together with our value all agree with respect to the negative sign of the constant. But our absolute value is about three to four times higher than the ones quoted in the literature.

b_o: This corresponds to the interaction between two carbon torsions in the ortho position. No value is quoted by Ferguson[43]. He again transferred the relevant symmetry force constant from benzene. The value quoted by Scherer[23] is of the same absolute order of magnitude as ours. However, they differ

with respect to the signs, ours being negative.

$\bar{c}_o$: This constant corresponds to the interaction between a fluorine bending and a carbon torsion in the ortho position. Once again no value is quoted by Ferguson[43], who either transferred the relevant force constant from benzene (F_{32} and F_{64}) or constrained it to zero (F_{31} and F_{65}) . He also assumed that $\bar{c}_o \approx c_o$ which is equivalent to the assumption that the interaction between a fluorine motion out of the plane and a non-planar ring deformation is equal to the interaction between a hydrogen motion out of the plane and a non-planar ring deformation. The value quoted by Scherer[23] is about half our value.

c_o: This is an internal force constant which corresponds to an interaction between a fluorine bending motion and a carbon torsion in the ortho position. The value quoted by Scherer[23] once again is slightly lower than ours.

Due to the fact that both Scherer's force field[23] and ours reproduce the experimental frequencies reasonably well, the discrepancies in the values of the internal force constants are thought to arise from two reasons:

1. Due to the indeterminacy of the problem.

2. Due to the fact that different basic sets may have been used.

In view of the above sources of uncertainty, we consider our solution to be one of a whole family of alternative solutions rather than the unique one.

Table 4.1

Definition Of Internal Displacement Coordinates
For s-Trifluorobenzene

r_i	increase in length of C_i-H_i bond
l_i	increase in length of C_i-F_i bond
R_i	increase in length of C_i-C_{i+1} bond
α_i	increase in C_{i-1}-C_i(H)-C_{i+1} angle
γ_i	increase in C_{i-1}-C_i(F)-C_{i+1} angle
β_i	C_i-H_i bend, increase in angle between C_i-H_i and external bisector of C_{i-1}-C_i(H_i)-C_{i+1}; positive when H_i moves towards C_{i-1}.
ω_i	C_i-F_i bend, increase in angle between C_i-F_i and external bisector of C_{i-1}-C_i(F_i)-C_{i+1}; positive when F_i moves towards C_{i-1}.

Table 4.2
Symmetry Coordinates For s-Trifluorobenzene

Γ	S_i	1	2	3	4	5	6	N	s_i
A_1'	S_1	1	1	1	-	-	-	$3^{-1/2}$	r_i
	S_2	1	1	1	-	-	-	$3^{-1/2}$	l_i
	S_3	1	1	1	1	1	1	$6^{-1/2}$	R_i
	S_4	1	1	1	-	-	-	$6^{-1/2}$	$R_\emptyset\gamma_i$
		-1	-1	-1	-	-	-		$R_\emptyset\alpha_i$
A_2'	S_5	1	-1	1	-1	1	-1	$6^{-1/2}$	R_i
	S_6	1	1	1	-	-	-	$3^{-1/2}$	$r_\emptyset\beta_i$
	S_7	1	1	1	-	-	-	$3^{-1/2}$	$l_\emptyset\omega_i$
E'	S_{8a}	-1	2	-1	-	-	-	$6^{-1/2}$	r_i
	S_{9a}	2	-1	-1	-	-	-	$6^{-1/2}$	l_i
	S_{10a}	-1	2	-1	-1	2	-1	$12^{-1/2}$	R_i
	S_{11a}	-1	Ø	1	-	-	-	$2^{-1/2}$	$r_\emptyset\beta_i$
	S_{12a}	Ø	1	-1	-	-	-	$2^{-1/2}$	$l_\emptyset\omega_i$
	S_{13a}	2	-1	-1	-	-	-	$12^{-1/2}$	$R_\emptyset\gamma_i$
		-1	2	-1	-	-	-		$R_\emptyset\alpha_i$
	S_{14a}	-1	Ø	1	1	Ø	-1	$2^{-3/2}$	R_i
		2	-1	-1	-	-	-	$24^{-1/2}$	$R_\emptyset\gamma_i$
		1	-2	1	-	-	-		$R_\emptyset\alpha_i$
	S_{8b}	1	Ø	-1	-	-	-	$2^{-1/2}$	r_i
	S_{9b}	Ø	-1	1	-	-	-	$2^{-1/2}$	l_i
	S_{10b}	-1	Ø	1	-1	Ø	1	2^{-1}	R_i
	S_{11b}	-1	2	-1	-	-	-	$6^{-1/2}$	$r_\emptyset\beta_i$
	S_{12b}	2	-1	-1	-	-	-	$6^{-1/2}$	$l_\emptyset\omega_i$
	S_{13b}	Ø	-1	1	-	-	-	2^{-1}	$R_\emptyset\gamma_i$
		1	Ø	-1	-	-	-		$R_\emptyset\alpha_i$
	S_{14b}	1	2	1	-1	-2	-1	$24^{-1/2}$	R_i
	-	Ø	-1	1	-	-	-	$2^{-3/2}$	$R_\emptyset\gamma_i$
		-1	Ø	1	-	-	-		$R_\emptyset\alpha_i$

Note: $R_\emptyset$ = eqm C-C bond length, $r_\emptyset$ = eqm C-H bond length, $l_\emptyset$ = eqm C-F bond length.

Table 4.3

Internal Force Constant Notation For s-Trifluorobenzene

	R_i	r_i	l_i	$R_\emptyset{}^{\alpha}{}_i$	$R_\emptyset{}^{\gamma}{}_i$	$r_\emptyset{}^{\beta}{}_i$	$l_\emptyset{}^{\omega}{}_i$
R_i	D d_o d_m d_p	h_o h_m h_p	h_o^F h_m^F h_p^F	i_o i_m i_p	i_o^F i_m^F i_p^F	j_o j_m j_p	j_o^F j_m^F j_p^F
r_i		E e_m	e_o^F e_p^F	k k_m	k_o^F k_p^F	l_m	l_o^F l_p^F
l_i			E^F e_m^F	$k_o^{F'}$ k_p^F	k^F k_m^F	$l_o^{F'}$ $l_p^{F'}$	l^F l_m^F
$R_\emptyset{}^{\alpha}{}_i$				F f_m	f_o^F f_p^F	n_m	n_o^F n_p^F
$R_\emptyset{}^{\gamma}{}_i$					F^F f_m^F	$n_o^{F'}$ $n_p^{F'}$	n^F n_m^F
$r_\emptyset{}^{\beta}{}_i$						G g_m	g_o^F g_p^F
$l_\emptyset{}^{\omega}{}_i$							G^F G_m^F

Note: Capital letters indicate diagonal force constants.
Also, o = ortho, m = meta, p = para.

Table 4.4

Symmetry Force Constants For s-Trifluorobenzene

A_1': $F_{11} = E+2e_m$

$F_{21} = 2e_o^F+e_p^F$

$F_{22} = E^F+2e_m^F$

$F_{31} = 2^{1/2}(h_o+h_m+h_p)$

$F_{32} = 2^{1/2}(h_o^F+h_m^F+h_p^F)$

$F_{33} = D+2d_o+2d_m+d_p$

$F_{41} = 2^{-1/2}(-k+2k_o^F-2k_m+k_p^F)$

$F_{42} = 2^{-1/2}(k^F-2k_o^{F'}+2k_m^F-k_p^{F'})$

$F_{43} = -i_o-i_m-i_p+i_o^F+i_m^F+i_p^F$

$F_{44} = 2^{-1}(F+2f_m+F^F-4f_o^F+2f_m^F-2f_p^F)$

A_2': $F_{55} = D-2d_o+2d_m-d_p$

$F_{65} = 2^{1/2}(-j_o+j_m-j_p)$

$F_{66} = G+2g_m$

$F_{75} = 2^{1/2}(j_o^F-j_m^F+j_p^F)$

$F_{76} = 2g_o^F+g_p^F$

$F_{77} = G^F+2g_m^F$

E': $F_{88} = E-e_m$

$F_{98} = -e_o^F+e_p^F$

$F_{99} = E^F-e_m^F$

$F_{108} = 2^{-1/2}(-h_o+2h_m-h_p)$

$F_{109} = 2^{-1/2}(-h_o^F+2h_m^F-h_p^F)$

$F_{1010} = D-d_o-d_m+d_p$

$F_{118} = -3^{1/2}l_m$

$F_{119} = 3^{1/2}l_o^{F'}$

$F_{1110} = (3/2)^{1/2}(-j_o+j_p)$

$$F_{1111} = G-g_m$$

$$F_{128} = 3^{1/2}l_o^F$$

$$F_{129} = -3^{1/2}l_m^F$$

$$F_{1210} = (3/2)^{1/2}(-j_o^F+j_p^F)$$

$$F_{1211} = -g_o^F+g_p^F$$

$$F_{1212} = G^F-g_m^F$$

$$F_{138} = 2^{-1/2}(k-k_o^F-k_m+k_p^F)$$

$$F_{139} = 2^{-1/2}(k^F-k_o^{F'}-k_m^F+k_p^{F'})$$

$$F_{1310} = 2^{-1}(-i_o+2i_m-i_p-i_o^F+2i_m^F-i_p^F)$$

$$F_{1311} = (3/2)^{1/2}(n_o^{F'}-n_m)$$

$$F_{1312} = (3/2)^{1/2}(n_o^F-n_m^F)$$

$$F_{1313} = 2^{-1}(F-f_m+F^F-2f_o^F-f_m^F+2f_p^F)$$

$$F_{148} = 2^{-1}[3^{1/2}(h_o-h_p)-k-k_o^F+k_m+k_p^F]$$

$$F_{149} = 2^{-1}[3^{1/2}(-h_o^F+h_p^F)k^F+k_o^{F'}-k_m^F-k_p^{F'}]$$

$$F_{1410} = 2^{-3/2}(i_o-2i_m+i_p-i_o^F+2i_m^F-i_p^F)$$

$$F_{1411} = 2^{-1}[3^{1/2}(n_o^{F'}+n_m)-j_o-2j_m-j_p]$$

$$F_{1412} = 2^{-1}[3^{1/2}(-n_o^F-n_m^F)+j_o^F+2j_m^F+j_p^F]$$

$$F_{1413} = 2^{-3/2}[3^{1/2}(i_o-i_p-i_o^F+i_p^F)-F+f_m+F^F-f_m^F]$$

$$F_{1414} = 2^{-1}[D+d_o-d_m-d_p+4^{-1}(-F^F+3f_o^F+f_m^F+3f_p^F-2F+2f_m)+$$
$$+3^{1/2}(-i_o^F+i_p^F-i_o+i_p)]$$

Table 4.5

Observed And Calculated Data For Planar Vibrations Of s-Trifluorobenzene-h_3

		Observed	Uncertainty	Calculated	Error
A_1'	ν_1	3076.0[28]	31	3093.5	-17.5
	ν_2	1362.6[28]	14	1363.6	-1.0
	ν_3	1012.4[28]	10	1018.0	-5.6
	ν_4	579.9[28]	6	577.1	2.8
A_2'	ν_5	–	–	1304.6	-
	ν_6	–	–	1173.8	-
	ν_7	–	–	553.7	-
E'	ν_8	3113.0	31	3086.2	26.7
	ν_9	1629.0	16	1622.2	6.8
	ν_{10}	1475.4	15	1472.9	2.5
	ν_{11}	1127.6	11	1139.6	-12.0
	ν_{12}	996.3	10	1003.0	-6.7
	ν_{13}	502.4[28]	5	497.6	4.8
	ν_{14}	324.2[28]	3	323.3	1.0
	ζ_8	-0.00(2)	0.00(2)	-0.00(2)	0.00
	ζ_9	-	-	0.19	-
	ζ_{10}	-0.4	0.20	-0.19	-0.21
	ζ_{11}	-0.05	0.20	-0.02	0.03
	ζ_{12}	-0.35	0.05	-0.38	0.03
	ζ_{13}	-0.30[28]	0.02	-0.30	-0.00
	ζ_{14}	-0.20[28]	0.15	-0.34	0.14
	D_J	0.1573	0.02	0.0932	0.0641
	D_{JK}	-0.2949	0.10	-0.1540	-0.1409
	D_K	0.1425	0.10	0.0689	0.0736

Note: Wavenumbers are in cm^{-1}, Coriolis coupling constants are dimensionless and centrifugal distortion constants are in kHz.

Table 4.6

Observed And Calculated Data For Planar Vibrations Of s-Trifluorobenzene-d_3

		Observed	Uncertainty	Calculated	Error
A_1'	$\bar{\nu}_1$	2319.2[28]	23	2327.4	-8.2
	$\bar{\nu}_2$	1359.7[28]	14	1363.5	-3.7
	$\bar{\nu}_3$	969.2[28]	10	957.4	11.8
	$\bar{\nu}_4$	577.3[28]	6	577.1	0.2
A_2'	$\bar{\nu}_5$	–	–	1261.3	-
	$\bar{\nu}_6$	–	–	947.7	-
	$\bar{\nu}_7$	–	–	509.8	-
E'	$\bar{\nu}_8$	2314.0[28]	23	2312.4	1.6
	$\bar{\nu}_9$	1617.0[28]	16	1621.5	-4.5
	$\bar{\nu}_{10}$	1425.0[28]	14	1431.2	-6.2
	$\bar{\nu}_{11}$	1054.0[28]	11	1044.3	9.7
	$\bar{\nu}_{12}$	792.0[28]	8	785.1	6.9
	$\bar{\nu}_{13}$	487.0[28]	5	487.7	-0.7
	$\bar{\nu}_{14}$	322.4[28]	3	319.8	2.6
	ζ_8	-0.05[28]	0.04	0.00(4)	0.04(5)
	ζ_9	–	–	0.13	-
	ζ_{10}	-0.40[28]	0.4	-0.24	-0.16
	ζ_{11}	0.02[28]	0.02	0.02	0.00
	ζ_{12}	-0.40[28]	0.1	-0.32	-0.08
	ζ_{13}	-0.25[28]	0.1	-0.30	0.05
	ζ_{14}	-0.25[28]	0.05	-0.29	0.04
	D_J	–	–	0.0829	-
	D_{JK}	–	–	-0.1367	-
	D_K	–	–	0.0611	-

Note: See note at the bottom of Table 4.5.

Table 4.7

Model Force Field For Planar Vibrations
Of s-Trifluorobenzene

Force Constant	Typical Coefficient	Best Value	Dispersion
D	R_i^2	7.460	0.455
E	r_i^2	5.081	0.115
E^F	l_i^2	6.238	0.315
F	$(R_o\alpha_i)^2$	0.206	0.120
F^F	$(R_o\gamma_i)^2$	1.249	0.101
G	$(r_o\beta_i)^2$	0.758	0.023
G^F	$(l_o\omega_i)^2$	1.749	0.208
d	(R_iR_j)	0.468	0.093
h_o^F	R_il_i	0.346	0.201
i_o	$R_oR_i\alpha_i$	0.528	0.172
j_o	$r_oR_i\beta_i$	0.536	0.061
j_o^F	$l_oR_i\omega_i$	1.038	0.207
j_m^F	$l_oR_i\omega_{i+1}$	-0.457	0.109
k^F	$R_ol_i\gamma_i$	0.856	0.135
n_o^F	$R_ol_o\alpha_i\omega_i$	0.191	0.098
$k_o^{F'}$	$R_ol_i\alpha_i$	0.765	0.093
k	$R_or_i\alpha_i$	0.319	0.166
g_o^F	$r_ol_o\beta_i\omega_i$	-0.015	0.023
g_p^F	$r_ol_o\beta_i\omega_{i+1}$	-0.088	0.039

Note: All constants are in units of mdyn.$Å^{-1}$.

Table 4.8

Symmetry Force Constants For The Planar Vibrations Of s-Trifluorobenzene

Γ	Symmetry Force Constants	Best Value	Γ	Symmetry Force Constants	Best Value
A_1'	F_{11}	5.081	E′	F_{118}	0.000
	F_{21}	0.000		F_{119}	0.000
	F_{22}	6.238		F_{1110}	-0.653
	F_{31}	0.000		F_{1111}	0.758
	F_{32}	0.488		F_{128}	0.000
	F_{33}	7.928		F_{129}	0.000
	F_{41}	-0.227		F_{1210}	-1.266
	F_{42}	-0.471		F_{1211}	-0.073
	F_{43}	0.000		F_{1212}	1.749
	F_{44}	0.727		F_{138}	0.226
A_2'	F_{55}	5.119		F_{139}	0.065
	F_{65}	-0.755		F_{1310}	-0.528
	F_{66}	0.758		F_{1311}	0.000
	F_{75}	2.108		F_{1312}	0.233
	F_{76}	-0.117		F_{1313}	0.727
	F_{77}	1.749		F_{148}	-0.159
E′	F_{88}	5.081		F_{149}	0.510
	F_{98}	0.000		F_{1410}	0.000
	F_{99}	6.238		F_{1411}	-0.268
	F_{108}	0.000		F_{1412}	-0.105
	F_{109}	-0.246		F_{1413}	0.365
	F_{1010}	7.928		F_{1414}	2.837

Note: All force constants are in units of mdyn.$Å^{-1}$.

Table 4.9

L Matrix Elements For a_1' Normal Coordinates
Of s-Trifluorobenzene -h_3 and -d_3.
(Planar Vibrations)(a.m.u.)$^{-1/2}$

s-$C_6F_3H_3$

ν_i(calculated)	3093.53	1363.58	1018.01	577.13
	Q_1	Q_2	Q_3	Q_4
S_1	1.03	0.02	0.07	0.01
S_2	-0.01	0.35	0.04	-0.10
S_3	-0.06	-0.21	0.16	-0.09
S_4	-0.26	0.56	0.76	0.22

s-$C_6F_3D_3$

ν_i(calculated)	2327.39	1363.45	957.44	577.08
	Q_1	Q_2	Q_3	Q_4
S_1	0.75	0.02	0.11	0.01
S_2	-0.01	0.35	0.03	-0.10
S_3	-0.09	-0.21	0.15	-0.09
S_4	-0.39	0.57	0.69	0.21

Table 4.1Ø

L Matrix Elements For a_2'' Normal Coordinates Of s-Trifluorobenzene $-h_3$ and $-d_3$. $(a.m.u)^{-1/2}$

	$s\text{-}C_6F_3H_3$		
ν_i(calculated)	1304.64	1173.78	553.70
	Q_5	Q_6	Q_7
S_5	Ø.40	Ø.21	-Ø.22
S_6	-Ø.39	Ø.98	-Ø.24
S_7	-Ø.Ø9	Ø.18	Ø.46
	$s\text{-}C_6F_3D_3$		
ν_i(calculated)	1261.32	947.7Ø	5Ø9.78
	Q_5	Q_6	Q_7
S_5	Ø.45	-Ø.Ø7	-Ø.19
S_6	Ø.2Ø	Ø.73	-Ø.3Ø
S_7	-Ø.Ø1	Ø.31	Ø.4Ø

Table 4.11

L Matrix Elements For e´ Normal Coordinates $^{-1/2}$
Of s-Trifluorobenzene $-h_3$ and $-d_3$. (a.m.u.)

$s\text{-}C_6H_3F_3$

ν_i(calc.) 3086.25 1622.18 1472.86 1139.61 1003.01 497.59 323.26

	Q_8	Q_9	Q_{10}	Q_{11}	Q_{12}	Q_{13}	Q_{14}
S_8	1.03	-0.02	-0.06	0.00	-0.04	-0.02	0.01
S_9	0.00	0.28	-0.11	-0.14	0.14	-0.08	-0.02
S_{10}	0.05	0.29	0.32	0.14	-0.02	-0.02	0.01
S_{11}	-0.00	0.34	-0.31	0.93	0.32	-0.02	0.06
S_{12}	0.09	0.01	0.41	-0.03	0.27	-0.02	0.16
S_{13}	0.19	0.53	0.22	-0.05	0.31	0.37	-0.14
S_{14}	-0.09	0.30	-0.29	0.04	-0.24	0.03	0.10

$s\text{-}C_6D_3F_3$

ν_i(calc.) 2312.42 1621.49 1431.19 1044.27 785.08 487.74. 319.82

	Q_8	Q_9	Q_{10}	Q_{11}	Q_{12}	Q_{13}	Q_{14}
S_8	0.75	-0.03	-0.10	0.05	-0.03	-0.02	0.01
S_9	0.01	0.28	-0.12	-0.19	0.02	-0.08	-0.02
S_{10}	0.09	0.28	0.33	0.08	0.03	-0.02	0.01
S_{11}	-0.00	0.35	-0.08	0.38	0.64	-0.05	0.07
S_{12}	0.15	-0.00	0.39	-0.25	0.10	-0.00	0.16
S_{13}	0.29	0.52	0.19	-0.25	0.16	0.35	-0.14
S_{14}	-0.14	0.31	-0.27	0.21	-0.09	0.04	0.10

Table 4.12

Definition Of The Out-Of-Plane Internal Displacement Coordinates For s-Trifluorobenzene

ϕ_i	The perpendicular displacement of the ith hydrogen atom out of the plane defined by the 2 adjacent C-C bonds.
ϑ_i	The perpendicular displacement of the ith fluorine atom out of the plane defined by the 2 adjacent C-C bonds.
τ_i	The out-of-plane ring bending deformations which are regarded as torsions around C-C bonds.

Table 4.13

Out-Of-Plane Symmetry Coordinates For s-Trifluorobenzene

Γ	S_i	1	2	3	4	5	6	N	s_i
A_2''	S_1	1	-	1	-	1	-	$6^{-1/2}$	$l_\emptyset \vartheta_i$
		-	1	-	1	-	1		$r_\emptyset \phi_i$
	S_2	1	-	1	-	1	-	$6^{-1/2}$	$l_\emptyset \vartheta_i$
		-	-1	-	-1	-	-1		$r_\emptyset \phi_i$
	S_3	1	-1	1	-1	1	-1	$6^{-1/2}$	$R_\emptyset \tau_i$
E''	S_{4a}	-	-	1	Ø	-1	-	2^{-1}	$l_\emptyset \vartheta_i$
		Ø	-1	-	-	-	1		$r_\emptyset \phi_i$
	S_{5a}	-	-	1	Ø	-1	-	2^{-1}	$l_\emptyset \vartheta_i$
		Ø	1	-	-	-	-1		$r_\emptyset \phi_i$
	S_{6a}	-1	2	-1	-1	2	-1	$12^{-1/2}$	$R_\emptyset \tau_i$
	S_{4b}	-2	-	1	-	1	-	$12^{-1/2}$	$l_\emptyset \vartheta_i$
		-	-1	-	2	-	-1		$r_o \phi_i$
	S_{5b}	-2	-	1	-	1	-	$12^{-1/2}$	$l_\emptyset \vartheta_i$
		-	-1	-	2	-	-1		$r_\emptyset \phi_i$
	S_{6b}	1	Ø	-1	1	Ø	-1	2^{-1}	$R_\emptyset \tau_i$

Note: $R_\emptyset$= equilibrium C-C bond length; $r_\emptyset$ = equilibrium C-H bond length; $l_\emptyset$ = equilibrium C-F bond length.

Table 4.14

Internal Force Constant Notation
(Out-Of-Plane Vibrations)

	$l_o\vartheta_i$	$r_o\phi_i$	$R_o\tau_i$
$l_o\vartheta_i$	H, h_m	$\bar{a}_o, \bar{a}_p$	$\bar{c}_o$, $\bar{c}_m$, $\bar{c}_p$
$r_o\phi_i$		A, a_m	c_o, c_m, c_p
$R_o\tau_i$			B, b_o, b_m, b_p

Table 4.15

Symmetry Force Constant Notation
(Out-Of-Plane Vibrations)

A_2'' :

$$F_{11} = (1/2)[(A+4\bar{a}_o+2a_m+2\bar{a}_p)+(H+2h_m)]$$

$$F_{21} = (1/2)[(H+2h_m)-(A+a_m)]$$

$$F_{22} = (1/2)[(A-4\bar{a}_o+2a_m-2\bar{a}_p)+(H+2h_m)]$$

$$F_{31} = c_o+c_p-c_m-\bar{c}_o-\bar{c}_p+\bar{c}_m$$

$$F_{32} = -c_o-c_p+c_m-\bar{c}_o-\bar{c}_p+\bar{c}_m$$

$$F_{33} = B-2b_o+2b_m-b_p$$

E'' :

$$F_{44} = (1/2)[A-2\bar{a}-a_m+2a_p)+(H-h_m)]$$

$$F_{54} = (1/2)[(-A+a_m)+(H-h_m)]$$

$$F_{55} = (1/2)[(A+2\bar{a}_o-a_m-2\bar{a}_p)+(H-h_m)]$$

$$F_{64} = (3^{1/2}/2)(c_o-c_p+\bar{c}_o-\bar{c}_p)$$

$$F_{65} = (3^{1/2}/2)(-c_o+c_p+\bar{c}_o-\bar{c}_p)$$

$$F_{66} = B-b_o-b_m+b_p$$

Table 4.16

Observed And Calculated Data For Out-Of-Plane Vibrations Of s-Trifluorobenzene-h_3 (cm^{-1}).

		Observed	Uncertainty	Calculated	Error
A_2'':	$\bar{\nu}_1$	848.13	9	841.83	6.3
	$\bar{\nu}_2$	664.69	7	665.33	-Ø.6
	$\bar{\nu}_3$	2Ø7.Ø[28]	2	2Ø7.93	-Ø.9
E''	$\bar{\nu}_4$	792.Ø[28]	8	793.74	-1.7
	$\bar{\nu}_5$	598.Ø[28]	6	594.42	3.6
	$\bar{\nu}_6$	245.8[28]	3	242.35	3.5

Table 4.17
Observed And Calculated Data For Out-Of-Plane Vibrations Of s-Trifluorobenzene-d_3

		Observed	Uncertainty	Calculated	Error
A_2''	$\bar{\nu}_1$	777.2[28]	8	779.4	-2.2
	$\bar{\nu}_2$	522.Ø[28]	5	521.2	Ø.8
	$\bar{\nu}_3$	2Ø5.Ø[28]	2	2Ø5.1	Ø.8
E''	$\bar{\nu}_4$	646.Ø[28]	7	651.3	-5.3
	$\bar{\nu}_5$	537.6[28]	5	538.1	-Ø.5
	$\bar{\nu}_6$	231.3[28]	2	234.5	-3.2

Table 4.18
Model Force Field For Out-Of-Plane Vibrations
Of s-Trifluorobenzene

Force Constant	Typical Coefficient	Best Value	Dispersion
H	$(l_{\emptyset}{}^{\vartheta}{}_{i})^{2}$	Ø.845	Ø.Ø7Ø
A	$(r_{\emptyset}{}^{\phi}{}_{i})^{2}$	Ø.433	Ø.ØØ7
B	$(R_{\emptyset}{}^{\tau}{}_{i})^{2}$	Ø.254	Ø.Ø18
$\bar{a}_{o}$	$l_{\emptyset}{}^{\vartheta}{}_{i} r_{\emptyset}{}^{\phi}{}_{i}$	-Ø.218	Ø.Ø2Ø
b_{o}	$R^{2}_{\emptyset}{}^{\tau}{}_{i}{}^{\tau}{}_{i+1}$	-Ø.Ø32	Ø.ØØ6
$\bar{c}_{o}$	$l_{\emptyset}{}^{\vartheta}{}_{i} R_{\emptyset}{}^{\tau}{}_{i}$	Ø.299	Ø.Ø36
c_{o}	$r_{\emptyset}{}^{\vartheta}{}_{i} R_{\emptyset}{}^{\tau}{}_{i}$	Ø.213	Ø.Ø11

Note: All constants are in units of $mdyn.A^{-1}$.

Table 4.19
Symmetry Force Constants For The Out-Of-Plane Vibrations
Of s-Trifluorobenzene

	Symmetry Force Constants	Our Field	E.Ferguson's[43]	J.R.Scherer's[23]
A_2''	F_{11}	Ø.2Ø2	Ø.223	Ø.217
	F_{21}	Ø.2Ø6	-Ø.Ø23	Ø.Ø16
	F_{22}	1.Ø76	Ø.515	Ø.485
	F_{31}	-Ø.Ø87	Ø	Ø.ØØ4
	F_{32}	-Ø.513	Ø.373	-Ø.234
	F_{33}	Ø.318	Ø.339	Ø.178
E''	F_{44}	Ø.857	Ø.427	Ø.418
	F_{54}	Ø.2Ø6	Ø.ØØ6	Ø.Ø16
	F_{55}	Ø.421	Ø.226	Ø.284
	F_{64}	Ø.446	-Ø.515	Ø.2Ø3
	F_{65}	Ø.Ø76	Ø	-Ø.ØØ3
	F_{66}	Ø.286	Ø.757	Ø.19Ø

Note: All force constants are in units of mdyn.$Å^{-1}$.

Table 4.20
L Matrix Elements For a_2'' Normal Coordinates
Of s-Trifluorobenzene $-h_3$ and $-d_3$.
(Out-Of-Plane Vibrations)

	$s\text{-}C_6F_3H_3$			$s\text{-}C_6F_3D_3$		
ν_i(calculated)	841.83	665.33	207.93	779.4	521.2	205.1
	Q_1	Q_2	Q_3	Q_1	Q_2	Q_3
S_1	-0.32	0.48	0.36	-0.01	0.38	0.36
S_2	1.22	0.35	-0.09	1.19	-0.07	-0.09
S_3	1.39	1.42	-0.17	1.89	0.64	-0.16

Table 4.21
L-Matrix Elements For e'' Normal Coordinates
Of s-Trifluorobenzene $-h_3$ and $-d_3$.

	$s\text{-}C_6F_3H_3$			$s\text{-}C_6F_3D_3$		
ν_i(calculated)	793.74	594.42	242.35	651.3	538.1	234.5
	Q_4	Q_5	Q_6	Q_4	Q_5	Q_6
S_4	0.93	-0.45	-0.35	0.94	-0.10	-0.33
S_5	-0.52	-0.56	0.14	0.01	0.64	0.11
S_6	-0.46	0.75	0.74	-0.87	-0.24	0.72

Note: The units are $(a.m.u.)^{-1/2}$

Figures

Figure 4.1

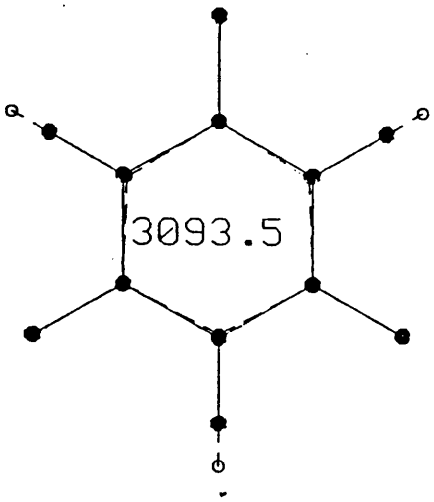

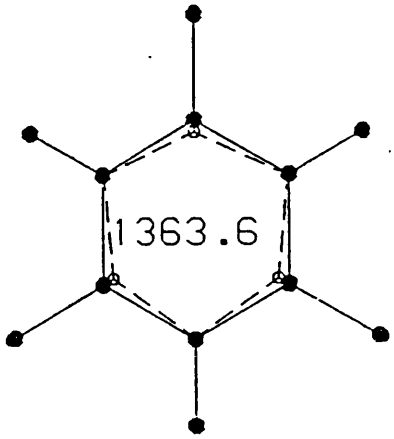

a_1'

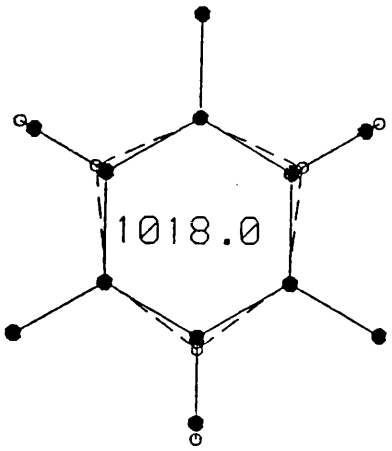

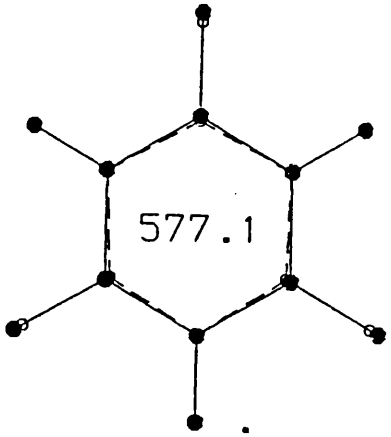

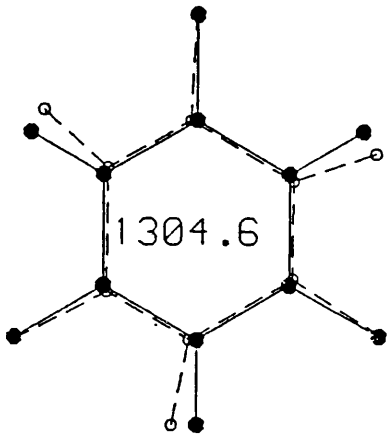

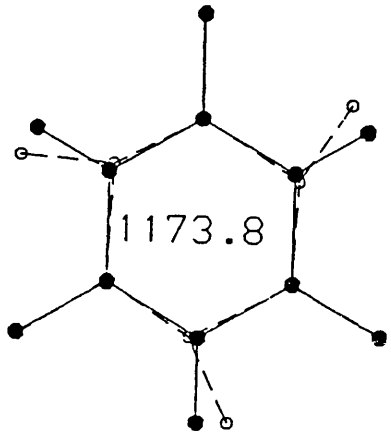

a_2'

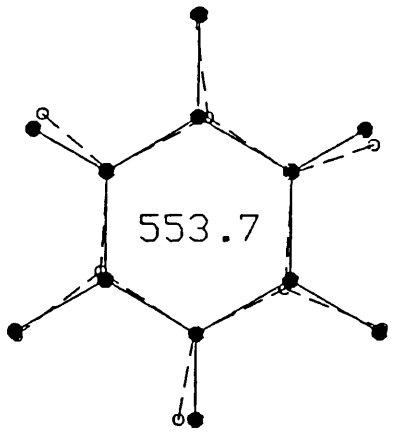

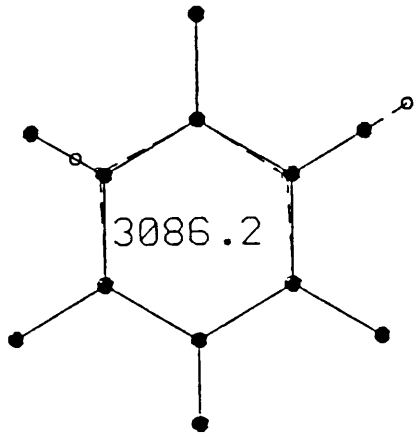

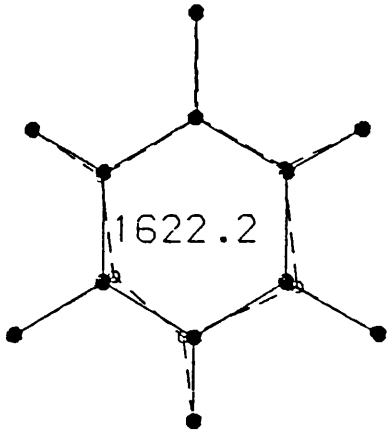

e´(a)

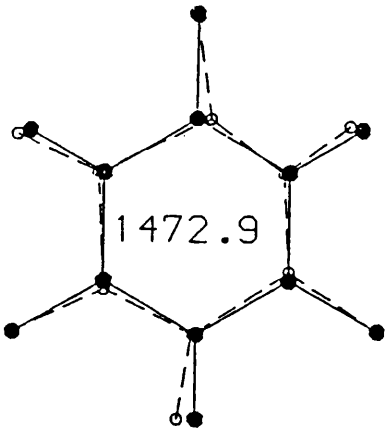

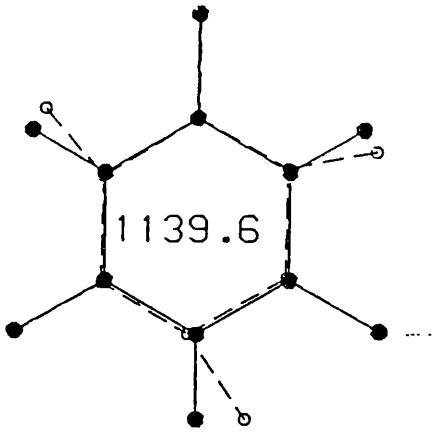

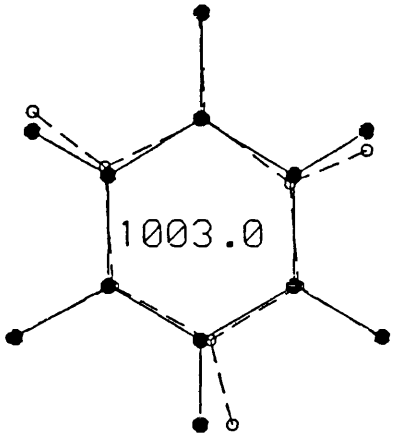

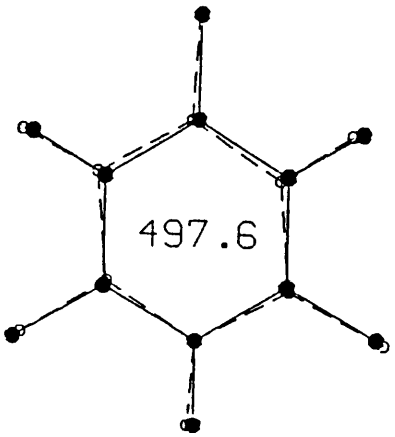

e´(a)

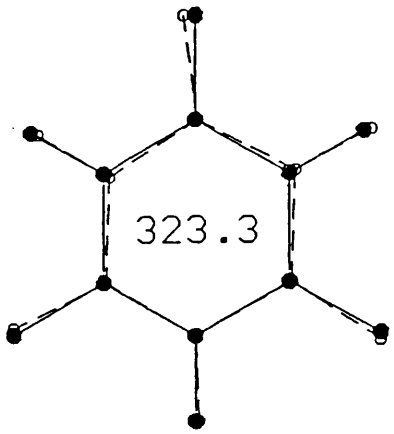

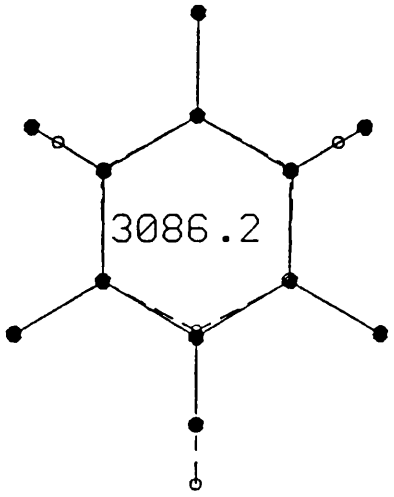

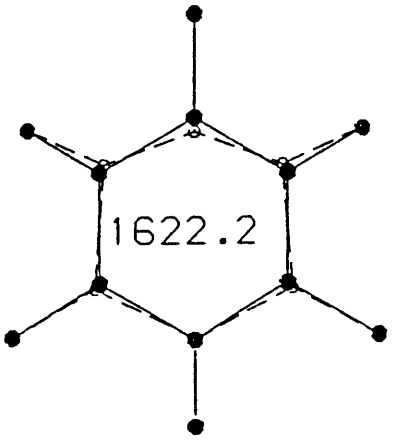

e´(b)

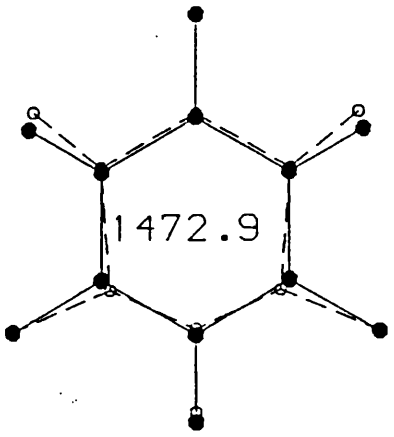

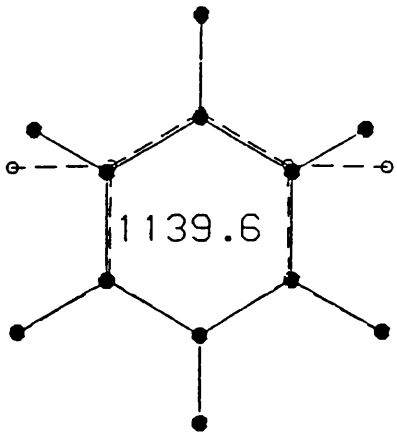

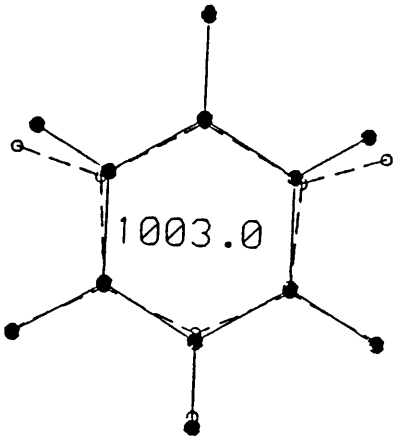

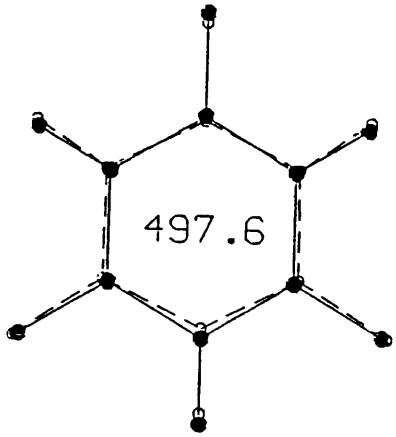

e´(b)

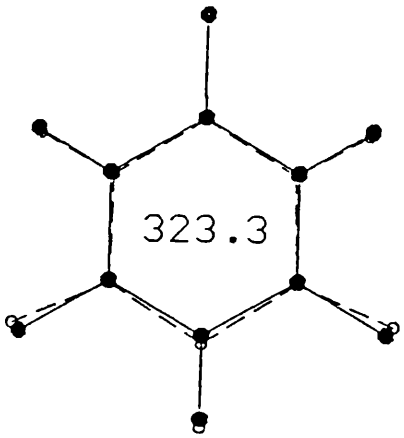

Figure 4.2

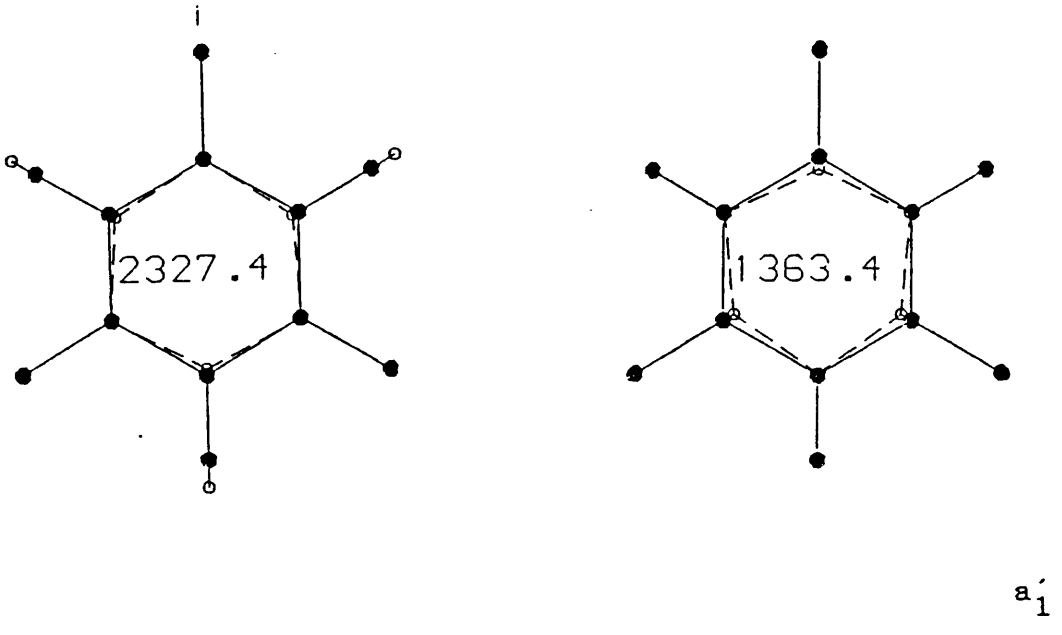

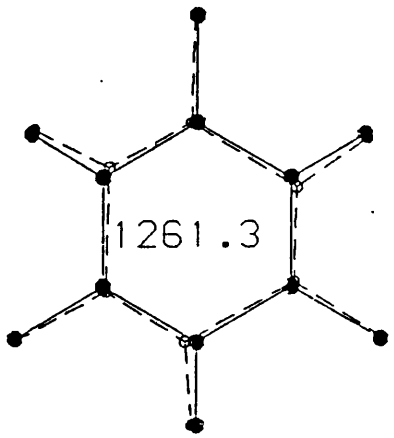

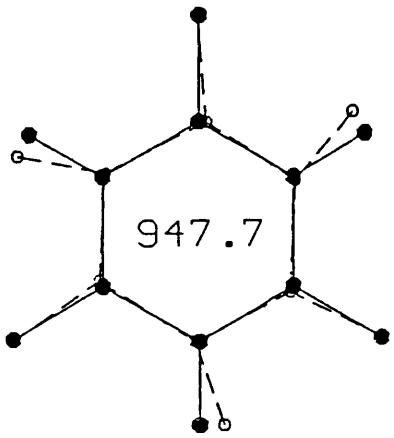

a_2'

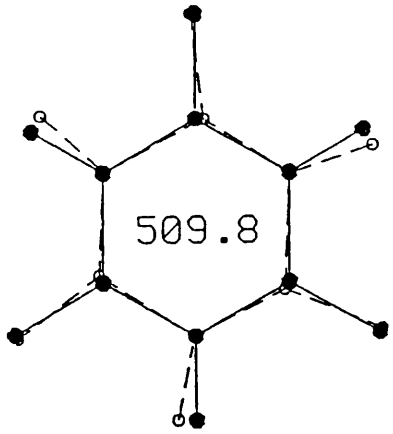

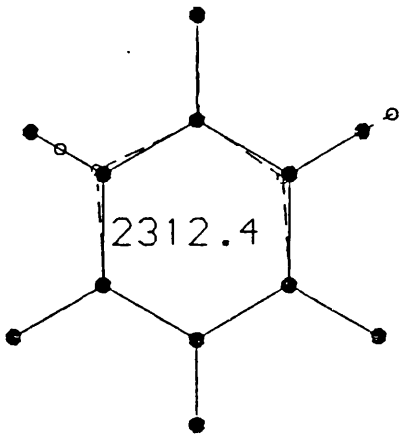

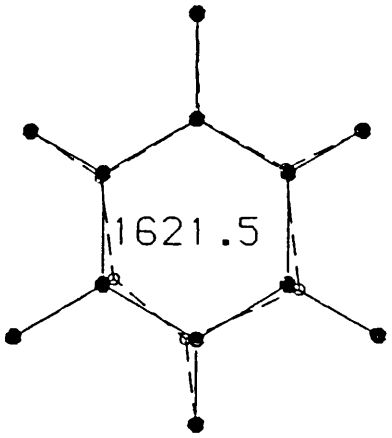

e´(a)

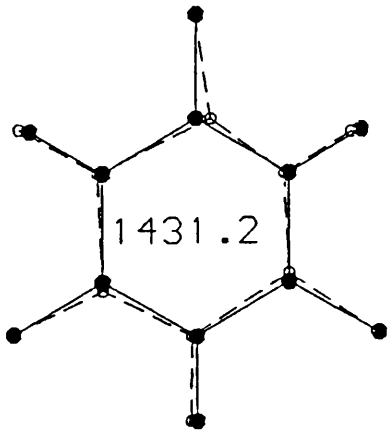

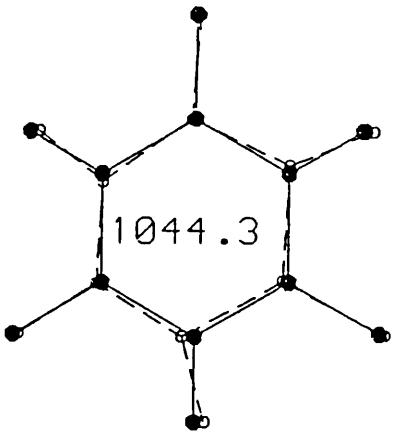

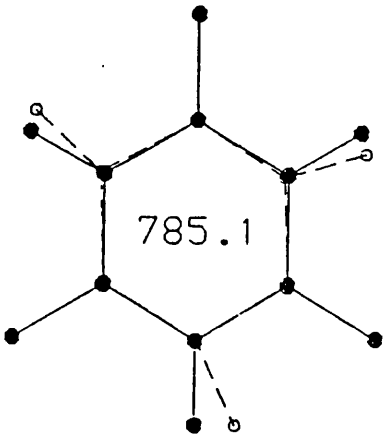

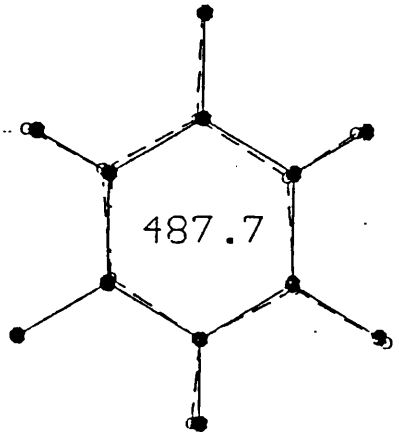

e´(a)

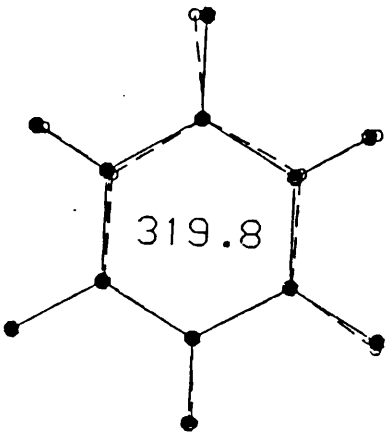

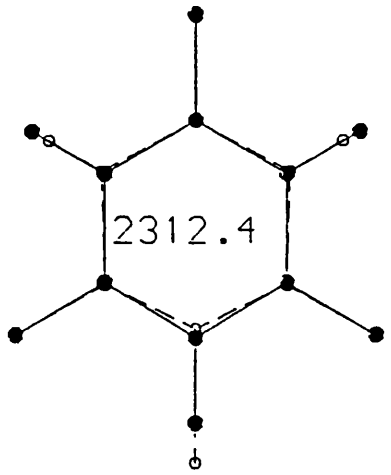

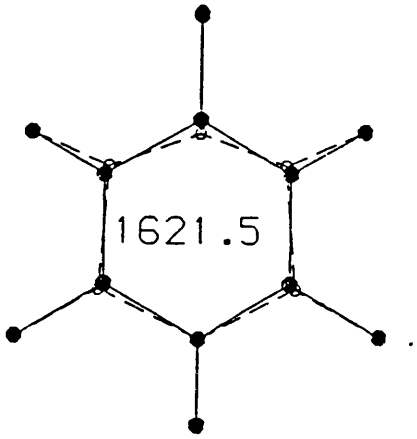

e´(b)

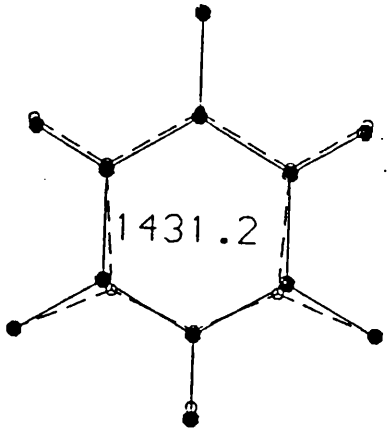

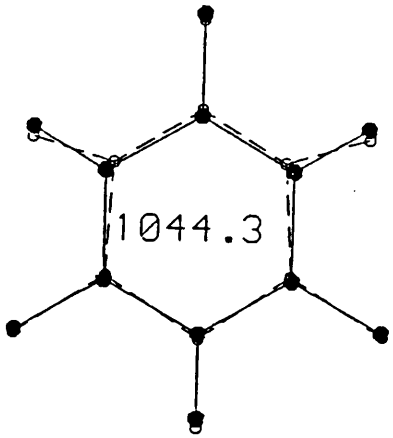

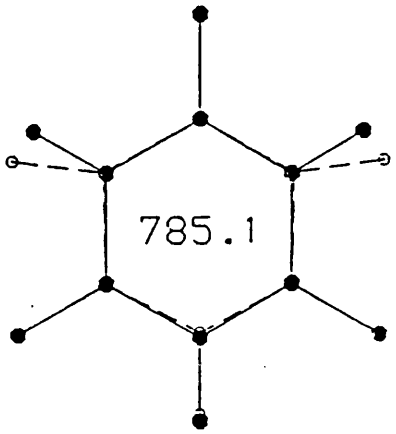

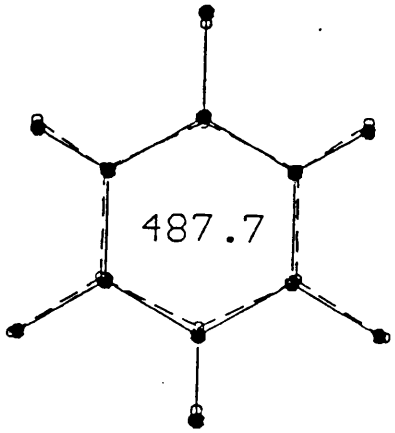

e´(b)

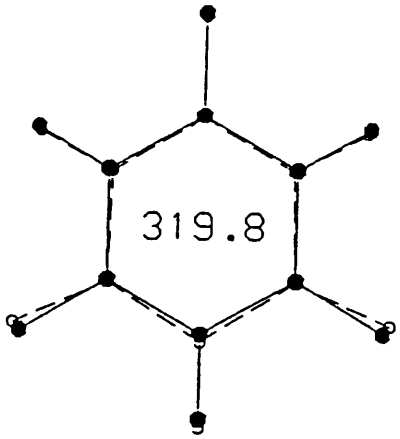

Chapter 5

Propynal: Preliminary Investigation Of The Mid-IR Spectrum Of The $C_2H.CDO$ And $C_2D.CDO$ Species Using FTIR Spectroscopy.

5.1 Introduction

The infrared spectrum of $C_2H.CHO$, $C_2D.CHO$ and $C_2H.CDO$ species was first observed at low resolution by Brand and Watson[45], in 1960. In their paper, they completed the vibrational assignments and quoted Coriolis constants for the $\nu_7(a')$,$\nu_{11}(a'')$ pair of fundamentals for all three species.

The infrared spectrum of the same species at low resolution was also observed by King and Moule[46] in 1961. They also completed the vibrational assignments of the same three species.

The assignments of the $\nu_7(a')$,$\nu_{11}(a'')$ fundamentals were later corrected in Watson's thesis[47] in 1962.

In 1971, Klaboe and Kremer[48] observed the Raman spectrum of the $C_2H.CHO$ species and confirmed the rectified assignment for the $\nu_7(a')$ and $\nu_{11}(a'')$.

Finally, Takami and Shimoda[49] and Takami and Suzuki[50] performed infrared-microwave double resonance experiments using the 3.51 μm He-Xe laser. As a result of their experiments accurate assignments for the $\nu_2(a')$ fundamentals in $C_2H.CHO$ and $C_2D.CHO$ species were obtained.They also performed rotational analyses for the same fundamentals for the two species.

In this study, the mid-infrared spectrum of the $C_2H.CDO$ was recorded at both low and high resolution using FTIR techniques. Also, the mid-infrared spectrum of the $C_2D.CDO$ species was recorded for the first time at both low and high resolution . The primary objectives of this investigation were the assignment of the fundamentals for the $C_2D.CDO$ species and also the partial rotational analysis of some of the observed fundamentals in the mid-infrared spectrum of the two species.

The propynal molecule belongs to the C_s point group. Since there are six atoms in the molecule, the total

number of vibrations is twelve - all of which are allowed in the infrared. The structure of their representation is as follows:

$$\Gamma(Q_v) = 9a' + 3a'' \qquad (5.1)$$

The molecule is a near-symmetric prolate rotor. This can be confirmed from Ray's asymmetry parameter $\varkappa$ which is defined as follows:

$$\varkappa = (2B - A - C) / (A - C) \qquad (5.2)$$

For a prolate symmetric rotor B = C therefore $\varkappa = -1$, while for an oblate symmetric rotor A = B therefore $\varkappa = +1$. By putting A'' = 1.7268 cm^{-1}, B'' = Ø.159828 cm^{-1} and C'' = Ø.146Ø63 cm^{-1} for the $C_2H.CDO$ species from the microwave study[51], the $\varkappa$ parameter has a value of -Ø.98 which is very close to the prolate symmetric rotor limit. It can be shown that the same is true for the $C_2D.CDO$ species.

Even though $\varkappa \cong -1$, the molecule is asymmetric enough to make the infrared bands characteristic of an asymmetric rotor. Therefore, in (5.1) the a'' modes are expected to give type C bands while the a' modes are expected to give type A and type B hybrids.

The type A band correlates with a parallel band in the prolate symmetric rotor limit and with a perpendicular band in the oblate symmetric rotor limit. The type B band correlates with a perpendicular band in both the prolate and oblate symmetric rotor limits. Finally, the type C band correlates with a perpendicular band in the prolate symmetric rotor limit and with a parallel band in the oblate symmetric rotor limit.

The survey spectra of the two species are given in Figures 5.1 and 5.2. They were recorded at a resolution of ca. 1 cm^{-1} in the range between 55Ø and 4ØØØ cm^{-1}. The same multipass cell was used as in the case of

s-trifluorobenzene-h_3 with a total pathlength of 12Ø cm. The samples which were generously given by Simon Edwards were used at a pressure of ca. 1 Torr. The Bruker IFS spectrometer was again used with the MCT detector cooled down to 77 K.

The fundamental frequencies for all four species are listed in Table 5.1. They are compiled from earlier work[47,49,50], from a recent analysis of the electronic spectra by Edwards[52] and from the present investigation.

5.2 Theory Of Asymmetric Rotors.

A minimum theory is given here, sufficient for an understanding of the later discussions in this chapter. Fuller treatments are given in standard texts[20].

The rotational term values for asymmetric rotors, excluding distortion constants are given by the following expression:

$$F(J,\tau) = (1/2)(A+C)J(J+1) + (1/2)(A-C)E(\varkappa)_{J,\tau} \qquad (5.3)$$

where $\varkappa$ is the asymmetry parameter defined by (5.2),
τ takes the values J,J-1 ... Ø,-J and labels in order 2J+1 energy levels for a given J,
$E(\varkappa)_{J,\tau}$ is a reduced energy term and is determined by the diagonalization of a matrix whose elements depend only on J, τ and $\varkappa$. The full diagonalization procedure can be programmed for a computer for any value of $\varkappa$. We use the method described by Bennett, Ross and Wells[53].
The rest of the symbols have their usual meaning.

In the limiting symmetric rotor cases expression (5.3) reduces to the following one:

$$F(J,K_{-1}) = BJ(J+1) + (A-B)K_{-1}^2 \qquad (5.4)$$

$$F(J,K_{+1}) = BJ(J+1) + (C-B)K_{+1}^2 \qquad (5.5)$$

where K_{-1} refers to the prolate rotor limit and K_{+1} refers to the oblate rotor limit. K takes the values from -J...Ø...+J and a particular level is labeled by J, K_{-1}, K_{+1}. The post-subscripts in K refer to the values of the asymmetry parameter κ in the two symmetric limits.

The selection rules for the three types of asymmetric bands are as follows:

i. Type A bands: In the prolate symmetric rotor limit these give rise to parallel bands with the selection rules:

$$K_{-1} = Ø \;;\; \Delta J = \pm 1 \;;\; \Delta K_{-1} = Ø$$
$$K_{-1} \neq Ø \;;\; \Delta J = Ø, \pm 1 \;;\; \Delta K_{-1} = Ø \qquad (5.6)$$

In the oblate symmetric rotor limit these give rise to perpendicular bands with the selection rules:

$$\Delta J = Ø, \pm 1 \;;\; \Delta K_{+1} = \pm 1 \qquad (5.7)$$

Therefore, the overall selection rules are a combination of (5.6) and (5.7).

ii. Type B bands : In both the prolate and oblate symmetric rotor limits these give rise to perpendicular bands. Therefore the overall selection rules of such bands are:

$$\Delta J = Ø, \pm 1 \;;\; \Delta K_{-1} = \pm 1 \;;\; \Delta K_{+1} = \pm 1 \qquad (5.8)$$

iii. Type C bands : In the prolate symmetric rotor limit these give rise to perpendicular bands with the selection rules:

$$\Delta J = Ø, \pm 1 \;;\; \Delta K_{-1} = \pm 1 \qquad (5.9)$$

In the oblate symmetric rotor limit these give rise to parallel bands with the selection rules:

$$K_{+1} = Ø \;;\; \Delta J = \pm 1 \;;\; \Delta K_{+1} = Ø$$
$$K_{+1} \neq Ø \;;\; \Delta J = Ø, \pm 1 \;;\; \Delta K_{+1} = Ø \qquad (5.10)$$

Therefore the overall selection rules are a combination of (5.9) and (5.1Ø).

These are the selection rules for the strong transitions in asymmetric rotors. They are expected to be strong because they are allowed transitions in both symmetric rotor limits. Strictly in asymmetric rotors the selection rules for ΔK_{-1} and ΔK_{+1} relax to:

$$\Delta K_{-1} = Ø, \pm 2, \pm 4 \ldots$$
$$\Delta K_{+1} = \pm 1, \pm 3, \pm 5 \ldots \qquad (5.11)$$

However, the extra transitions are usually weak and can often be ignored when the rotor is not too asymmetric.

The intensities of the transitions are expressed as follows[9]:

$$I_{n'',n'} = C.g_n.\exp(-E_{n''}/kT).|A|^2 \qquad (5.12)$$

where n'',n' are a summary of ground and excited states constants,

C is nearly constant for a vibrational transition ,

g_n is the multiplicity of the lower state of the transition in an absorption

and $|A|$ is the electric dipole transition matrix element between the two states, which for an asymmetric rotor can not be expressed in a simple closed form. Its calculation involves setting up a matrix of the appropriate symmetric rotor quantities for a specific $J'' \Rightarrow J'$ (for all K values) and transforming these to an asymmetric rotor representation using the eigenvectors of the reduced energy matrices of the lower and upper states respectively . These operations can easily be done with a computer. Programs used in this work are outlined in Appendix 3.

5.3 Second Order Coriolis Interaction Between B And C Type Bands

Perturbations of this kind have been observed in the present investigation and the rotational band contour program KONTUR has been modified to include them (see Appendix 3).

In a prolate asymmetric rotor with a small value of I_A (large value of A) the perturbation term $(-p_z J_z/I_A)$ is large and can produce important interactions[54]. Additionally, if the asymmetry parameter $\kappa \approx -1$ (as in the case of propynal) then asymmetric rotor effects can largely be ignored except at very low K.

In the case of an interaction between two fundamental vibrational levels where $Q_r \times Q_s \supset R_A$ and $Q_r \supset T_B$, $Q_s \supset T_C$ the two fundamental levels combine with the ground state to give B and C type perpendicular bands. Assuming that the molecule is close to a symmetric rotor about the A-axis and k (K = |k|) is considered a good quantum number except for the lowest values, the perturbation term $(-p_z J_z/I_A)$ will be diagonal in J and the Hamiltonian factorises into 2x2 blocks of the type shown below:

$$\begin{array}{c} \quad |v_r=1,v_s=\emptyset;J,k\rangle \qquad |v_r=\emptyset,v_s=1;J,k\rangle \\ \left[\begin{array}{ll} \nu_r + F(J,k) & +2iA\zeta_{rs}\Omega_{rs}k \\ \text{Hermitian} & \nu_s + F(J,k) \end{array}\right] \end{array} \qquad (5.13)$$

where ν_r, ν_s are the vibrational energies measured from the ground vibrational state.

F(J,k) in this case denotes the rigid symmetric rotor approximation to the rotational energy which is expressed as follows:

$$F(J,k) = \bar{B}J(J+1) + (A-\bar{B})k^2 \qquad (5.14)$$

where $\bar{B} = (B+C)/2$

and $\Omega_{rs} = (1/2)[(\nu_r/\nu_s)^{1/2} + (\nu_s/\nu_r)^{1/2}]$ (5.15)

In expression (5.15) it is worth noting that for $\nu_r \approx \nu_s \Rightarrow \Omega_{rs} \approx 1$. After diagonalising (5.13) the energy levels are given as follows:

$$E_{\pm}(J,k) = (1/2)(\nu_r+\nu_s) + F(J,k) \pm \Delta_k \qquad (5.16)$$

where $\Delta_k = \{ \delta^2 + 16A^2k^2\zeta_{rs}^2\Omega_{rs}^2 \}^{1/2}$ (5.17)

and $\delta = \nu_r - \nu_s$ (5.18)

The perturbed wavefunctions are given as follows:

$$|\psi_+\rangle = a_k |\psi_r\rangle - i\sigma_{jk}b_k|\psi_s\rangle$$

$$|\psi_-\rangle = -i\sigma_{jk}b_k |\psi_r\rangle + a_k|\psi_s\rangle \qquad (5.19)$$

where $|\psi_r\rangle$, $|\psi_s\rangle$ denote the unperturbed vibrational functions $|v_r=1,v_s=0\rangle$, $|v_r=0,v_s=1\rangle$,

$$a_k = [(\Delta_k + \delta)/2\Delta_k]^{1/2}$$
$$b_k = [(\Delta_k - \delta)/2\Delta_k]^{1/2}$$

and $\sigma_{jk} = (\text{sign } j_{rs})(\text{sign } k) = \pm 1$ which comes from the sign of the crossterm in the original matrix.

Assuming $\nu_r > \nu_s$ and for small values of k, the upper energy levels E_+ correlate strongly with ν_r and the lower energy levels E_- correlate strongly with ν_s. For large values of k the wavefunctions become strongly mixed and $a_k, b_k \Rightarrow (1/2)^{1/2}$.

An energy level diagram for second order Coriolis interactions between B and C type bands for the

C_s symmetry species to which propynal belongs is given in Figure 5.3.

By combining (5.14) with (5.15) expressions can be obtained for the line positions in the two observed bands. Because of the fact that the perturbation is independent of J, only the relative positions of the sub-band origins are affected in the two bands. Therefore, the expressions for the line positions are given as follows:

From (5.14) we have :

$$F(J,K\pm1) - F(J,K) = \bar{B}J(J+1) - \bar{B}J(J+1) + (A-\bar{B})K^2 - (A-\bar{B})K^2 \pm$$

$$\pm 2(A-\bar{B})K + (A-\bar{B}) = (A-\bar{B}) \pm 2(A-\bar{B})K$$

Therefore,

$$^{r,p}Q_K(\nu_+) = (1/2)(\nu_r+\nu_s) + (A-\bar{B}) \pm 2(A-\bar{B})K +$$

$$+ (1/2)[\delta^2+16A^2\zeta_{rs}^2\Omega_{rs}^2(K\pm1)^2]^{1/2}$$

$$^{r,p}Q_K(\nu_-) = (1/2)(\nu_r+\nu_s) + (A-\bar{B} \pm 2(A-\bar{B})K -$$

$$- (1/2)[\delta^2+16A^2\zeta_{rs}^2\Omega_{rs}^2(K\pm1)^2]^{1/2} \qquad (5.20)$$

where the upper and lower signs in the above expressions refer to $\Delta K = +1$ (r type) and $\Delta K = -1$ (p type) transitions respectively.

It can be shown[54], that the vibration line strengths M_+ and M_- can be obtained as follows:

$$M_+ = a_K^2 M_r^2 + b_K^2 M_s^2 \mp \sigma_\zeta a_K b_K M_r M_s$$
$$M_- = b_K^2 M_r^2 + a_K^2 M_s^2 \pm \sigma_\zeta a_K b_K M_r M_s \qquad (5.21)$$

where M_r, M_s are the unperturbed vibrational transition moments in the B and C axes,

σ_ζ denotes the sign of ζ_{rs}

and the upper and lower signs refer to $\Delta K = +1$ and $\Delta K = -1$ transitions respectively.

The first two terms on the right hand side of expression (5.21) lead to a transfer of intensity from the stronger to the weaker band at high K. The third term leads to an asymmetry of intensity about the band centre in both bands.

Since a_K, $b_K > 0$ the asymmetry is determined by the sign of $\zeta_{rs}(M_r)(M_s)$. In other words, for the fundamental bands considered here the sign is determined by the following expression:

$$(\zeta^z_{rs})(d\mu^x/dQ_r)(d\mu^y/dQ_s) \qquad (5.22)$$

If expression (5.22) has a positive sign in front of it, we have a positive perturbation. In that case, the p-type sub-bands of the high frequency band and the r-type ones of the low frequency band are enhanced, and the r-type sub-bands of the high frequency band and the p-type ones of the low frequency band are depleted.

On the other hand, if expression (5.22) has a negative sign in front of it, we have a negative perturbation and the converse intensity perturbation is observed.

5.4 The ν_1 Band Of $C_2H.CDO$

The $\nu_1(a')$ band of $C_2H.CDO$ is due to a C-H stretching vibration. The band extends from about 3300 cm^{-1} to about 3350 cm^{-1} with the band centre at 3325.42 cm^{-1} as can be seen in Figure 5.4. At low resolution it looks like an A type band with a central maximum Q branch and P and R wings. At a relatively high resolution of 0.08 cm^{-1}, the central maximum branch remains unresolved, but the P and R branches are sufficiently resolved to allow assignment of J values .

A prominent peak to low frequency of the band centre is due to a 'sequence band' of the type $\nu_i+\nu_j-\nu_j$ discussed in the third chapter. The two primary candidates for ν_j are the two low frequency vibrations $\nu_9(a')$ = 201.5 cm^{-1} due to C-C≡C in plane vibration and $\nu_{12}(a'')$ = 249.9 cm^{-1} due to C-C≡C out of plane vibration. The rotational fine structure of such a 'sequence band' could interfere with the rotational fine structure of the main band producing a 'beating' phenomenon. Finally, we must recognise that in principle the in-plane vibrations of propynal give rise to A/B hybrid bands and so some type B structure might be present.

The method which was used in the analysis of this band can be divided into the following steps:

α. An initial non-linear least squares analysis was performed utilising the observed transitions with their J'', ΔJ assignments. Then, by using similar P and R branch expressions to the case of a symmetric rotor parallel band, a rough value for the $\bar{B}$ = (B+C)/2 constant for the upper state was obtained .

β. This value together with accurate ground state constants from the microwave study of the same species by Costain and Morton[51] were then used as data for the Mainir program . The transitions with their full ΔJ, ΔK_{-1} and ΔK_{+1} assignments were also included in the relevant datafile. A full least squares analysis was then performed using the full Hamiltonian, taking into account the asymmetry of the molecule. As a result, calculated line positions together with new rotational constants for the upper state were derived. This analysis only provides $\overline{B}'$ because of the nature of the transitions used. The A' constant is a trial value and was not solved for, since there is no information in the observed data to allow a better estimate for this constant.

γ. The new upper state rotational constants were then used as input data for the Kontur program which produced a simulated band contour, without taking into account any effects due to 'sequence bands'. These could include some shifting to the line positions. Then, a series of calculations was performed increasing the type B component until a best fit with the observed spectrum was achieved. It was found that the type B component was no more than 5% of the total band intensity.

The observed and calculated line positions together with their assignments are given in Table 5.2 and the rotational constants which were used in the computer simulation of the band contour are given in Table 5.3. The observed and calculated band contours are given in Figure 5.4. As can be seen from that Figure the agreement between the observed and calculated band contours is satisfactory.

5.5 The ν_5 Band Of $C_2H.CDO$

The $\nu_5(a')$ band of $C_2H.CDO$ is due to a C-D in plane rocking vibration. The band extends from about 1030 cm^{-1} to about 1130 cm^{-1} with the band centre at 1078.96 cm^{-1} as can be seen in Figure 5.5. At low resolution the band is characterised by a central minimum with P and R branches. At the relatively high resolution of 0.08 cm^{-1} the P and R branches are partially resolved revealing detailed fine structure which was found to be due to the A type component of the band. Also, a relatively simple K structure is present in the wings of the band which was found to be due to the B type component of the band. This structure is sufficiently resolved to allow assignment of K values.

The R branch of the main band is slightly perturbed by the presence of at least one other band which extends from about 1115 cm^{-1} to about 1140 cm^{-1}. The band centre of that weaker band is at 1127 cm^{-1}. That second band seems also to be an A/B hybrid type combination band. Once again there is also the possibility of the presence of 'sequence bands' perturbing the centre of the main band, as was the case for the ν_1 band of the same species.

The $\nu_5(a')$ band of $C_2H.CDO$ appears to be a hybrid since both type A and type B features were present.

The method which was used in the analysis of this band can be divided into the following steps:

α. Initial trial computer simulations were performed starting with the excited rotational constants from the analysis of the ν_1 band. Initially only the A' rotational constant was allowed to vary. When a relatively satisfactory match with the observed band was accomplished, the $\overline{B}'$ and also the individual B' and C' rotational constants were allowed to vary until an optimum set of upper state rotational

constants was found. All these simulations were carried out for a purely type A band ,which as it was noted above, was found to be the dominant component of the centre of the hybrid band. Then, further simulations were carried out by increasing the type B component , which contributes to the sharp features in the wings of the band, and decreasing the type A component by the same amount. After a satisfactory mixture of the two components was found, the excited state rotational constants were again allowed to vary, until the calculated K structure of the B component matched roughly the observed structure. The type A component was found to be 80% ± 5% of the total band intensity.

β. It can be shown that the positions of the Q heads for the P and R branches of a perpendicular band are given by the following formula, in the symmetric rotor approximation:

$$
\begin{aligned}
{}^{r,P}Q_{JK} = {} & \{\nu_o + (A-\bar{B})' - D_K'\} \pm \\
& \pm \{2(A-\bar{B})' - 4D_K'\}K + \\
& + \{(A-\bar{B})' - (A-\bar{B})'' - 6D_K'\}K^2 \pm \\
& \pm \{-4D_K'\}K^3 + \\
& + \{-D_K' + D_K''\}K^4
\end{aligned}
\qquad (5.23)
$$

where the upper sign refers to the R branch and the lower sign refers to the P branch.

The D_K centrifugal distortion constants for the ground and excited states were found to play a crucial role in the calculation of the Q heads. This is due to the relatively high values associated with these constants for these species which are of the order of 10^{-4} cm^{-1}.

In calculating the positions of the Q-heads, trial values of the rotational constants were used and the D_K constants

were set to zero. The differences between the observed Q-heads and those calculated from the simulated spectrum were fitted into a fourth order polynomial whose coefficients were:

a = correction in ν_o

b = $2\Delta(A-\bar{B})'$

c = $\Delta\delta(A-\bar{B})$

d = $-4D_K'$

e = $-D_K' + D_K''$ (5.24)

where Δ refers to the difference between observed and calculated values and δ refers to the difference between ground and excited state rotational constants. The effects of the centrifugal distortion constants were ignored in the coefficients a, b, c, in this initial iteration.

γ. The refined A' and D_K' constants were then used for a final iteration of the solution procedure. D_K'' was taken from the microwave determination of the ground state constants[51] and D_K' was calculated from coefficient e. Within experimental error, this value of D_K' agreed with the value obtained from coefficient d.

The observed and calculated line positions together with their assignments are given in Table 5.4 and the rotational constants used in the final computer simulation of the contour are given in Table 5.5. The observed and calculated band contours are given in Figure 5.5. The agreement between the observed and calculated K structure in the wings of the band is satisfactory. Also, the overall fine structure in the centre of the band seems to be reproduced quite well.

5.6 The ν_6, ν_{10} Pair Of Bands Of $C_2H.CDO$.

The ν_6 (a′) band of $C_2H.CDO$ species is due to a C-C stretching vibration. The band extends from about 850 cm^{-1} to about 920 cm^{-1} with the band centre at 876.5 cm^{-1} as can be seen in Figure 5.6. At low resolution the band is characterised by a central minimum with P and R branches. At the relatively high resolution of 0.08 cm^{-1} the two branches are partially resolved revealing detailed rotational structure which was found to be due to the A type component. Unfortunately, unlike the ν_5(a′) band no sharp features were present in the wings of the band. Nevertheless, the overall band could not be reproduced satisfactory without the addition of some B type component.

The central maximum of the ν_{10}(a′′) band which is due to a C-Dout of plane wagging vibration lies at 848 cm^{-1} slightly higher than the previously reported value of 841 cm^{-1}[47]. In fact, there is a weaker peak at 841 cm^{-1} which we assign to a ′sequence band′ of the ν_{10}(a′′) band. The ν_{10}(a′′) is a purely type C band. After a series of computer simulations for the observed band, it was found that the ν_6(a′) band is a hybrid of an A type band (ca. 70%) and a B type band (ca. 30%). In Watson′s thesis[47] a ζ Coriolis constant is predicted of ca. 0.40 assuming that the two bands interact with each other. Although such an interaction is expected, we have found in this case no evidence on the basis of our simulations for such a strong interaction. Consequently, it was assumed that ζ could be set to 0 pending the availability of higher resolution spectra.

The rotational constants which were used in the computer simulation of the band contour are given in Table 5.6. The observed and calculated band contours are given in Figure 5.6. The overall agreement between the observed and calculated ν_6(a′) band is found to be satisfactory.

5.7 The ν_7,ν_{11} Pair Of Bands Of $C_2H.CDO$.

The $\nu_7(a')$ band of $C_2H.CDO$ species is due to a C-H rocking vibration. The band extends from about 590 cm^{-1} to about 670 cm^{-1} with the central minimum at 651.17 cm^{-1}. As can be seen in Figure 5.7 this band appears to be 100% B type band. It exibits a typical K structure in the P branch. Close to this band is the $\nu_{11}(a'')$ band of the same species, due to a C-H out of plane wagging vibration. It extends from about 670 cm^{-1} to about 740 cm^{-1} with the central maximum at 692.67 cm^{-1}. The $\nu_{11}(a'')$ band is a purely type C one which exibits a typical K structure in the r branch. At low resolution the p branch of the C band and the r branch of the B band remain unresolved, while at the relatively high resolution of 0.08 cm^{-1} these are both resolved revealing their strongly perturbed K structures.

We have analysed the ν_7,ν_{11} pair of bands by making a series of computer simulations. They are a good example of a Coriolis interaction between B and C types of bands. The theory behind this type of interaction was covered in the relevant section of this chapter. In the present case, it was found that the interaction between the two bands is a strong one with a ζ Coriolis constant of 0.92. The sign of the Coriolis constant is determined from the relative intensities of the p and r branches of the two bands. In the present case, the p type sub-bands of the high frequency C type band and the r type sub-bands of the low frequency B type band are enhanced while the r type sub-bands of the C type band and the p type sub-bands of the B type band are depleted. Therefore, according to the convention described earlier, we have a positive perturbation which means that the vibrational angular momentum and the effective charge are rotating in the same sense when the two vibrations

are excited classically with a 90° phase shift[54].

From the computer simulations an optimum set of parameters was found. A relatively prominent feature could not be reproduced at ca. 667 cm^{-1}. This could be due to another band. Also, the appearance of the observed r branch of the B type band seems to be more complicated than the calculated one. Finally, 'hot bands' are also present and can be seen near the prominent band centre of the C type band. These 'hot bands' could give rise to a secondary, weaker K structure which can ,in fact, be observed in the r branch of the C type band and the p branch of the B type band.

The observed and calculated line positions together with their assignments are given in Table 5.7. The rotational constants which were used in the computer simulation of the band contour are given in Table 5.8. The observed and calculated band contours are given in Figure 5.7. The agreement between the observed and the calculated spectra with respect to the p and r branches of the C type band and the p branch of the B type band is excellent. The agreement between the observed and the calculated spectra with respect to the r branch of the B type band is satisfactory. The remaining discrepancies await spectra at higher resolution.

5.8 Other Observed Fundamentals Of $C_2H.CDO$.

There are another three fundamentals which were observed in the mid-IR spectrum of the $C_2H.CDO$ species.

The $\nu_2(a')$ band which is due to a C-D stretching vibration with a band centre at 2119 cm^{-1} and the $\nu_3(a')$ band which is due to a C≡C stretching vibration with a band centre at 2104.5 cm^{-1} can be seen in Figure 5.8. Both of

them seem to be hybrids of A and B type bands. In both cases, the A type component seems to be the predominant one but the B type component seems to be significant too. The evidence of the presence of the A type component comes from the central maxima of the two bands while the evidence of the presence of the B type component comes from the apparent K structure. Again, there are also 'hot bands' which complicate the appearance of the spectrum. Another major complication is the fact that the two bands are very close to each other. As a result, the P branch of the $\nu_2(a')$ band is buried underneath the R branch of the $\nu_3(a')$ band and there may be Coriolis interaction between the bands. The theory of this type of interaction has not been examined here and these bands await further investigation.

Another fundamental band which was observed was the $\nu_4(a')$ band which is due to a C=O stretching vibration with a band centre at 1678 cm^{-1}. Unfortunately, the spectrum was partially obscured by the presence of H_2O lines. Nevertheless, its overall appearance indicated that it is an A/B type hybrid band, as expected.

These three bands have been stored digitally for further analysis.

5.9 The ν_6,ν_{10} Pair Of Bands Of $C_2D.CDO$.

The $\nu_6(a')$ band of $C_2D.CDO$ species is due to a C-C stretching vibration. The band extends from about 830 cm^{-1} to about 910 cm^{-1} with the band centre at 870.0 cm^{-1} as can be seen in Figure 5.9. At low resolution the band is characterised by a central minimum with P and R branches. At the relatively high resolution of 0.08 cm^{-1} the two branches are partially resolved revealing detailed

rotational structure which , as for the $C_2H.CDO$ species, was found to be due to the A type component. Yet again no sharp features were present in the wings of the band. Nevertheless, the overall band could not be reproduced satisfactorily without the addition of a B type component.

The central maximum of the $\nu_{10}(a'')$ band which is due to a $C-D_2$ (see note at the bottom of Table 5.1) out of plane wagging vibration, lies at 849 cm^{-1}. The $\nu_{10}(a'')$ band is a purely type C band.

After a series of computer simulations with the observed band it was found that the $\nu_6(a')$ band is a hybrid of 65% type A band and 35% type B band. Again, as in $C_2H.CDO$, it was assumed that there was a negligible Coriolis interaction between $\nu_6(a')$ and $\nu_{10}(a'')$ bands, so ζ was set to Ø.

The rotational constants which were used in the computer simulation of the observed $\nu_6(a')$ band are given in Table 5.9. The observed and calculated band contours are given in Figure 5.9.

The overall agreement between the observed and calculated $\nu_6(a')$ bands is found to be satisfactory.

5.1Ø Other Observed Fundamentals Of The $C_2D.CDO$.

There are another four fundamentals which were observed in the mid-IR spectrum of the $C_2D.CDO$ species.

The $\nu_2(a')$ band is due to a $C-D_2$ stretching vibration. It extends from about 2Ø6Ø cm^{-1} to about 216Ø cm^{-1} with a band centre at 211Ø cm^{-1}as can be seen in Figure 5.1Ø. It is an almost 1ØØ% type B band which seems relatively unperturbed.

The $\nu_3(a')$ band is due to a C≡C stretching vibration.

It extends from about 1950 cm^{-1} to about 2010 cm^{-1} with a band centre at 1984 cm^{-1} as seen in Figure 5.11 . There is also a possible prominent 'hot band' at 1980 cm^{-1}. This band seems to be an almost 100% type A band.

The $\nu_4(a')$ band which is due to a C=C stretching vibration with a band centre at 1689 cm^{-1} was again partially obscured by the presence of H_2O lines.

Finally, the $\nu_5(a')$ band which is due to a C-D_2 out of plane rocking vibration, extends from about 1050 cm^{-1} to 1120 cm^{-1} with a band centre at 1071 cm^{-1} and is seen in Figure 5.12. This band has the appearance of an A/B hybrid type band. The spectrum seems to be complicated by the presence of a strong feature at 1090 cm^{-1} possibly due to another unassigned band.

These four bands have been stored digitally to await futher analysis.

5.11 Suggested Further Work

Apart from the rotational analysis of the remaining observed bands for the two species described in sections 5.8 and 5.10, it would be useful to:

α. Study the spectrum at longer absorption path lengths using the same MCT detector in order to observe the $\nu_1(a')$ band of $C_2D.CDO$ species and the $\nu_8(a')$ band of the $C_2H.CDO$ and $C_2D.CDO$ species which seem to be relatively weak.

β. Use a far-infrared detector to observe the low frequency ν_9 (a') and $\nu_{12}(a'')$ bands of the two species and more importantly the $\nu_7(a')$,$\nu_{11}(a'')$ Coriolis interacting pair of bands of the $C_2D.CDO$ species.

γ. Record the spectrum at higher resolution for a complete

analysis of all the fine structure in these bands. Unfortunately, the Bruker spectrometer used for this work has an ultimate resolution of Ø.Ø3 cm^{-1} but even this was unattainable due to mulfunction of the instrument.

The present partial rotational analysis should provide a starting point for further work.

Table 5.1

Fundamental Wavenumbers For Propynal

Γ	ν_r	mode	ν/cm^{-1}			
			$C_2H.CHO$	$C_2D.CHO$	$C_2H.CDO$	$C_2D.CDO$
a′	ν_1	C-H_1stretching	3326[47]	2605[47]	3325.42	-
	ν_2	C-H_2stretching	2858.231[49]	2857.888[50]	2119	2110
	ν_3	C≡C stretching	2106[47]	1977[47]	2104.5	1984
	ν_4	C=O stretching	1696.9[47]	1697.0[47]	1678	1689
	ν_5	C-H_2rocking	1388[47]	1387.6[47]	1078.96	1071
	ν_6	C-C stretching	943.7[47]	933.6[47]	876.5	870
	ν_7	C-H_1rocking	650.0[47]	507.9[47]	651.17	507.9[52]
	ν_8	C-C=O bending	613.7[47]	609.9[47]	611.9[47]	607[52]
	ν_9	C-C≡C bending	205.3[47]	195.6[47]	201.5[47]	192.8[52]
a″	ν_{10}	C-H_2wagging	981.2[47]	980.9[47]	848	849
	ν_{11}	C-H_1wagging	692.7[47]	548.6[47]	692.67	542.5[52]
	ν_{12}	C-C≡C bending	260.6[47]	248.5[47]	249.9[47]	237.1[52]

Note: H_2 refers to the hydrogen in CHO group while H_1 refers to the hydrogen in C_2H group. Also, ν_7-ν_9 and ν_{11}-ν_{12} fundamentals for the $C_2D.CDO$ species have been taken from Edward's electronic analysis of the spectrum[52].

Table 5.2

Observed And Calculated Lines For $\nu_1(a')$ Fundamental Band Of $C_2H.CDO$ (cm^{-1})

J′	K'_{-1}	K'_{+1}	J′′	K''_{-1}	K''_{+1}	ν(Obs.)	ν(Obs.-Calc.)
74	5	69	75	5	70	3300.96	0.33
73	5	68	74	5	69	3301.26	0.20
72	5	67	73	5	68	3301.59	0.12
71	5	66	72	5	67	3301.94	0.07
70	5	65	71	5	66	3302.30	0.03
69	5	64	70	5	65	3302.62	-0.03
68	5	63	69	5	64	3302.96	-0.06
67	5	62	68	5	63	3303.32	-0.06
66	5	61	67	5	62	3303.66	-0.08
65	5	60	66	5	61	3304.00	-0.10
64	5	59	65	5	60	3304.32	-0.12
63	5	58	64	5	59	3304.65	-0.13
62	5	57	63	5	58	3304.99	-0.14
61	5	56	62	5	57	3305.31	-0.16
60	5	55	61	5	56	3305.66	-0.14
59	5	54	60	5	55	3305.98	-0.16
58	5	53	59	5	54	3306.32	-0.15
57	5	52	58	5	53	3306.71	-0.09
56	5	51	57	5	52	3307.08	-0.05
55	5	50	56	5	51	3307.41	-0.06
54	5	49	55	5	50	3307.75	-0.05
53	5	48	54	5	49	3308.07	-0.06
52	5	47	53	5	48	3308.40	-0.06
51	5	46	52	5	47	3308.75	-0.04
50	5	45	51	5	46	3309.06	-0.06
49	5	44	50	5	45	3309.40	-0.05
48	5	43	49	5	44	3309.73	-0.06
47	5	42	48	5	43	3310.04	-0.08
46	5	41	47	5	42	3310.38	-0.07
45	5	40	46	5	41	3310.71	-0.07
43	5	38	44	5	39	3311.34	-0.10
42	5	37	43	5	38	3311.69	-0.08
41	5	36	42	5	37	3311.99	-0.11
40	5	35	41	5	36	3312.29	-0.13
39	5	34	40	5	35	3312.61	-0.14
38	5	33	39	5	34	3313.07	-0.01
37	5	32	38	5	33	3313.39	-0.02

J'	K'_{-1}	K'_{+1}	J''	K''_{-1}	K''_{+1}	ν(Obs.)	ν(Obs.-Calc.)
36	5	31	37	5	32	3313.72	-0.01
35	5	30	36	5	31	3313.96	-0.10
34	5	29	35	5	30	3314.29	-0.09
33	5	28	34	5	29	3314.62	-0.09
32	5	27	33	5	28	3314.97	-0.06
31	5	26	32	5	27	3315.27	-0.08
30	5	25	31	5	26	3315.60	-0.07
29	5	24	30	5	25	3315.92	-0.08
28	5	23	29	5	24	3316.25	-0.07
27	5	22	28	5	23	3316.57	-0.07
26	5	21	27	5	22	3316.88	-0.08
25	5	20	26	5	21	3317.20	-0.08
24	5	19	25	5	20	3317.52	-0.08
23	5	18	24	5	19	3317.83	-0.08
22	5	17	23	5	18	3318.15	-0.08
21	5	16	22	5	17	3318.47	-0.08
20	5	15	21	5	16	3318.78	-0.08
19	5	14	20	5	15	3319.10	-0.08
18	5	13	19	5	14	3319.43	-0.07
17	5	12	18	5	13	3319.73	-0.08
16	5	11	17	5	12	3320.06	-0.06
15	5	10	16	5	11	3320.38	-0.06
14	5	9	15	5	10	3320.76	0.01
13	5	8	14	5	9	3321.09	0.03
12	5	7	13	5	8	3321.39	0.02
11	5	6	12	5	7	3321.71	0.02
10	5	5	11	5	6	3322.01	0.01
9	5	4	10	5	5	3322.34	0.03
8	5	3	9	5	4	3322.65	0.03
7	5	2	8	5	3	3322.94	0.01
6	5	1	7	5	2	3323.26	0.02
5	5	0	6	5	1	3323.62	0.07
8	5	3	7	5	2	3327.88	0.06
9	5	4	8	5	3	3328.17	0.05
10	5	5	9	5	4	3328.47	0.05
11	5	6	10	5	5	3328.77	0.04
12	5	7	11	5	6	3329.06	0.03
13	5	8	12	5	7	3329.36	0.03
14	5	9	13	5	8	3329.66	0.03
15	5	10	14	5	9	3329.96	0.03
16	5	11	15	5	10	3330.26	0.03
17	5	12	16	5	11	3330.56	0.04
18	5	13	17	5	12	3330.87	0.05
19	5	14	18	5	13	3331.17	0.06

J'	K'_{-1}	K'_{+1}	J''	K''_{-1}	K''_{+1}	ν(Obs.)	ν(Obs.-Calc.)
20	5	15	19	5	14	3331.45	0.03
21	5	16	20	5	15	3331.74	0.03
22	5	17	21	5	16	3332.06	0.05
23	5	18	22	5	17	3332.36	0.06
24	5	19	23	5	18	3332.66	0.06
25	5	20	24	5	19	3332.93	0.04
26	5	21	25	5	20	3333.23	0.04
27	5	22	26	5	21	3333.52	0.04
28	5	23	27	5	22	3333.82	0.05
29	5	24	28	5	23	3334.09	0.02
30	5	25	29	5	24	3334.38	0.01
31	5	26	30	5	25	3334.66	0.01
32	5	27	31	5	26	3334.95	0.01
33	5	28	32	5	27	3335.24	-0.01
34	5	29	33	5	28	3335.51	-0.03
35	5	30	34	5	29	3335.79	-0.03
36	5	31	35	5	30	3336.09	-0.02
37	5	32	36	5	31	3336.35	-0.04
38	5	33	37	5	32	3336.65	-0.03
39	5	34	38	5	33	3336.88	-0.09
40	5	35	39	5	34	3337.13	-0.13
41	5	36	40	5	35	3337.43	-0.12
42	5	37	41	5	36	3337.80	-0.04
43	5	38	42	5	37	3338.05	-0.07
44	5	39	43	5	38	3338.38	-0.03
45	5	40	44	5	39	3338.70	0.00
46	5	41	45	5	40	3338.97	-0.01
47	5	42	46	5	41	3339.26	-0.01
48	5	43	47	5	42	3339.53	-0.03
49	5	44	48	5	43	3339.80	-0.04
50	5	45	49	5	44	3340.07	-0.06
51	5	46	50	5	45	3340.33	-0.09
52	5	47	51	5	46	3340.59	-0.12
53	5	48	52	5	47	3340.89	-0.10
54	5	49	53	5	48	3341.16	-0.12
55	5	50	54	5	49	3341.41	-0.16
56	5	51	55	5	50	3341.68	-0.18
57	5	52	56	5	51	3341.94	-0.21
58	5	53	57	5	52	3342.26	-0.18
59	5	54	58	5	53	3342.48	-0.25
60	5	55	59	5	54	3342.75	-0.27
61	5	56	60	5	55	3342.96	-0.34
62	5	57	61	5	56	3343.25	-0.34
63	5	58	62	5	57	3343.52	-0.35

J'	K'_{-1}	K'_{+1}	J''	K''_{-1}	K''_{+1}	ν(Obs.)	ν(Obs.-Calc.)
64	5	59	63	5	58	3343.75	-Ø.4Ø
65	5	6Ø	64	5	59	3343.98	-Ø.45
66	5	61	65	5	6Ø	3344.24	-Ø.46
67	5	62	66	5	61	3344.5Ø	-Ø.47
68	5	63	67	5	62	3344.76	-Ø.46
69	5	64	68	5	63	3345.Ø3	-Ø.44
7Ø	5	65	69	5	64	3345.3Ø	-Ø.42
71	5	66	7Ø	5	65	3345.53	-Ø.42
72	5	67	71	5	66	3345.75	-Ø.42
73	5	68	72	5	67	3346.Ø5	-Ø.32
74	5	69	73	5	68	3346.31	-Ø.26
75	5	7Ø	74	5	69	3346.56	-Ø.18
76	5	71	75	5	7Ø	3346.82	-Ø.Ø9

Table 5.3

Derived Constants For $\nu_1(a')$ Fundamental Band

Of $C_2H.CDO$.

Parameter	Derived Value
Type A	95%-100%
Type B	Ø-5%
ν_o/ cm^{-1}	3325.42
A''/cm^{-1}	1.7268[51]
α_1^A/cm^{-1}	Ø.ØØ48
B''/cm^{-1}	Ø.159828[51]
α_1^B/cm^{-1}	-Ø.ØØ1699
C''/cm^{-1}	Ø.146Ø63[51]
α_1^C/cm^{-1}	Ø.ØØ2158
σ/cm^{-1}	Ø.Ø98

Note: α^A= A''-A' etc., σ = standard deviation

Table 5.4

Observed And Calculated Lines For $\nu_5(a')$ Fundamental Band Of $C_2H.CDO$ (cm^{-1})

J'	K'_{-1}	J''	K''_{-1}	ν(Obs.)	ν(Obs.-Calc.)
29	5	29	4	1094.19	0.07
29	6	29	5	1097.60	-0.03
29	7	29	6	1101.11	-0.05
29	8	29	7	1104.66	-0.04
29	9	29	8	1108.23	-0.02
29	10	29	9	1111.80	0.02
29	11	29	10	1115.29	0.01
29	12	29	11	1118.78	0.06
29	13	29	12	1122.20	0.12
28	5	28	6	1062.84	-0.01
28	6	28	7	1060.08	-0.01
28	7	28	8	1057.36	-0.05
28	8	28	9	1054.75	-0.04
28	9	28	10	1052.16	-0.05
28	10	28	11	1049.66	-0.01
28	11	28	12	1047.09	-0.05
28	12	28	13	1044.61	0.00

Table 5.5

Derived Constants For $\nu_5(a')$ Fundamental Band

Of $C_2H.CDO$.

Parameter	Derived Value
Type A	75-85%
Type B	15-25%
ν_o/cm^{-1}	1078.96
α_5^A/cm^{-1}	-0.0392
α_5^B/cm^{-1}	-0.002247
α_5^C/cm^{-1}	0.002558
D_K''/cm^{-1}	0.000102[51]
β_5^K/cm^{-1}	-0.000076
σ/cm^{-1}	0.056

Note: See note at the bottom of Table 5.3 , $\beta^K = D_K''-D_K'$.

Table 5.6

Best Fit Constants For $\nu_6(a')$ Fundamental Band

Of $C_2H.CDO$.

Parameter	Best Fit Value
Type A	65-75%
Type B	25-35%
ν_o/cm^{-1}	876.5
α_6^A/cm^{-1}	-0.0632
α_6^B/cm^{-1}	0.0009
α_6^C/cm^{-1}	0.0009

Note: See note at the bottom of Table 5.3.

Table 5.7

Observed And Calculated Lines For $\nu_7(a'),\nu_{11}(a'')$ Pair Of Fundamental Bands Of $C_2H.CDO$. (cm^{-1})

J′	K'_{-1}	J″	K''_{-1}	ν(Obs.)	ν(Obs.-Calc.)
24	4	24	3	706.90	-0.01
24	5	24	4	711.95	-0.05
24	6	24	5	717.25	-0.06
24	7	24	6	722.73	-0.08
24	8	24	7	728.34	-0.13
24	9	24	8	734.03	-0.20
24	3	24	4	683.30	0.01
24	4	24	5	681.81	0.13
24	5	24	6	680.64	0.08
24	6	24	7	679.70	0.03
24	7	24	8	678.96	0.00
24	8	24	9	678.39	-0.01
24	9	24	10	677.94	-0.03
24	10	24	11	677.55	-0.10
24	3	24	4	637.62	-0.01
24	4	24	5	632.89	-0.05
24	5	24	6	627.84	-0.16
24	6	24	7	622.59	-0.15
24	7	24	8	617.16	-0.16
24	8	24	9	611.54	-0.22
24	9	24	10	606.03	-0.02
24	10	24	11	600.42	-0.04
24	11	24	12	594.86	0.07

Table 5.8

Best Fit Constants For $\nu_7(a')$,$\nu_{11}(a'')$ Pair

Of Fundamental Bands Of $C_2H.CDO$.

Parameter	Best Fit Value
Type B	100%
ν_7 /cm^{-1}	651.17
Type C	100%
ν_{11}/cm^{-1}	692.67
$\alpha^A_{7,11}$/cm^{-1}	-0.0114
$\alpha^B_{7,11}$/cm^{-1}	-0.0008
$\alpha^C_{7,11}$/cm^{-1}	0.0011
$\zeta_{7,11}$	0.92±0.01
$\delta_{7,11}$/cm^{-1}	41.5

Note: See note at the bottom of Table 5.3, $\delta_{7,11} = \nu_{11}-\nu_7$.

Table 5.9

Best Fit Constants For $\nu_6(a')$ Fundamental Band

Of $C_2D.CDO$.

Parameter	Best Fit Value
Type A	60-70%
Type B	30-40%
$\tilde{\nu}_o/cm^{-1}$	870.0
A''/cm^{-1}	1.7037[51]
α_6^A/cm^{-1}	-0.0632
B''/cm^{-1}	0.147739[51]
α_6^B/cm^{-1}	0.0009
C''/cm^{-1}	0.135747[51]
α_6^C/cm^{-1}	0.0009

Note: See note at bottom of Table 5.3.

Figures

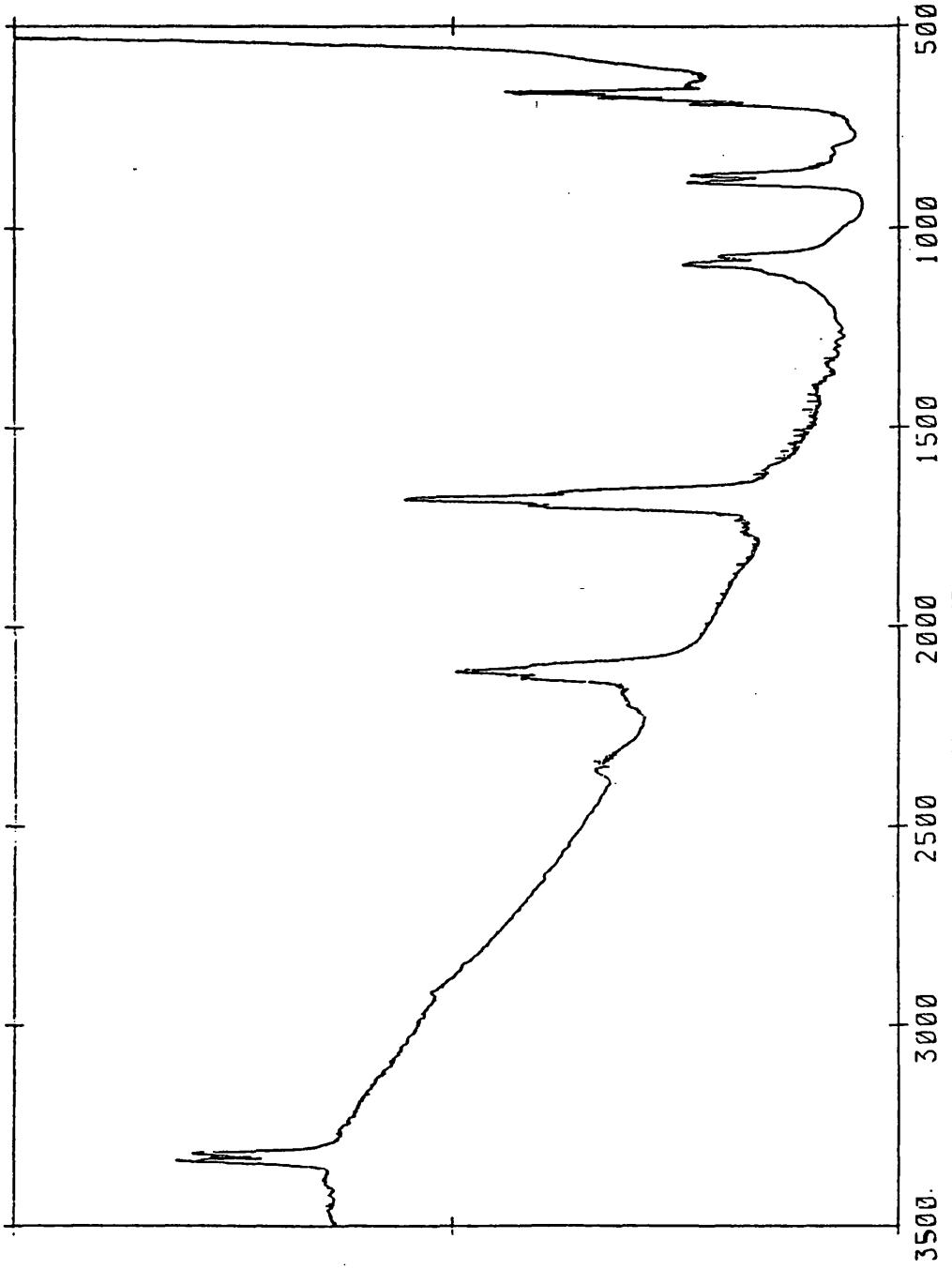

Figure 5.1

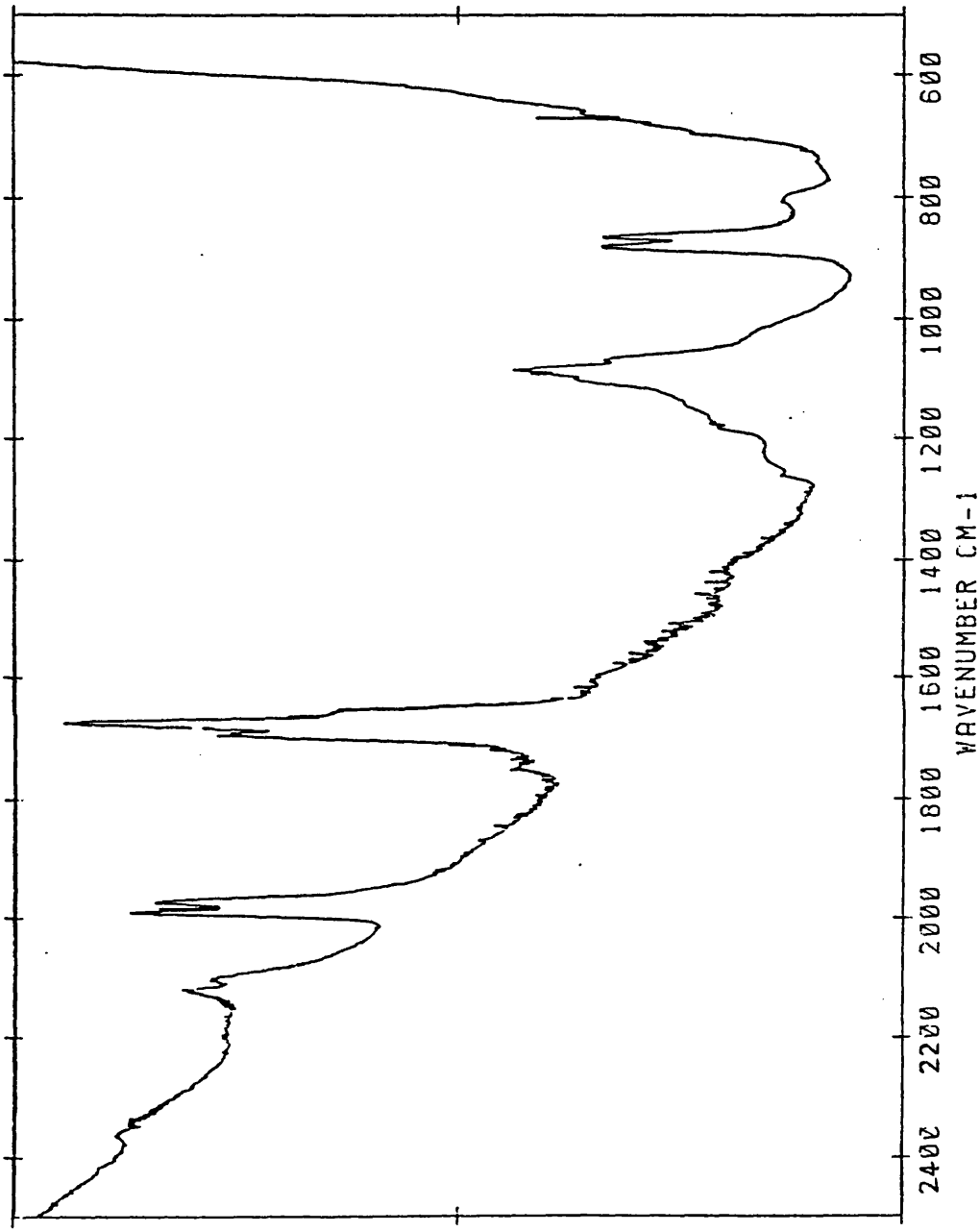
2400
2200
2000
1800
1600
1400
1200
1000
800
600
WAVENUMBER CM-1

Figure 5.2

Figure 5.3
Second Order Coriolis Interaction Between B And C Type Bands
For A Prolate Asymmetric Rotor Belonging
To The C_s Point Group

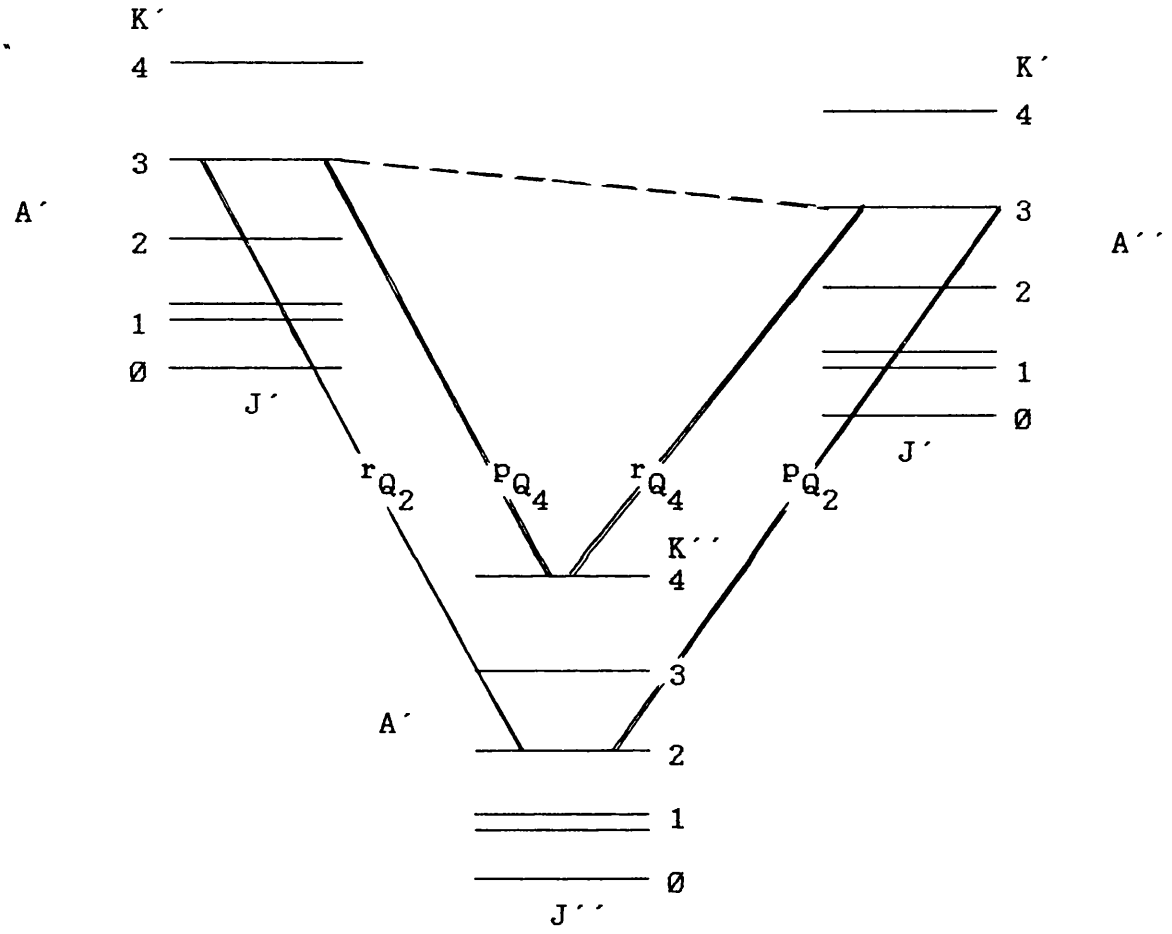

Note : α. The pre-superscript to Q ($\Delta J = Ø$) indicates the value of ΔK. In this case ΔK can be either +1 ,-1 which is indicated by p,r. The post-subscript to Q indicates the value of K´´ as it is obvious from the diagram.

β. In theory, all the energy levels (except K=Ø) are doublets but in practice only for the first levels these doublets are sufficiently resolved.

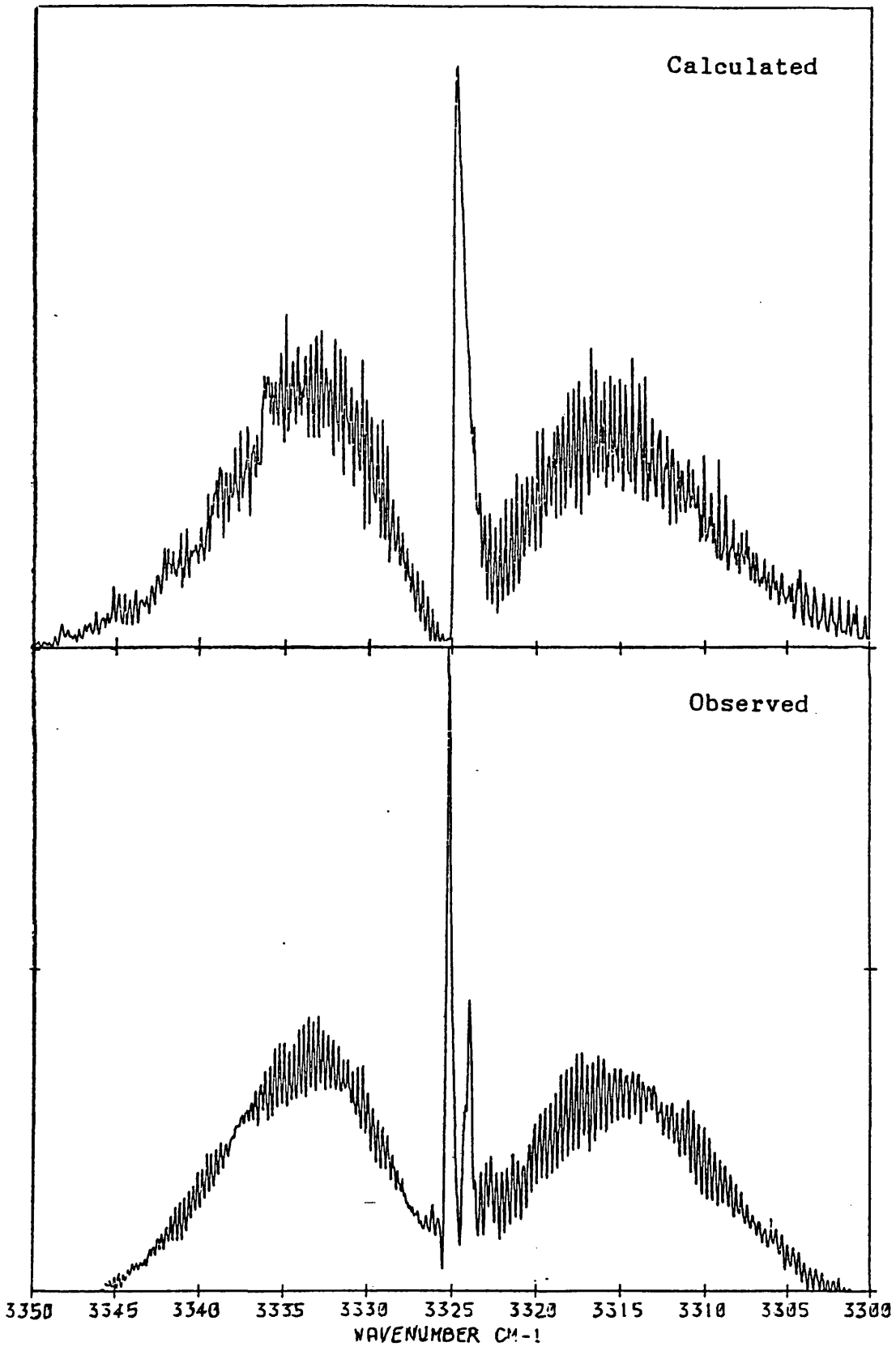
Calculated
Observed
3350
3345
3340
3335
3330
3325
3320
3315
3310
3305
3300
WAVENUMBER CM-1

Figure 5.4

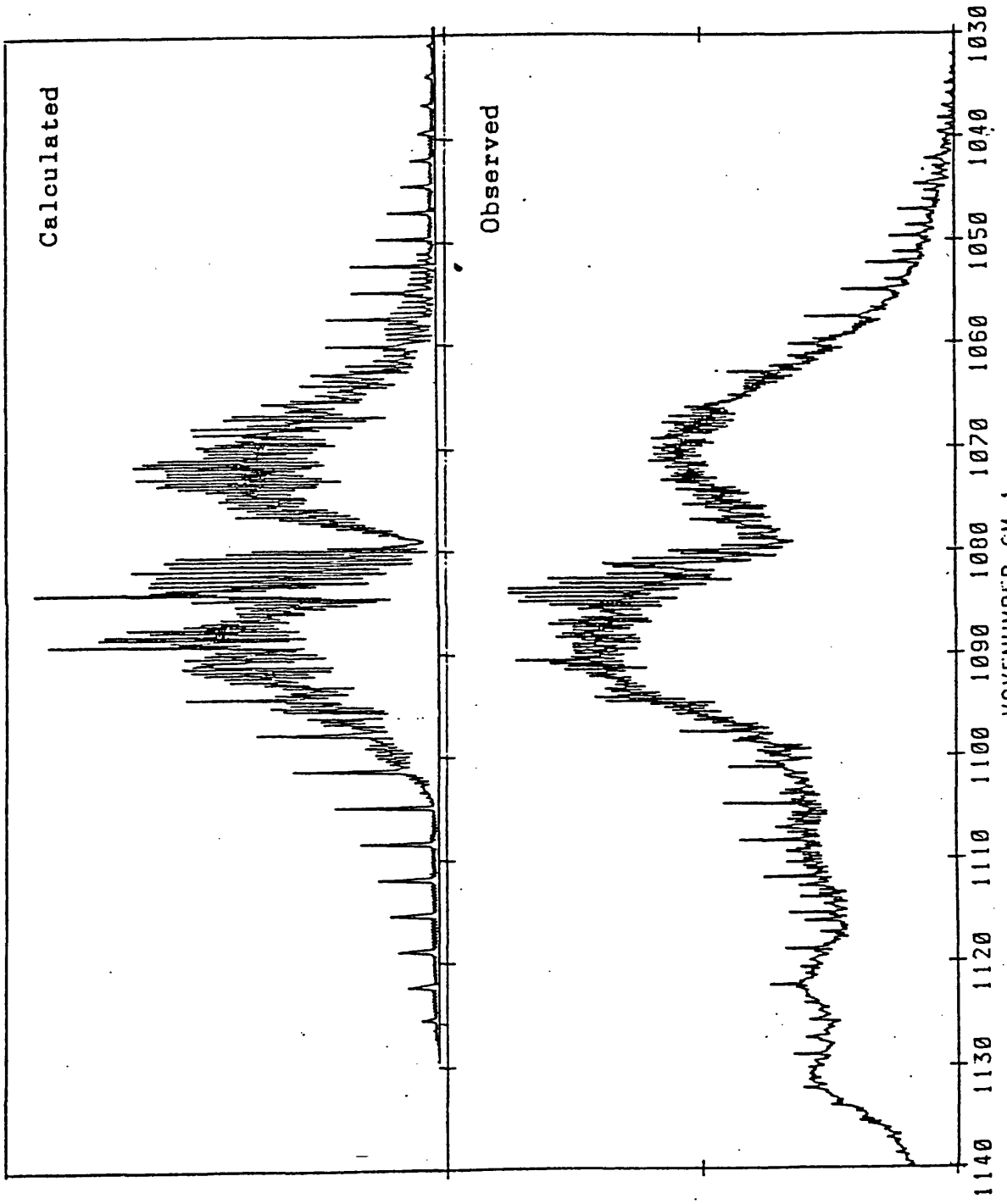
Calculated
Observed
1030
1040
1050
1060
1070
1080
1090
1100
1110
1120
1130
1140
WAVENUMBER CM-1

Figure 5.5

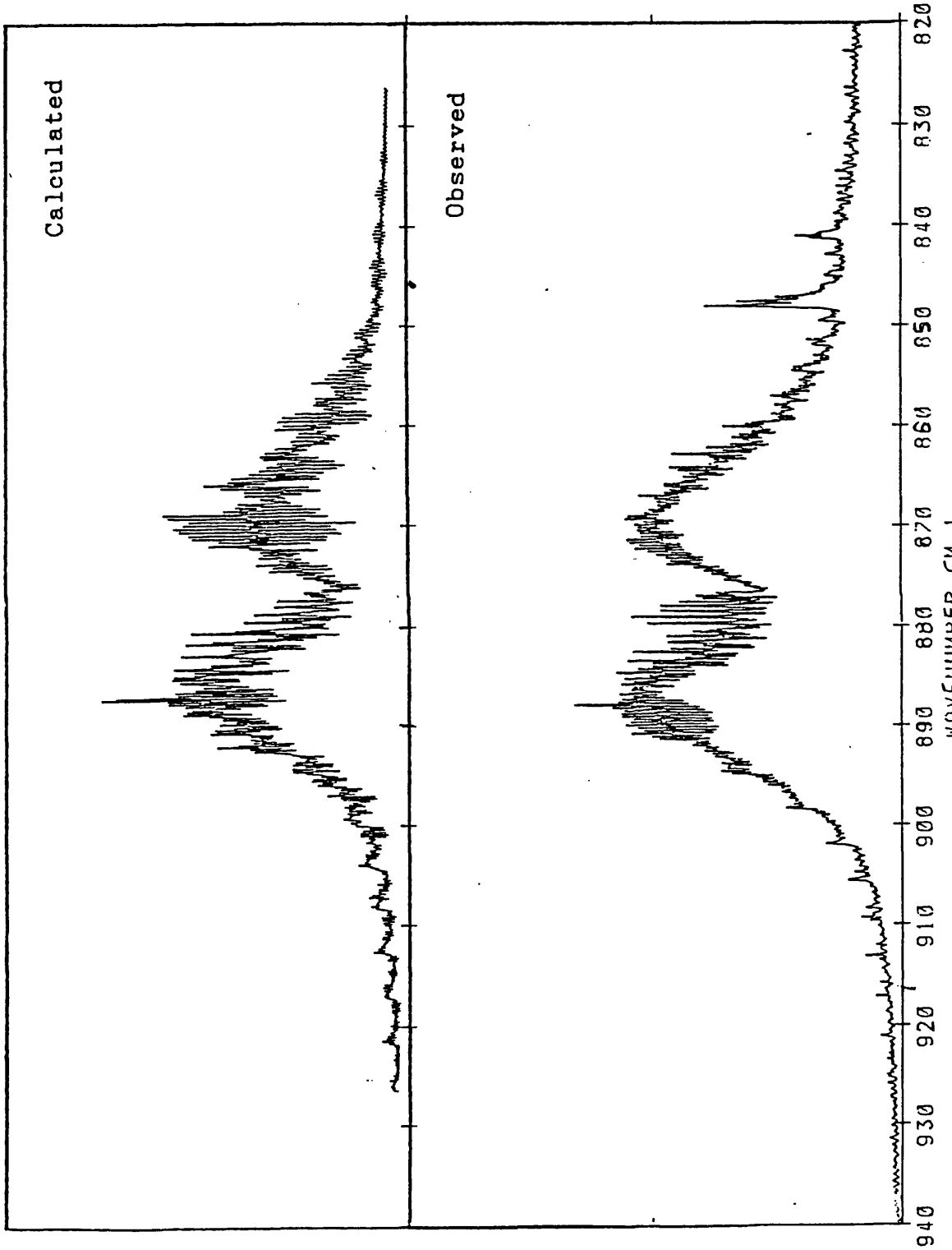
Calculated
Observed
820
830
840
850
860
870
880
890
900
910
920
930
940
WAVENUMBER CM-1

Figure 5.6

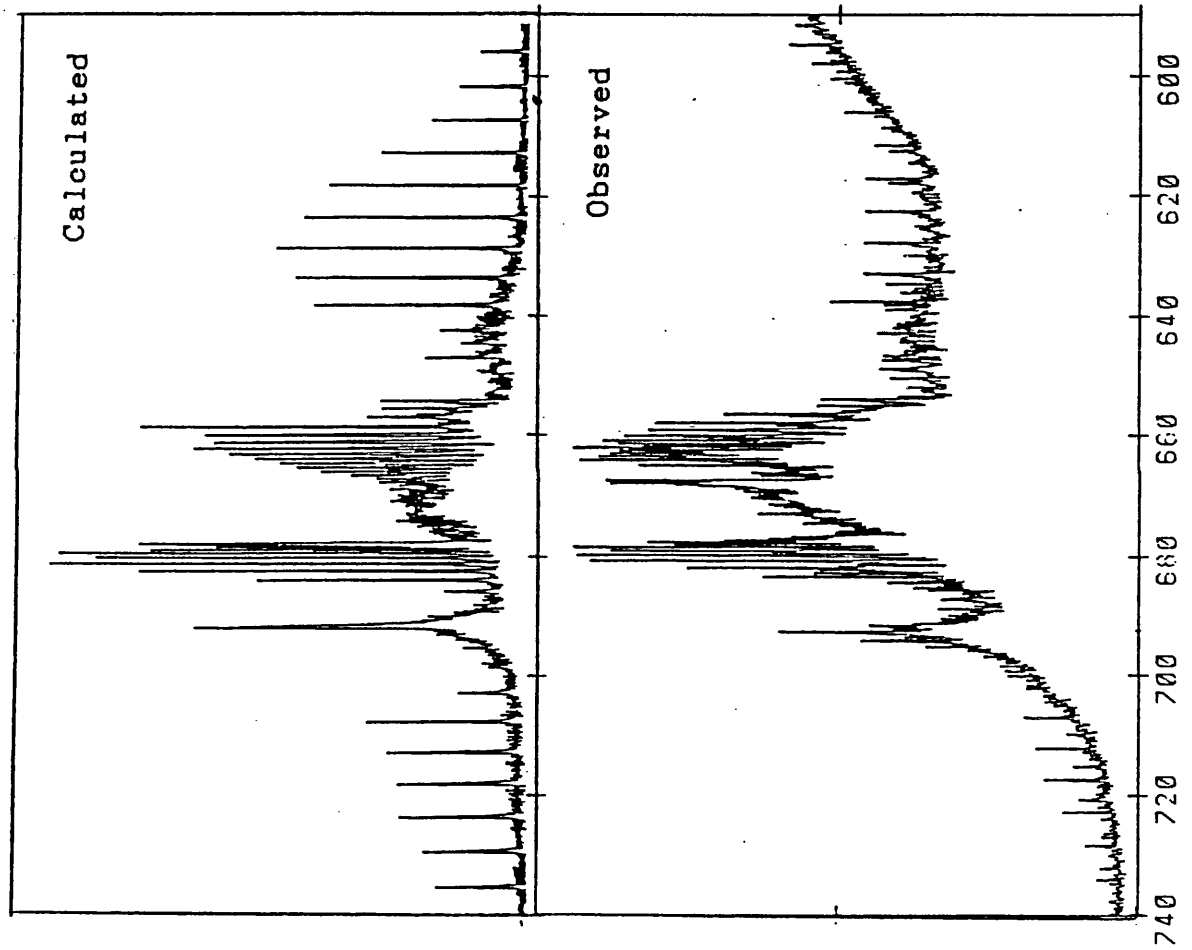
Calculated
Observed
740
720
700
680
660
640
620
600
WAVENUMBER CM-1

Figure 5.7

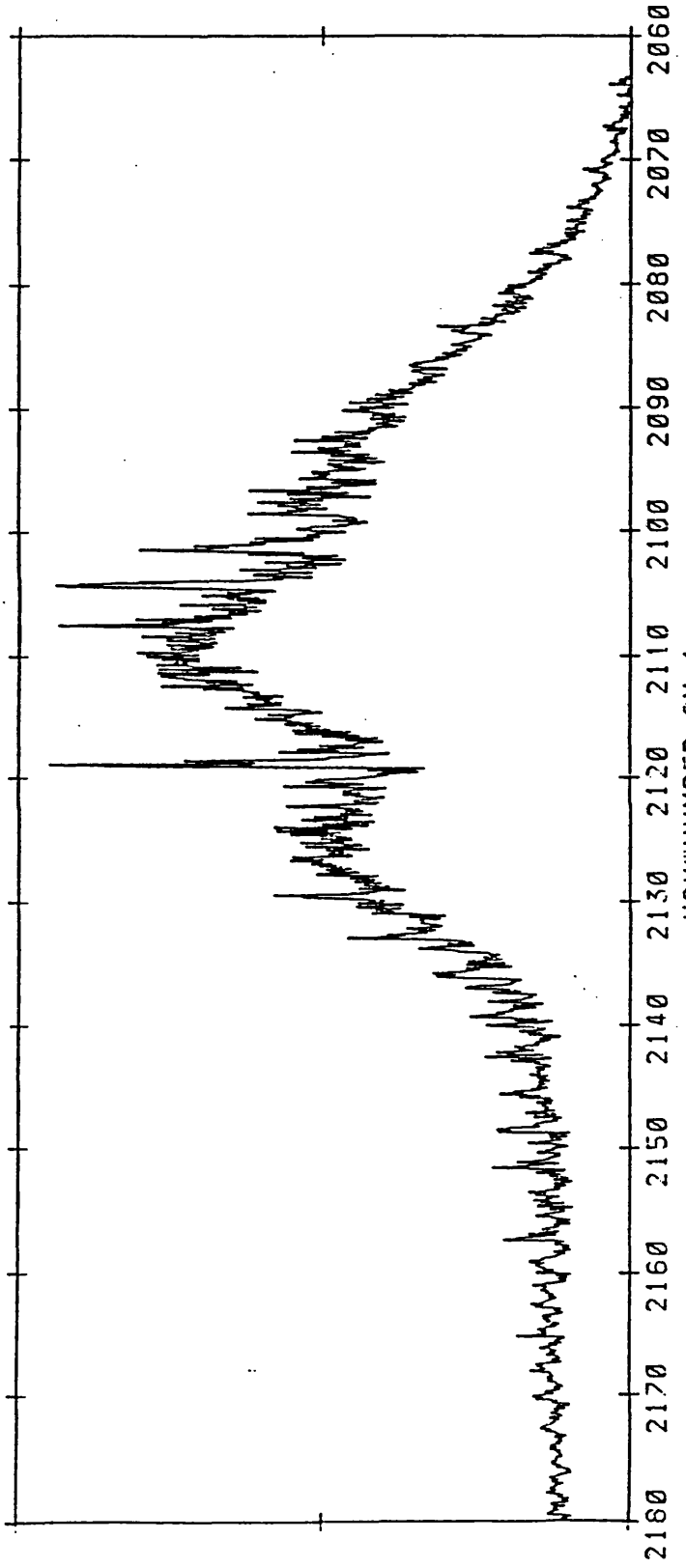
2060
2070
2080
2090
2100
2110
2120
2130
2140
2150
2160
2170
2180
WAVENUMBER CM-1

Figure 5.8

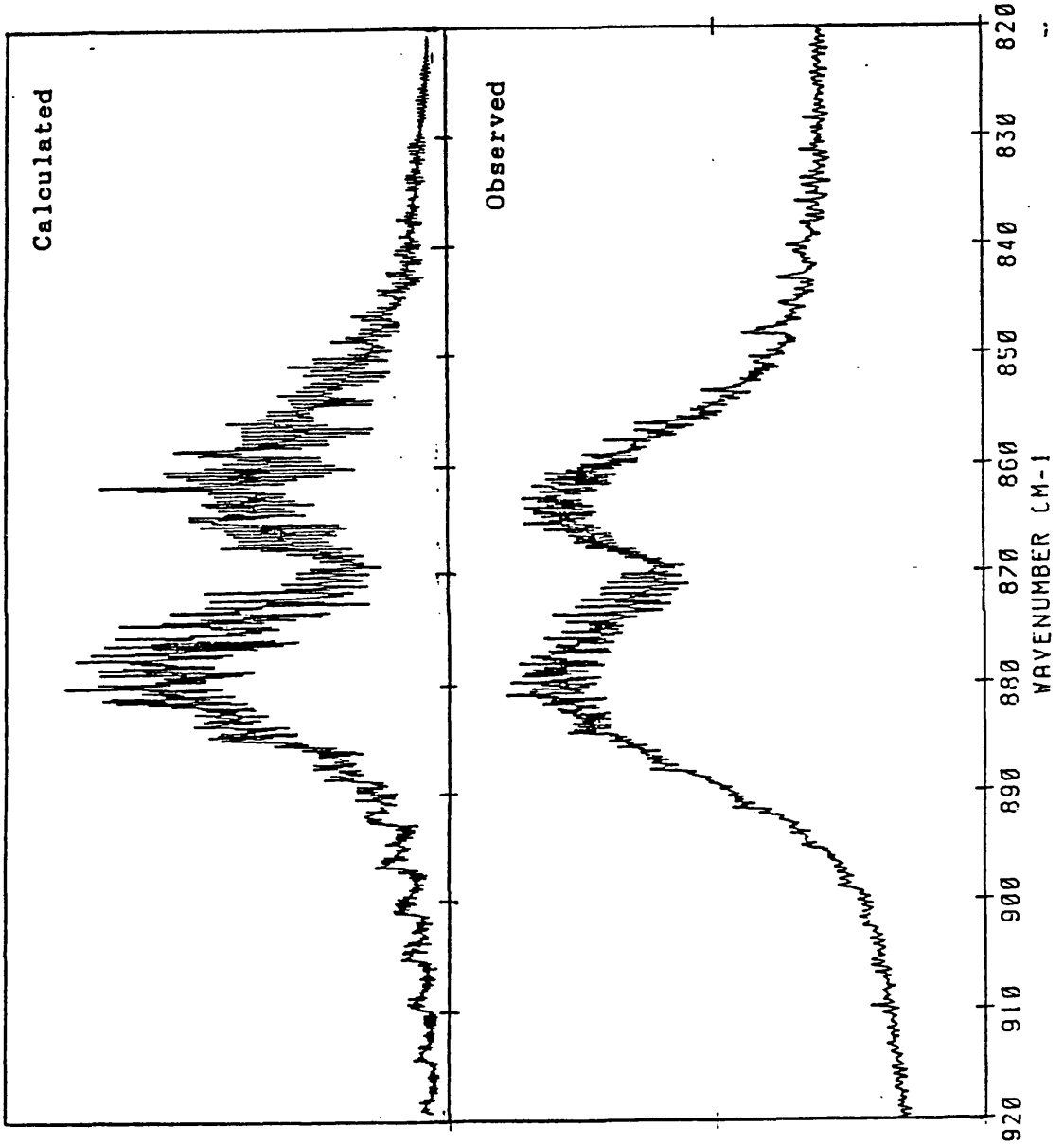
Calculated
Observed
920
910
900
890
880
870
860
850
840
830
820
WAVENUMBER (M-1

Figure 5.9

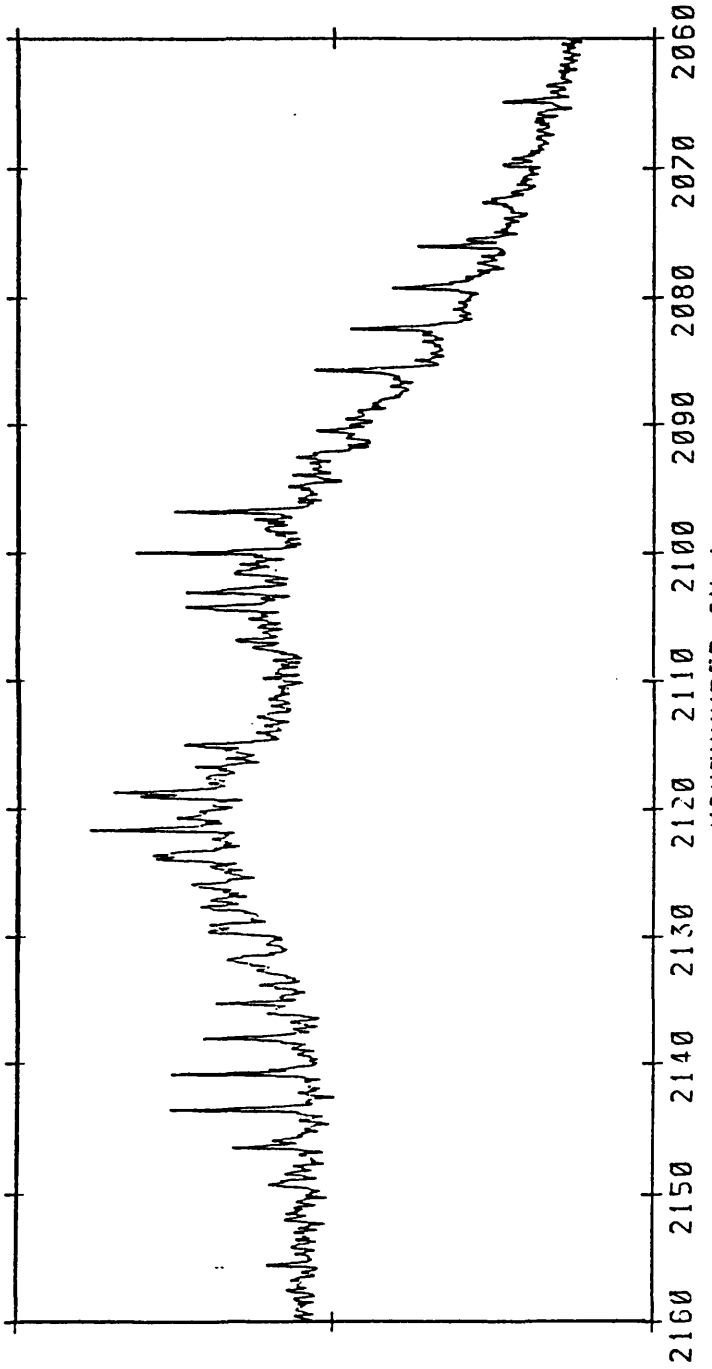
2160
2150
2140
2130
2120
2110
2100
2090
2080
2070
2060
WAVENUMBER CM-1

Figure 5.10

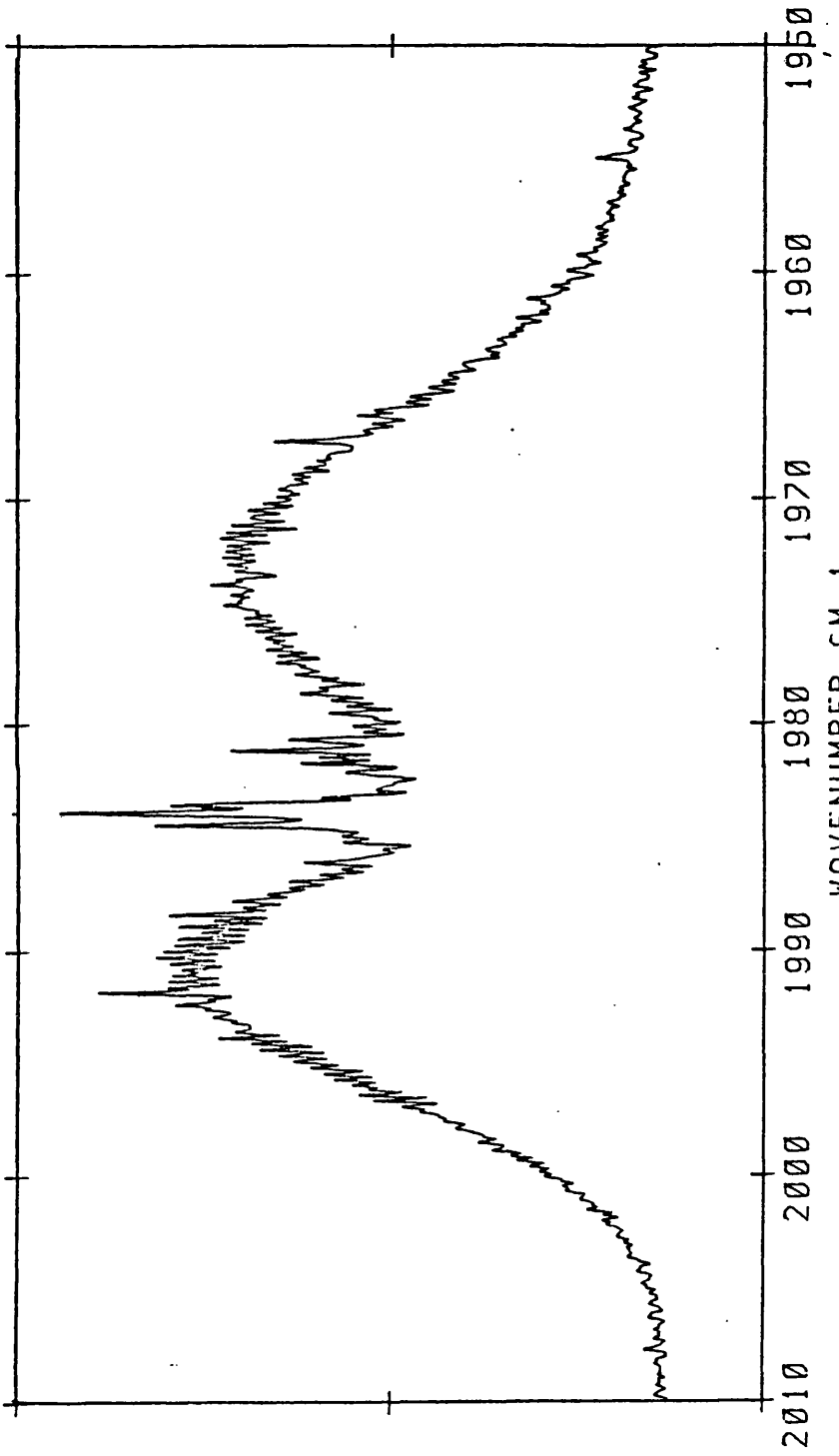

Figure 5.11

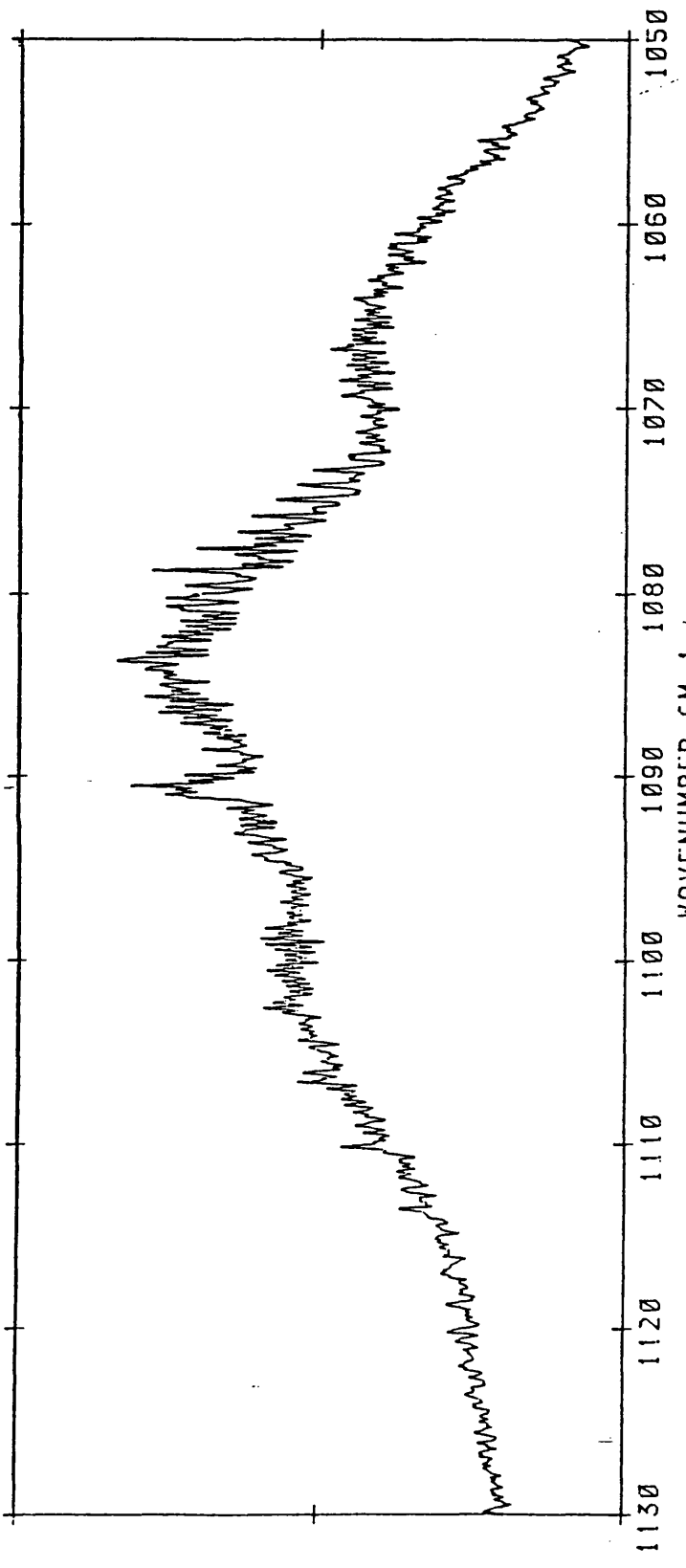

Figure 5.12

Appendix 1

Subroutine For The Calculation Of 1-Resonance In Symmetric Rotors.

```
      SUBROUTINE PEBAND
CCCC
CCCC  K.TAYLAJORAKIS -1987
CCCC  THIS SUBROUTINE DEALS WITH L RESONANCE PERTURBATION.
CCCC  IT IS A MODIFICATION OF AN EARLIER SUBROUTINE WHICH
CCCC  DID NOT INCLUDE SUCH A PERTURBATION.
CCCC
      IMPLICIT REAL*8(A-H,O-Z)
      DIMENSION EFACT(200),ENERG(200),CONT(6001),ENEU(200),CJ(200),
     1ENEJP(200),KSTN(5),JSTN(2)
      COMMON CONT,EFACT,ENERG,ENEU,CJ,COEF(2),AG,BG,AU,BU,AGZET,AUZET,
     1AGBG,AUBU,FACT,FREQ,CLW,EMIN,EMAX,PI,DELNU,DJG,DJKG,DKG,DJJ,DJKJ,
     2DKU,VFREQ,OPLUS,KSTN,IAXIS,JMAX,KMAX,NC1,JSTN,IGAUZ,INAUZ,LRES
C
      WRITE(6,200)
  200 FORMAT('0 PEBAND ENTERED',/)
C
      IK = 1
      II = 1
      K = 0
      JJMX = JMAX + 1
      JJJMX = JJMX + 1
C
  202 IKT = IAXIS - IK
      IF(IKT.LT.0) IK=1
      STWT = DFLOAT(KSTN(IK))
C
C     *** CALCULATE ENERGIES
      CK = DFLOAT(K*K)
      CKP = DFLOAT((K-1)*(K-1))
      CKR = DFLOAT((K+1)*(K+1))
      ZJJKG = DJKG*CK
      ZPDJKJ = DJKU*CKP
      ZRDJKJ = DJKU*CKR
      ZK = (AGBG-DKG*CK)*CK
      ZKP = (AUBU-DKU*CKP)*CKP + AUZET*DFLOAT(K-1)
      ZKR = (AUBU-DKU*CKR)*CKR - AUZET*DFLOAT(K+1)
CCCC
CCCC  DEFINITION OF VARIABLES NEEDED FOR L-RESONANCE CALCULATION.
CCCC  OPLUS IS THE L RESONANCE PARAMETER.
CCCC
      IF(LRES.NE.1) GO TO 600
      AB1 = (AUBU-AUZET/2.0D0)*(AUBU-AUZET/2.0D0)
      AB2 = (AUBU-AUZET/2.0D0)
      CK3 = DFLOAT(K*(K+1))
      CK5 = DFLOAT((K-1)*K)
      CK7=DFLOAT(K)
      OFACTI = (OPLUS/(4.0D0*CK7))*(OPLUS/(4.0D0*CK7))
  600 JJMN=K+1
      DO 203 J=JJMN,JJJMX
      CJ(J)=DFLOAT(J*(J-1))
      ENEG = CJ(J)*(BG-ZDJKG-DJG*CJ(J)) + ZK
      ENERG(J) = FREQ-ENEG
      EFACT(J) = DEXP(FACT*ENEG)
      ENEJ(J) = CJ(J)*(BU - ZRDJKJ - DJU*CJ(J)) + ZKR
      IF (LRES.NE.1) GO TO 203
      XER = OFACTI*(CJ(J)-CK3)*(CJ(J)-CK5)/AB1
CCCC
CCCC  PERTURBATION IN R BRANCH
CCCC
```

```
      PERT1 = -CK7*AB2*(XFR-(XFR*XFR)/4.0D0
     1+(XFR*XFR*XFR)/3.0D0-5.0D0*(XFR*XFR*XFR*XFR)/64.0D0
     2+7.0D0*(XFR*XFR*XFR*XFR*XFR)/128.0D0
     3-63.0D0*(XFR*XFR*XFR*XFR*XFR*XFR)/1536.0D0)
      ENEU(J) = ENEU(J) + PERT1
  203 CONTINUE
      IF (K.EQ.0) GO TO 205
C
      JJMN = K
      DO 204 J=JJMN,JJMX
      ENEUP(J) = CU(J)*(3U - ZPDJKU - DJU*CJ(J)) + ZKP
      IF(LRES.NE.1.OR.K.EQ.1) GO TO 204
      XFP = DFACT1*(CJ(J)-CK3)*(CJ(J)-CK5)/AB1
CCCC
CCCC  PERTURBATION IN P BRANCH
CCCC
      PERT2 = CK7*AB2*(XFP-(XFP*XFP)/4.0D0
     1+(XFP*XFP*XFP)/3.0D0-5.0D0*(XFP*XFP*XFP*XFP)/64.0D0
     2+7.0D0*(XFP*XFP*XFP*XFP*XFP)/128.0D0
     3-63.0D0*(XFP*XFP*XFP*XFP*XFP*XFP)/1536.0D0)
      ENEUP(J) = ENEUP(J) + PERT2
  204 CONTINUE
C
C     *** P TYPE SUB BANDS
C     *** P BRANCH
      JJMN = K+1
      DO 209 J=JJMN,JJMX
      JJ = J-1
      PFRQ=ENEUP(JJ) + ENFRQ(J)
      IF(PFRQ.LE.FMIN) GO TO 210
      IF(PFRQ.GT.FMAX) GO TO 210
      ST = DFLOAT(2*(J-K-2)*(JJ-K))/DFLOAT(JJ)
      PINY = STREACT(J)*STWT*VFREQ
      N = IDINT((FMAX-PFRQ)/CI + 1.0D0)
      CONT(N) = CONT(N) + PINY
C
C     *** Q BRANCH
  210 QFRQ = ENEUP(J) + ENFRQ(J)
      IF(QFRQ.LE.FMIN) GO TO 211
      IF(QFRQ.GT.FMAX) GO TO 211
      ST = DFLOAT(2*(J-K-1)*(J-K)*(2*J-1))/CU(J)
      QINY = ST*EFACT(J)*STWT*VFREQ
      N = IDINT((FMAX-QFRQ)/CI + 1.0D0)
      CONT(N) = CONT(N) + QINY
C
C     *** R BRANCH
  211 JJ = J+1
      RFRQ = ENEUP(JJ) + ENFRQ(J)
      IF(RFRQ.GT.FMAX) GO TO 209
      IF(RFRQ.LE.FMIN) GO TO 209
      ST = DFLOAT(2*(J-K)*(JJ-K))/DFLOAT(J)
      RINY = ST*EFACT(J)*STWT*VFREQ
      N = IDINT((FMAX-RFRQ)/CI + 1.0D0)
      CONT(N) = CONT(N) + RINY
  209 CONTINUE
C
  205 CONTINUE
C
C     *** R TYPE SUB BANDS
C     *** P BRANCH
```

```
      DO 212 M=1,2
      IF(K.EQ.0) GO TO 213
      GO TO 214
  213 SIMI = DFLOAT(ISTAG(M))
  214 JJMN = K + M + 2
      IF (JJMN.GT.JJMX) GO TO 211
C
      DO 206 J=JJMN,JJMX,2
      JJ = J-1
      PERJ = ENEU(JU) + ENERO(J)
      IF(PERO.LE.FMIN) GO TO 206
      IF(PERO.GT.FMAX) GO TO 206
      SI = DFLOAT(2*(J-K-2)*(JU-K))/DFLOAT(JU)
      PINY = STAFFACT(J)*STNT*VFREQ
      N = TOTNT((FMAX-FERO)/CI + 1.000)
      CONI(N) = CONI(N) + PINY
  206 CONTINUE
  211 CONTINUE
C
C
C     *** P BRANCH
      JJMN = K+1
      IF (JJMN.GT.JJMX) GO TO 212
      DO 208 J=JJMN,JJMX,2
      JJ = J+1
      PERJ = ENEU(JU) + ENERO(J)
      IF(PERO.GT.FMAX) GO TO 208
      IF(PERO.LE.FMIN) GO TO 208
      SI = DFLOAT(2*(J+K)*(JU+K))/DFLOAT(J)
      PINY = STAFFACT(J)*STNT*VFREQ
      N = TOTNT((FMAX-FERO)/CI + 1.000)
      CONI(N) = CONI(N) + PINY
  208 CONTINUE
  212 CONTINUE
C     *** Q BRANCH
      DO 215 M=1,2
      JJMN = K + 4 - M
      IF (JJMN.GT.JJMX) GO TO 215
      IF(K.EQ.0) GO TO 215
      GO TO 217
  216 SIMI = DFLOAT(ISTAG(M))
  217 DO 207 J=JJMN,JJMX,2
      PERJ = ENEU(J) + ENERO(J)
      IF(PERO.LE.FMIN) GO TO 207
      IF(PERO.GT.FMAX) GO TO 207
      SI = DFLOAT(2*(J+K)*(J-K-1)*(2*J-1))/CJ(J)
      PINY = STAFFACT(J)*STNT*VFREQ
      N = TOTNT((FMAX-FERO)/CI + 1.000)
      CONI(N) = CONI(N) + PINY
  207 CONTINUE
  215 CONTINUE
C
      IK = IK + 1
      II = 2
      K = K+1
      IF(K.LE.KMAX) GO TO 202
      RETURN
      END
```

Appendix 2

Program For The Construction Of A Pictorial Representation Of The Cartesian Displacements For s-Trifluorobenzene.

```
CCCC   K TAVLADORAKIS -1989
CCCC   THIS PROGRAM CONSTRUCTS A PICTORIAL REPRESENTATION
CCCC   OF THE ATOMIC DISPLACEMENTS FOR EACH NORMAL
CCCC   MODE FOR TRIFLUOROBENZENE.
CCCC   IT IS A MODIFICATION OF AN EARLIER PROGRAM WHICH
CCCC   DID THE SAME FOR TRIAZINE.
CCCC
       COMMON POS(40),CPOS(40),NAME(20)
       DIMENSION DPOS(1000),FREQ(30)
CCCC
CCCC   INPUT NUMBER OF ATOMS, NUMBER OF MODES, SCALE
CCCC
       READ(5,30) NATOMS,NMODES,SKALE
       NA2=NATOMS*2
       NORD=NA2*NMODES
       XDIM=200.0
       YDIM=300.0
CCCC
CCCC   INPUT THE WAVENUMBERS
CCCC
       READ(5,33)(FREQ(I),I=1,NMODES)
       J2=0
       DO 1 I=1,NATOMS
       J1=J2+1
       J2=J2+2
CCCC
CCCC   INPUT THE EQUILIBRIUM COORDINATES
CCCC
     1 READ(5,31)NAME(I),(POS(J),J=J1,J2)
CCCC
CCCC   INPUT THE ATOMIC DISPLACEMENTS FOR EACH NORMAL MODE
CCCC
       DO 2 I=1,NA2,2
       READ(5,33)(DPOS(K),K=I,NORD,NA2)
       M=I+1
       READ(5,33)(DPOS(K),K=M,NORD,NA2)
     2 CONTINUE
CCCC
CCCC   CALCULATION OF THE NEW COORDINATES
CCCC
       CALL V8GL
       CALL DEVMAP(XDIM,YDIM,0)
       DO 3 I=1,NMODES
       DO 4 K=1,NA2
     4 CPOS(K)=0.0
       INT=(I-1)*NA2
       DO 5 M=1,NA2
     5 CPOS(M)=POS(M)+DPOS(INT+M)
       FREQI=FREQ(I)
       CALL PLOT(I,NATOMS,NA2,SKALE,XDIM,YDIM,FREQI)
     3 CONTINUE
       CALL DEVEND
    30 FORMAT(2I5,F5.2)
    31 FORMAT(I4,2F13.6)
    33 FORMAT(8F10.4/(8F10.4)/(8F10.4))
       STOP
       END
       SUBROUTINE PLOT(IMODES,NATOMS,NA2,SKALE,XDIM,YDIM,FREQI)
       COMMON POS(40),CPOS(40),NAME(20)
       DIMENSION X1(40),X2(40),Y1(40),Y2(40)
```

```
      XORG=XDIM/2.0
      YORG=YDIM/2.0
      TPOSX=XDIM/3.0
      TPOSY=YDIM/2.0
      DO 2 I=1,NA2
      X1(I)=0.0
      X2(I)=0.0
      Y1(I)=0.0
    2 Y2(I)=0.0
      NIND=0
      DO 1 I=1,NA2,2
      NIND=NIND+1
      X1(NIND)=POS(I)*SKALE
      X2(NIND)=CPOS(I)*SKALE
      Y1(NIND)=POS(I+1)*SKALE
      Y2(NIND)=CPOS(I+1)*SKALE
    1 CONTINUE
      CALL WINDOW(2)
      CALL CHAHAR(3,0)
      CALL ARCTOL(0.2)
      CALL AXIPOS(0,XORG,YORG,1.0,1)
      CALL AXIPOS(0,XORG,YORG,1.0,2)
      CALL PENSEL(1,0.0,1)
      DO 3 N=1,NATOMS
      XP=X1(N)
      YP=Y1(N)
      CALL GRAMOV(XP,YP)
    3 CALL DOT(1.5)
      CALL LINE(X1,Y1,0)
      CALL PENSEL(2,1.0,1)
      DO 4 N=1,NATOMS
      XP=X2(N)
      YP=Y2(N)
      CALL GRAMOV(XP,YP)
    4 CALL SYMBOL(7)
      CALL LINE(X2,Y2,1)
      CALL PENSEL(1,0.0,1)
      CALL ITALIC(10.0)
      CALL CHAHAR(5,0)
      CALL MOVTO2(TPOSX+12.0,TPOSY+132.0)
      CALL CHAFIX(FREQI,7,1)
      CALL PICCLE
      CALL VBOL
      RETURN
      END
      END
      SUBROUTINE LINE(X,Y,IBROK)
      DIMENSION X(20),Y(20)
      CALL DASHED(1,1.5,1.0,0.0)
      CALL BROKEN(IBROK)
      DO 1 I=4,6
      XP=X(I)
      YP=Y(I)
      CALL GRAMOV(XP,YP)
      XPO=X(I+3)
      YPO=Y(I+3)
      CALL GRALIN(XPO,YPO)
      II=I+1
      IF(II.EQ.7)II=4
      XP=X(II)
```

```
      YP=Y(II)
    1 CALL GPALIN(XP,YP)
      DO 2 I=1,3
      XP=X(I)
      YP=Y(I)
      CALL GPAMOV(XP,YP)
      XP=X(I+3)
      YP=Y(I+3)
    2 CALL GPALIN(XP,YP)
      DO 3 I=10,12
      XP=X(I)
      YP=Y(I)
      CALL GPAMOV(XP,YP)
      XP=X(I-3)
      YP=Y(I-3)
    3 CALL GPALIN(XP,YP)
      CALL BROKEN(0)
      RETURN
      END
```

Appendix 3

Computer Programs Used In The Present Study

1.PLLBAND program: The PLLBAND program, which was first described by Barnard[19], calculates and plots parallel and perpendicular band contours for symmetric rotors. It has been modified specifically for interactive use for the PYRAMID computer system at UCL, utilising the GINO graphics library. The general form of the program is as follows:

Input Data: α. Number of bands to be superimposed, scale(cm^{-1}/cm), marks/cm^{-1}, transmission maximum, y-height/cm.

β. Temperature in Kelvin, contour interval, contour linewidth (Lorentzian), contour minimum, contour maximum, contour origin.

γ. Ground state Coriolis constants, excited state Coriolis constants, maximum intensity.

δ. Limit on J,K and order of axis.

ε. Ground state rotational constants, excited state rotational constants.

Output: Calculated band contour.

2. ASYM20 program: All our force field calculations were performed using the ASYM20 program which was written by Duinker and Mills[42] and was kindly provided to us by Professor Mills. The general form of the program is as follows:

Input Data: α. Number of different isotopic species, number of atoms in the molecule, number of each symmetry species.

β. Number of refinement cycles, number of observed Coriolis constants, number of observed centrifugal distortion

constants, factor used to multiply the indicated corrections to the parameters at the end of the first cycle. The factor is gradually increased and reaches 1 in the last cycle.

γ. The axis used for the calculation of the centrifugal distortion constants and the refinement of the constants. (A-axis, B-axis or C-axis), symmetric or asymmetric reduction used in the refinement of the distortion constants.

δ. Force constants which are already symmetrised or contants which are not going to be symmetrised.

ε. Values of elements of the Z matrix together with their positions in it.

$\sigma\tau$. Cartesian coordinates of each atom.

ζ. Number of internal coordinates, number of non-redundant or symmetry coordinates, number of bond stretches, number of angle bends, number of out of plane bends, number of torsions.

η. Identification of atoms taking part in a specific internal coordinate.

ϑ. U matrix.

ι. Atom weights of each atom in the molecule.

$\iota\alpha$ Observed wavenumbers with uncertainties, [weight = $1/(\text{uncertainty})^2$], Coriolis constants, x, y or z axis, normal modes coupled with uncertainties [weight = $1/(\text{uncertainty})^2$, distortion constants with uncertainties.

Output: Calculated values for frequencies, Coriolis constants, distortion constants together with Cartesian

displacements, normal coordinates, refined parameters and symmetry force constants. Also, several other matrices can be printed if required (e.g. Jacobian matrices etc.).

3. KONTUR program: This program which is based on an original one of Pierce[55] constructs simulated band contours for A or B or C or hybrid type bands of an asymmetric rotor molecule utilising the GINO graphics library (see PLLBAND program). It was modified recently by Parkin[56] to include second order Coriolis interactions like, for instance, between B and C type bands in prolate asymmetric rotors. The input and output of data has been approximately the same form as for the PLLBAND program discussed in Chapter 2 so it will not be repeated here.

4. MAINIR program: This program uses the so called A matrix formulation to sixth order for centrifugal distortion by Watson[57]. The rotational constants are determined by the method of least squares from a set of input transitions. Energy levels can also be calculated either from the least squares treatment or from input constants. Finally, the frequencies from these energy levels can be computed according to set selection rules. The energies are calculated by diagonalisation of the asymmetric rotor matrices. The general form of the datafile used is as follows:

α. Number of data sets, data in MHz or cm^{-1} or both, relative weight for data.

β. Provision for least squares treatment, number of constants to be fitted (from 2 to 31), full or reduced output, maximum frequency difference for least squares.

γ. Constants to be fitted include the following (for both upper and lower states) : B_x, B_y, B_z, D_J, D_{JK}, D_K, etc., vibrational frequency. Note : $B_x = B$, $B_y = C$, $B_z = A$ for a near prolate asymmetric rotor while $B_x = A$, $B_y = B$, $B_z = C$ for a near oblate asymetric rotor.

δ. Provision for calculation of energy levels, first J value, last J value, K maximum.

ε. Provision for calculation of frequencies, type of band (all combinations are possible).

$\sigma\tau$. Specified selection rules if required (ie ΔJ or ΔK_{-1} or ΔK_{+1}), frequencies by band type or ordered frequencies or both, lower frequency limit, upper frequency limit.

ζ. Transitions which are specified as follows: J', K'_{-1}, K'_{+1}, J'', K''_{-1}, K''_{+1}, resolved member of K doublet or mean of two unresolved components, weight for line frequency.

The output includes the observed and calculated transitions and the new constants derived from the least squares analysis.

References

1. S.J.Daunt, H.F.Shurvell, Spectrochim.Acta, 32A, 1545, (1976).

2. R.S.McDowell, 'Advances In Ir And Raman Spectroscopy', V5, ed.R.J.H.Clark, R.H.Hester, Heyden, (1978).

3. P.R.Griffiths, 'Advances In Ir And Raman Spectroscopy', V10, ed.R.J.H.Clark, R.H.Hester, Wiley, (1983).

4. S.Gherseti, K.Rao, J.Mol.Spec., 28, 27, (1968).

5. I.Nagakawa, J.Overend, J.Mol.Spec., 50, 333, (1974).

6. P.R.Griffiths, J.A.de Hesells 'FTIR Spectroscopy', Willey, New York, (1986).

7. T.Hirtschfeld, Appl.Opt., 17, 1400, (1978).

8. R.J.Anderson, P.R.Griffiths, Anal.Chem., 47, 2339, (1975).

9. W.H.Fletcher, 'Vibrational Spectroscopy - Modern Trends', Elsevier, New York, (1977).

10. W.S.Benedict, R.Herman, G.E.Moore, S.Silverman, Can.J.Phys., 34, 830,850, (1956).

11. G.I.Cartwright, I.M.Mills, J.Mol.Spec., 34, 415, (1970).

12. J.Sellors, Ph.D Thesis, University College London, (1984).

13. D.R.J.Boyd, H.C.Longuet-Higgins, Proc.Roy.Soc.A, 213, 55, (1952).

14. J.H.Meal, S.R.Polo, J.Chem.Phys., 24, 1119, (1956).

15. T.Oka, J.Chem.Phys., 47, 5140, (1967).

16. I.M.Mills, Mol.Phys., 7, 549, (1964).

17. G.Herzberg, 'Ir And Raman Spectra Of Polyatomic Molecules', Van Nostrand, (1945).

18. M.Grenier-Besson, J.Phys.Radium., 21, 555, (1960).

19. J.Barnard, Ph.D Thesis, University College london, (1974).

20. H.Allen, P.Cross, 'Molecular Vib-Rotors', Willey, (1963).

21. J.R.Nielsen, C.Y.Liang, D.C.Smith, Trans.Faraday.Soc., 9, 177, (1950).

22. E.Ferguson, J.Chem.Phys., 21, 886, (1953).

23. J.R.Sherer, J.C.Evans, W.W.Muelder, Spectrochim.Acta, 18, 1579, (1962).

24. J.Schlupf, A.Weber, J.Raman.Spec., 1, 3, (1973).

25. V.J.Eaton, D.Steele, J.Mol.Spec., 54, 312, (1975).

26. V.J.Eaton, R.A.R.Pearce, D.Steele, J.W.Tindle, Spectrochim.Acta, 32A, 663, (1976).

27. H.F.Shurvell, T.E.Cameron, D.B.Baker, S.J.Daunt, Spectrochim.Acta, 35A, 757, (1979).

28. J.Korppi-Tommola, H.F.Shurvell, S.J.Daunt, D.Steele, J.Mol.Spec., 87, 382, (1981).

29. V.J.Eaton, D.Steele, J.Mol.Spec., 48, 446, (1973).

30. J.M.Dowling, J.Mol.Spec., 6, 550, (1961).

31. M.R.Aliev, S.J.Subbotin, V.J.Tyulin, Opt.Spec.(USSR), 24, 47, (1968).

32. L.C.Hoskins, J.Chem.Phys.,45, 4594, (1966).

33. T.Shimanouchi, I.Nagakawa, Ann.Rev.Phys.Chem.,23, 217, (1972).

34. P.Gans, 'Advances In IR And Raman Spectroscopy',V3, ed.R.J.H.Clark,R.E.Hester, (1977).

35. T.Shimanouchi, 'Physical Chemistry: An Advanced Treatise', V4, 233, (197Ø).

36. J.Overend, Ann.Rev.Phys.Chem., 21, 265, (197Ø).

37. E.Wilson,J.C.Decius,P.Cross, 'Molecular Vibrations' McGrow Hill, New York, (1955).

38. S.R.Califano, 'Vibrational States', Wiley, (1976).

39. J.Aldous,I.M.Mills, Spectrochim.Acta, 18, 1Ø73, (1962).

4Ø. J.Aldous,I.M.Mills, Spectrochim.Acta, 19, 1567, (1963).

41. J.R.Scherer,J.Overend, Spectrochim.Acta, 17, 719, (1961).

42. J.C.Duinker,I.M.Mills, Spectrochim.Acta, 24A, 417, (1968).

43. E.Ferguson, J.Chem.Phys., 21, 886, (1953).

44. F.A.Miller,B.C.Crawford, J.Chem.Phys., 14, 282, (1946).

45. J.C.D.Brand,J.K.G.Watson, Trans.Far.Soc., 56, 1582,- (196Ø).

46. G.W.King,D.Moule, Spectrochim.Acta, 17, 286, (1961).

47. J.K.G.Watson, Ph.D Thesis, University Of Glasgow, (1962).

48. P.Klaboe,G.Kramer, Spectrochim.Acta, 33, 947, (1971).

49. M.Takami,K.Shimada, J.Mol.Spec., 59, 35, (1976).

50. M.Takami,M.Suzuki, J.Chem.Phys., 72, 4089, (1980).

51. C.Costain, J.R. Morton, J.Chem.Phys., 31, 389, (1959).

52. S.Edwards, Ph.D. Thesis, University College London, (in preparation).

53. J.M.Bennett,I.G.Ross,E.J.Wells, J.Mol.Spec., 4, 342, (1960).

54. I.M.Mills, 'VIII European Congress On Molecular Spectroscopy', Butterworths, London, (1965).

55. L.Pierce, unpublished program provided by Prof. K.K.Innes.

56. J.E.Parkin, private communication.

57. J.K.G.Watson, J.Chem.Phys., 46, 1935, (1967).

58. A.G.Ozkabak,L.Goodman,S.N.Thakur,K.K.Jespersen, J.Chem.Phys., 83, 6047, (1985).

59. S.N.Thakur,L.Goodman,A.G.Ozkabak, J.Chem.Phys., 84, 6642, (1986).

60. A.G.Ozkabak,L.Goodman, J.Chem.Phys., 87, 2564, (1987).